

The numerical renormalization group method for quantum impurity systems

Ralf Bulla*

Theoretische Physik III, Elektronische Korrelationen und Magnetismus, Institut für Physik, Universität Augsburg, 86135 Augsburg, Germany

Theo Costi†

Institut für Festkörperforschung, Forschungszentrum Jülich, 52425 Jülich, Germany

Thomas Pruschke‡

Institut für Theoretische Physik, Universität Göttingen, 37077 Göttingen, Germany

(Dated: February 5, 2008)

In the beginning of the 1970's, Wilson developed the concept of a fully non-perturbative renormalization group transformation. Applied to the Kondo problem, this numerical renormalization group method (NRG) gave for the first time the full crossover from the high-temperature phase of a free spin to the low-temperature phase of a completely screened spin. The NRG has been later generalized to a variety of quantum impurity problems. The purpose of this review is to give a brief introduction to the NRG method including some guidelines of how to calculate physical quantities, and to survey the development of the NRG method and its various applications over the last 30 years. These applications include variants of the original Kondo problem such as the non-Fermi liquid behavior in the two-channel Kondo model, dissipative quantum systems such as the spin-boson model, and lattice systems in the framework of the dynamical mean field theory.

Contents

	1. Multi-orbital Anderson model	37
	2. NRG calculations – an overview	38
	3. Selected results on low-energy properties	39
	E. Bosonic degrees of freedom and dissipation	41
I. Introduction	1	
II. Introduction to the Numerical Renormalization Group Method	4	
A. Structure of the Hamiltonian	6	
B. Logarithmic discretization	6	
C. Mapping on a semi-infinite chain	8	
D. Iterative diagonalization	9	
E. Renormalization group flow	11	
III. Calculation of Physical Properties	13	
A. Thermodynamic and static properties	13	
1. Entropy, specific heat and susceptibility	13	
2. Other local properties	15	
3. Example: The Kondo model	15	
4. Improving the accuracy: The Z -averaging	16	
B. Dynamic properties	16	
1. Equilibrium dynamics and transport	16	
2. Self-energy and reduced density matrix approach	19	
3. The x-ray problem and transient dynamics	20	
IV. Application to Impurity Models	23	
A. Kondo effect and related phenomena	23	
1. Screening and photoemission	23	
2. Kondo effect in the bulk and underscreened models	24	
3. Kondo effect in nanostructures	26	
B. Two-channel Kondo physics	28	
C. Impurity quantum phase transitions	31	
1. Multi-impurity physics	31	
2. Local criticality	33	
3. Kondo effect in superconductors	35	
D. Orbital effects	37	
	V. Application to Lattice Models within DMFT	43
	A. Hubbard model	44
	1. Mott metal-insulator transition	44
	2. Ordering phenomena	45
	3. Multi-band Hubbard models	46
	4. Other generalizations of the Hubbard model	46
	B. Periodic Anderson and Kondo lattice models	47
	C. Lattice models with phonons	48
	VI. Summary	49
	Acknowledgments	50
	References	50

I. INTRODUCTION

The last decades saw a steadily increasing interest in a wide range of physical systems involving quantum impurities. The expression ‘quantum impurity system’ is used in a very general sense here, namely a small system (the impurity) with only a few degrees of freedom coupled to a large system (the environment or bath) with very many degrees of freedom, and where both subsystems have to be treated quantum mechanically.

The use of the terminology ‘impurity’ is due to historical reasons. In the Kondo problem, the small system is a magnetic impurity, such as an iron ion, interacting with the conduction electrons of a nonmagnetic metal such as gold (Hewson, 1993). Other realizations are for example artificial impurities such as quantum dots hosting only

*Electronic address: Ralf.Bulla@Physik.Uni-Augsburg.De

†Electronic address: t.costi@fz-juelich.de

‡Electronic address: pruschke@theorie.physik.uni-goettingen.de

a small number of electrons. Here, the environment is formed by the electrons in the leads. The term ‘quantum impurity systems’ can also be used for what are traditionally called ‘dissipative systems’. As an example, let the impurity correspond to a spin degree of freedom and the environment be built up by a bosonic bath; this describes the well-known spin-boson model experimentally relevant, for example, for dissipative two-level systems like tunneling centers in glasses (Leggett *et al.*, 1987).

Any theoretical method for the investigation of quantum impurity systems has to face a number of serious obstacles. First of all, because the environment typically consists of a (quasi-)continuum of quantum-mechanical degrees of freedom, one has to consider a wide range of energies – from a high-energy cut-off (which can be of the order of several eV) down to arbitrarily small excitation energies. On the other hand, because the impurity degrees of freedom usually form an interacting quantum-mechanical system, their coupling to a continuum of excitations with arbitrarily small energies can result in infrared divergencies in perturbational treatments. A well-known example for this difficulty is the Kondo problem: Its physics is governed by an energy scale, the Kondo temperature T_K , which depends non-analytically on the spin-exchange coupling J between the impurity and the conduction band of the host, $\ln T_K \propto 1/J$ (see Hewson (1993) for a detailed description of the limitations of the perturbational approach for the Kondo model and the single-impurity Anderson model). One is thus faced with the task to perform non-perturbative calculations for an interacting quantum-mechanical many-body system with a continuum of excitations covering a broad spectrum of energies.

A very efficient way to treat systems with such a broad and continuous spectrum of energies is the renormalization group approach. It allows, in general, to go in a certain sequence of renormalization group steps from high energies, such as the bandwidth, to low energies, such as the Kondo temperature. General introductions of renormalization group concepts have been given in Goldenfeld (1992); Ma (1976); Salmhofer (1999) (see also the original papers: Wilson and Kogut (1974) and Wilson (1975b)). Here we focus on a specific implementation of the renormalization group idea: Wilson’s numerical renormalization group method (Wilson, 1975a), referred to as ‘NRG’ in the remainder of the review. This approach is different from most renormalization group methods as it is non-perturbative in all system parameters; however, the price one has to pay is that the renormalization group steps have to be performed numerically.

The general strategy of the NRG is the following (more details are given in Sec. II). As specific example, let us consider the Kondo model which describes a magnetic impurity with spin \vec{S} coupled to the electrons of a conduction band, assumed to be non-interacting, via an interaction of the form $J\vec{S} \cdot \vec{s}$, with \vec{s} the spin of the electrons at the impurity site. The NRG starts with a logarithmic discretization of the conduction band in

intervals $[\Lambda^{-(n+1)}\omega_c, \Lambda^{-n}\omega_c]$ and $[-\Lambda^{-n}\omega_c, -\Lambda^{-(n+1)}\omega_c]$ ($n = 0, 1, 2, \dots$). We shall call $\Lambda > 1$ the NRG discretization parameter. After a sequence of transformations, the discretized model is mapped onto a semi-infinite chain with the impurity spin representing the first site of the chain. The Kondo model in the semi-infinite chain form is diagonalized iteratively, starting from the impurity site and successively adding degrees of freedom to the chain. Due to the logarithmic discretization, the hopping parameters between neighboring sites fall off exponentially, i.e. going along the chain corresponds to accessing decreasing energy scales in the calculation.

In this way, Wilson achieved a non-perturbative description of the full crossover from a free impurity spin at high temperatures to a screened spin at low temperatures (Wilson, 1975a), thus solving the so-called Kondo problem as discussed in detail in Hewson (1993). After this first application more than 30 years ago, the NRG has been successfully generalized and applied to a much wider range of quantum impurity problems. The first extension was the investigation of the single-impurity Anderson model (Anderson, 1961), which extends the Kondo model by including charge fluctuations at the impurity site. Krishna-murthy *et al.* (1980a,b) described all the technical details, the analysis of fixed points, and the calculation of static quantities for this model.

In the following, the development of the NRG concentrated on the analysis of more complicated impurity models, involving either more environment or impurity degrees of freedom. For example, in the two-channel Kondo model the impurity spin couples to two conduction bands. This model, which has a non-Fermi liquid fixed point with associated non-Fermi liquid properties, has been first investigated with the NRG by Cragg *et al.* (1980). The numerical calculations for such a two-channel model are, however, much more cumbersome because the Hilbert space grows by a factor 16 in each step of the iterative diagonalization, instead of the factor 4 in the single-channel case. Pang and Cox (1991) and Affleck *et al.* (1992) later analyzed the stability of the non-Fermi liquid fixed point with respect to various perturbations such as channel anisotropy.

The two-impurity Kondo model as paradigm for the competition of local Kondo screening and non-local magnetic correlations was studied with NRG by Jones and Varma (1987); Jones *et al.* (1988); Sakai and Shimizu (1992a,b); Sakai *et al.* (1990); Silva *et al.* (1996). Here, the focus was on the question, if the two regimes are connected by a quantum-phase transition or rather by a smooth crossover. Later on, such studies were extended to the two-channel situation, too (Ingersent *et al.*, 1992).

Originally, the NRG was used to determine thermodynamic properties of quantum impurity systems. The calculation of dynamic quantities with the NRG started with the $T = 0$ absorption and photoemission spectra of the x-ray Hamiltonian (Oliveira and Wilkins, 1981, 1985), followed by the $T = 0$ single-particle spectral func-

tion for the orbitally non-degenerate and degenerate Anderson model (Brito and Frota, 1990; Costi and Hewson, 1990, 1992b; Frota and Oliveira, 1986; Sakai *et al.*, 1989). The resulting spectral functions are obtained on all energy scales, with a resolution proportional to the frequency as discussed in detail in Sec. III.B. Calculation of finite-temperature spectral functions $A(\omega, T)$ are more problematic since all excitations can, in principle, contribute. Nevertheless, the NRG has been shown to give accurate results for $A(\omega, T)$, too, which also allows to calculate transport properties (Costi and Hewson, 1992b; Costi *et al.*, 1994a; Suzuki *et al.*, 1996). A subsequent development is the introduction of the concept of the reduced density matrix, which allows to calculate dynamic quantities in equilibrium in the presence of external fields (Hofstetter, 2000). The calculation of non-equilibrium transient dynamics requires a multiple-shell NRG procedure (Costi, 1997a) and has been accomplished with the aid of a complete basis set and the reduced density matrix (Anders and Schiller, 2005). The first applications of this approach show very promising results, both for fermionic and bosonic systems (Anders *et al.*, 2006; Anders and Schiller, 2005, 2006). Another recent generalization of the NRG approach is to quantum impurities coupled to a bosonic bath (bosonic NRG, see Bulla *et al.* (2005); for early related approaches see Evangelou and Hewson (1982)). The bosonic NRG has already been successfully applied to the sub-Ohmic spin-boson model which shows a line of quantum critical points separating localized and delocalized phases (Bulla *et al.*, 2003).

Additional motivation to further improve the NRG method came from the development of the dynamical mean-field theory (DMFT) (Georges *et al.*, 1996; Metzner and Vollhardt, 1989) in which a lattice model of correlated electrons, such as the Hubbard model, is mapped onto a single-impurity Anderson model with the impurity coupled to a bath whose structure has to be determined self-consistently. This requires the NRG to handle impurity models with an arbitrary density of states of the conduction electrons and to calculate directly the impurity self-energy (Bulla *et al.*, 1998). The first applications of the NRG within the DMFT framework concentrated on the Mott transition in the Hubbard model and accurate results could be obtained for both $T = 0$ (Bulla, 1999; Sakai and Kuramoto, 1994) and finite temperatures (Bulla *et al.*, 2001). Within DMFT, the NRG has been applied to the periodic Anderson model (Pruschke *et al.*, 2000), the Kondo lattice model (Costi and Manini, 2002), multi-band Hubbard models (Pruschke and Bulla, 2005), the ferromagnetic Kondo lattice model with interactions in the band (Liebsch and Costi, 2006), and to lattice models with a coupling to local phonon modes such as the Holstein model (Meyer *et al.*, 2002) and the Hubbard-Holstein model (Koller *et al.*, 2004b).

The observation that the coupling between electronic degrees of freedom in quantum dots and the surrounding

leads can give rise to Kondo-like features in the transport characteristics, has also led to a resurgence of interest in quantum impurity systems, both experimentally and theoretically. An important feature of quantum dot systems is their flexibility and a number of different set-ups have been realized so far, and investigated theoretically by various methods including the NRG. Applications of the NRG in this field include the standard Kondo effect (Borda *et al.*, 2005; Costi, 2001; Gerland *et al.*, 2000; Izumida *et al.*, 1998), coupled quantum dots (Borda *et al.*, 2003; Cornaglia and Grepel, 2005b; Galpin *et al.*, 2006b; Hofstetter and Schoeller, 2002; Hofstetter and Zaránd, 2004), quantum dots in a superconductor (Choi *et al.*, 2004a), and quantum dots coupled to ferromagnetic leads (Choi *et al.*, 2004b; Martinek *et al.*, 2003).

From this brief overview one can see that the range of applicability of the NRG has widened considerably since Wilson's original paper, covering physical phenomena such as the Mott transition, quantum dot physics, local criticality, dissipative quantum systems, etc. Further applications are still lying ahead and various optimizations of the technique itself are still being developed – we shall come back to this point in the summary section.

This paper is the first review of the NRG approach (since Wilson's original paper on the Kondo problem) which attempts to cover both the technical details and all the various applications. In this way, the reader should get an overview over the field, learn about the current status of the individual applications, and (hopefully) come up with ideas for further calculations. This review can only be a start for a deeper understanding of the NRG. The following shorter reviews on selected topics are also helpful: section 4 in Hewson (1993) contains a pedagogical introduction to the NRG as applied to the Kondo problem, Gonzalez-Buxton and Ingersent (1998) discuss the soft-gap Anderson and Kondo models, Costi (1999) gives a general overview of the key concepts, including the application to the anisotropic Kondo model, Bulla *et al.* (2005) present a detailed introduction to the bosonic NRG, and, finally, the two papers on the first calculations for the single-impurity Anderson model by Krishna-murthy *et al.* (1980a,b) are still valuable reading for an overview of the method and the details of the analysis of fixed points.

The review is organized as follows: in Sec. II we start with an introduction to the basic concepts of the NRG approach. The single-impurity Anderson model serves as an example here, but the strategy applies to quantum impurity systems quite generally. At the end of this section, we discuss the flow of the many-particle eigenenergies and the appearance of fixed points in this flow. This analysis already gives important insights into the physics of a given model, but the calculation of physical quantities needs some extra care, as described in Sec. III. This section is divided into Sec. III.A (thermodynamic and static quantities, such as entropy, specific heat and susceptibilities) and Sec. III.B (dynamic quantities, both

in equilibrium and non-equilibrium).

The following two sections deal with the various applications of the NRG and we distinguish here between quantum impurity systems (Sec. IV) and lattice models within DMFT (Sec. V). Section IV covers most of the work using the NRG which has been published so far. We shall present results for systems which show the standard Kondo effect (Sec. IV.A, this also includes most of the NRG-results on quantum dots), the two-channel Kondo problem (Sec. IV.B), models displaying impurity quantum phase transitions (Sec. IV.C), quantum impurity systems with orbital degrees of freedom (Sec. IV.D), and, finally, impurities coupled to bosonic degrees of freedom (Sec. IV.E). The section on lattice models within DMFT (Sec. V) covers calculations for the Hubbard model (Sec. V.A), the periodic Anderson and Kondo lattice models (Sec. V.B), and lattice models with coupling to phonons (Sec. V.C).

In the summary we shall discuss open problems as well as possible directions for future developments of the NRG approach.

Let us finish the introduction with a few remarks on the selection of the material presented and the references: Due to the flexibility of the NRG, the review covers a broad range of physical phenomena, in particular in Secs. IV and V. We shall, however, only give very brief introductions to these phenomena and refer the reader to the references given in the individual subsections, in particular reviews or seminal books. Furthermore, due to lack of space, we shall mostly not review the results from other theoretical approaches which have been applied to quantum impurity systems, such as Bethe ansatz, quantum Monte Carlo, resolvent perturbation theory, local-moment approach, etc, unless these appear crucial for an understanding of relevant NRG results. Comparisons between the results from NRG and these approaches are, in most cases, included in the papers cited here (see also Hewson (1993)). This means that we shall focus, almost completely, on references which use the NRG.

II. INTRODUCTION TO THE NUMERICAL RENORMALIZATION GROUP METHOD

The NRG method can be applied to systems of the following form: a quantum mechanical impurity with a small number of degrees of freedom (so that it can be diagonalized exactly) coupling to a bath of fermions or bosons, usually with continuous excitation spectrum. There is no restriction on the structure of the impurity part of the Hamiltonian; it might contain, for example, a Coulomb repulsion of arbitrarily large strength. The bath, however, is required to consist of non-interacting fermions or bosons, otherwise the various mappings described below cannot be performed.

Whenever we discuss, in this review, models of a different kind, such as the Hubbard model, these models will be mapped onto impurity models of the above type. For

the Hubbard model and other lattice models of correlated electrons this is achieved via the dynamical mean-field theory, see Sec. V.

Before we start with the technical details of the NRG approach, let us give a brief overview of the general strategy. For basically all NRG applications, one proceeds as follows:

- a) Division of the energy support of the bath spectral function into a set of logarithmic intervals.
- b) Reduction of the continuous spectrum to a discrete set of states (logarithmic discretization).
- c) Mapping of the discretized model onto a semi-infinite chain.
- d) Iterative diagonalization of this chain.
- e) Further analysis of the many-particle energies, matrix elements, etc., calculated during the iterative diagonalization. This yields information on fixed points, static and dynamic properties of the quantum impurity model.

Parts a), b) and c) of this strategy are sketched in Fig. 1, where we consider a constant bath spectral function within the interval $[-1, 1]$. The NRG discretization parameter Λ defines a set of discretization points, $\pm\Lambda^{-n}$, $n = 0, 1, 2, \dots$, and a corresponding set of intervals. The continuous spectrum in each of these intervals (Fig. 1a) is approximated by a single state (Fig. 1b). The resulting discretized model is mapped onto a semi-infinite chain with the impurity (filled circle) corresponding to the first site of this chain. Due to the logarithmic discretization, the hopping matrix elements decrease exponentially with distance from the impurity, $t_n \propto \Lambda^{-n/2}$.

While the various steps leading to the semi-infinite chain are fairly straightforward from a mathematical point of view, the philosophy behind this strategy is probably not so obvious.

Quite generally, a numerical diagonalization of Hamiltonian matrices allows to take into account the various impurity-related terms in the Hamiltonian, such as a local Coulomb repulsion, non-perturbatively. Apparently, the actual implementation of such a numerical diagonalization scheme requires some sort of discretization of the original model, which has a continuum of bath states. There are, however, many ways to discretize such a system, so let us try to explain why the logarithmic discretization is the most suitable one here. As it turns out, quantum impurity models are very often characterized by energy scales orders of magnitudes smaller than the bare energy scales of the model Hamiltonian. If the ratio of these energy scales is, for example, of the order of 10^5 , a linear discretization would require energy intervals of size at most 10^{-6} to properly resolve the lowest scale in the system. Since for a finite system the splitting of energies is roughly inversely proportional to the system size, one would need of the order of 10^6 sites, which renders an exact diagonalization impossible.

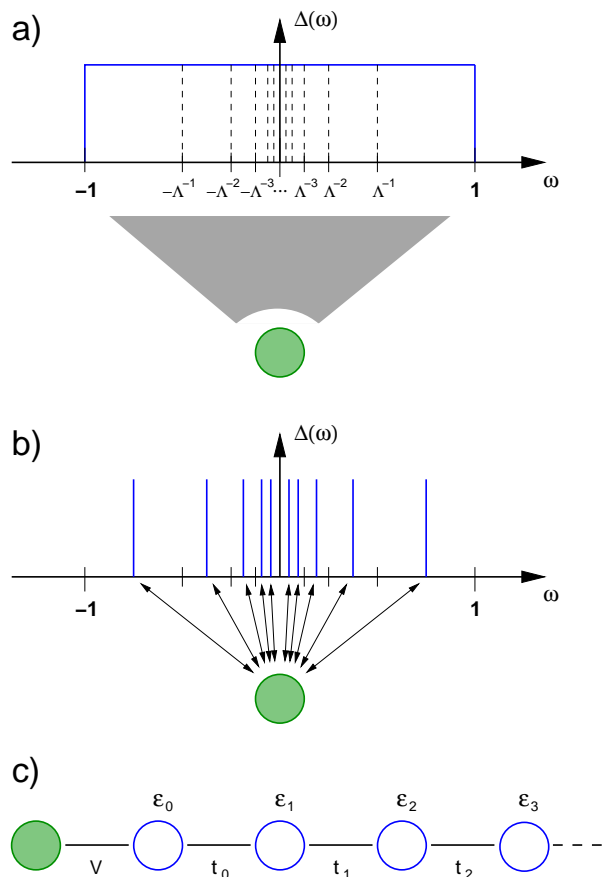


FIG. 1 Initial steps of the NRG illustrated for the single-impurity Anderson model in which an impurity (filled circle) couples to a continuous conduction band via the hybridization function $\Delta(\omega)$; a) a logarithmic set of intervals is introduced through the NRG discretization parameter Λ ; b) the continuous spectrum within each of these intervals is approximated by a single state; c) the resulting discretized model is mapped onto a semi-infinite chain where the impurity couples to the first conduction electron site via the hybridization V ; the parameters of the tight-binding model (see Eq. (26)) are ϵ_n and t_n .

Apparently, the logarithmic discretization reduces this problem in that the low-energy resolution now depends exponentially on the number of sites in the discretized model. Of course, the accuracy of such an approach has to be checked by suitable extrapolations of the discretization parameters, in particular a $\Lambda \rightarrow 1$ extrapolation, which recovers the original continuum model. Very often it turns out that already for Λ of the order of 2 the results are accurate to within a few percent and a $\Lambda \rightarrow 1$ extrapolation indeed reproduces exact results, if these are available.

However, this argument in favor of the logarithmic discretization does neither explain the need for a mapping to a chain Hamiltonian as in Fig. 1c, nor how the problem of an exponentially growing Hilbert space with increasing chain length is resolved. As far as the first point is concerned, an iterative diagonalization for the discretized

model with a star geometry as in Fig. 1b has been implemented for the spin-boson model (Bulla *et al.*, 2005). For reasons which are not yet completely clear, such a ‘star-NRG’ is only partly successful. Let us just mention here that for a fermionic model such as the single-impurity Anderson model, the iterative diagonalization of the model in the semi-infinite chain form is much more convenient since one site of the chain can be added in each step without violating particle-hole symmetry (for a detailed discussion of this point see Bulla *et al.* (2005)).

The quantum impurity model in the semi-infinite chain form is solved by iterative diagonalization, which means that in each step of the iterative scheme one site of the chain is added to the system and the Hamiltonian matrices of the enlarged cluster are diagonalized numerically. As already pointed out, without taking further steps to reduce the size of the Hilbert space this procedure would have to end for chain sizes of ≈ 10 . Here the renormalization group concept enters the procedure through the dependence of the hopping matrix elements on the chain length, $t_n \propto \Lambda^{-n/2}$. Adding one site to the chain corresponds to decreasing the relevant energy scale by a factor $\sqrt{\Lambda}$. Furthermore, because the coupling t_n to the newly added site falls off exponentially, only states of the shorter chain within a comparatively small energy window will actually contribute to the states of the chain with the additional site. This observation allows to introduce a very simple truncation scheme: after each step only the lowest lying N_s many-particle states are retained and used to build up the Hamiltonian matrices of the next iteration step, thus keeping the size of the Hilbert space fixed as one walks along the chain.

All these technical steps will be discussed in detail in the following. Let us briefly remark on the general set-up of this section. We would of course like to keep this section as general as possible, because it should serve as an introduction to the NRG technique, whose application to a variety of problems is then the subject of the remainder of this review. This quest for generality is, however, contrasted by the large variety of possible impurity-bath interactions. Instead of presenting explicit formulae for all possible quantum impurity models, we restrict ourselves to the single-impurity Anderson model as a specific – and most important – example here. The original introductions to the technique for the Kondo model (Wilson, 1975a) and the single-impurity Anderson model (Krishna-murthy *et al.*, 1980a,b) were restricted to a constant bath density of states (or better, a constant hybridization function $\Delta(\omega)$ as defined below). Here, we consider a general frequency dependent $\Delta(\omega)$ from the outset. This generalization is essential for various applications of the NRG (the soft-gap models, see Sec. IV.C.2, and lattice models within DMFT, see Sec. V) where the physics is largely determined by the frequency dependence of $\Delta(\omega)$. If the hybridization function is non-zero for positive frequencies only, the manipulations of the bath degrees of freedom equally hold for a bosonic bath, see Bulla *et al.* (2005).

In this section we cover the steps a), b), c) and d) of the list given above. Concerning the analysis of the data [step e) in the list], we discuss the flow of the many-particle spectra and all related issues here. The calculation of static and dynamic quantities will be described in Sec. III.

A. Structure of the Hamiltonian

The Hamiltonian of a general quantum impurity model consists of three parts, the impurity H_{imp} , the bath H_{bath} , and the impurity-bath interaction $H_{\text{imp-bath}}$:

$$H = H_{\text{imp}} + H_{\text{bath}} + H_{\text{imp-bath}} . \quad (1)$$

For the single-impurity Anderson model (SIAM) (Anderson, 1961) with the Hamiltonian $H = H_{\text{SIAM}}$, these three terms are given by:

$$\begin{aligned} H_{\text{imp}} &= \sum_{\sigma} \varepsilon_f f_{\sigma}^{\dagger} f_{\sigma} + U f_{\uparrow}^{\dagger} f_{\uparrow} f_{\downarrow}^{\dagger} f_{\downarrow} , \\ H_{\text{bath}} &= \sum_{k\sigma} \varepsilon_k c_{k\sigma}^{\dagger} c_{k\sigma} , \\ H_{\text{imp-bath}} &= \sum_{k\sigma} V_k \left(f_{\sigma}^{\dagger} c_{k\sigma} + c_{k\sigma}^{\dagger} f_{\sigma} \right) . \end{aligned} \quad (2)$$

In this Hamiltonian, the fermionic operators $c_{k\sigma}^{(\dagger)}$ correspond to band states with spin σ and energy ε_k , and the $f_{\sigma}^{(\dagger)}$ to the impurity states with energy ε_f . The Coulomb interaction between two electrons occupying the impurity site is parametrized by U and both subsystems are coupled via a k -dependent hybridization V_k .

The influence of the bath on the impurity is completely determined by the so-called hybridization function $\Delta(\omega)$:

$$\Delta(\omega) = \pi \sum_k V_k^2 \delta(\omega - \varepsilon_k) . \quad (3)$$

Thus, if we are only interested in the impurity contributions to the physics of the SIAM, we can rewrite the Hamiltonian in a variety of ways, provided the manipulations involved do not change the form of $\Delta(\omega)$. Without loss of generality, we assume that the support of $\Delta(\omega)$ completely lies within the interval $[-D, D]$, with $D > 0$ chosen suitably. Henceforth, we will use $D = 1$ as energy unit.

One such possible reformulation is given by the following Hamiltonian:

$$\begin{aligned} H &= H_{\text{imp}} + \sum_{\sigma} \int_{-1}^1 d\varepsilon g(\varepsilon) a_{\varepsilon\sigma}^{\dagger} a_{\varepsilon\sigma} \\ &+ \sum_{\sigma} \int_{-1}^1 d\varepsilon h(\varepsilon) \left(f_{\sigma}^{\dagger} a_{\varepsilon\sigma} + a_{\varepsilon\sigma}^{\dagger} f_{\sigma} \right) . \end{aligned} \quad (4)$$

Here we introduced a one-dimensional energy representation for the conduction band with band cut-offs at energies ± 1 , a dispersion $g(\varepsilon)$ and a hybridization $h(\varepsilon)$. The

band operators fulfill the standard fermionic commutation relations: $[a_{\varepsilon\sigma}^{\dagger}, a_{\varepsilon'\sigma'}]_{\pm} = \delta(\varepsilon - \varepsilon') \delta_{\sigma\sigma'}$. It has been shown in Bulla *et al.* (1997b) that the two functions $g(\varepsilon)$ and $h(\varepsilon)$ are related to the hybridization function $\Delta(\omega)$ via

$$\Delta(\omega) = \pi \frac{d\varepsilon(\omega)}{d\omega} h[\varepsilon(\omega)]^2 , \quad (5)$$

where $\varepsilon(\omega)$ is the inverse function to $g(\varepsilon)$, $g[\varepsilon(\omega)] = \omega$. For a given $\Delta(\omega)$ there are obviously many possibilities to divide the ω -dependence between $\varepsilon(\omega)$ and $h(\varepsilon(\omega))$. This feature will turn out to be useful later.

For a constant $\Delta(\omega) = \Delta_0$ within the interval $[-1, 1]$, Eq. (5) can be fulfilled by choosing $\varepsilon(\omega) = \omega$ (this corresponds to $g(\varepsilon) = \varepsilon$ and $h^2(\varepsilon) = \Delta_0/\pi$).

B. Logarithmic discretization

The Hamiltonian in the integral representation Eq. (4) is a convenient starting point for the logarithmic discretization of the conduction band. As shown in Fig. 1a, the parameter $\Lambda > 1$ defines a set of intervals with discretization points

$$x_n = \pm \Lambda^{-n} , \quad n = 0, 1, 2, \dots . \quad (6)$$

The width of the intervals is given by

$$d_n = \Lambda^{-n} (1 - \Lambda^{-1}) . \quad (7)$$

Within each interval we now introduce a complete set of orthonormal functions

$$\psi_{np}^{\pm}(\varepsilon) = \begin{cases} \frac{1}{\sqrt{d_n}} e^{\pm i\omega_n p \varepsilon} & \text{for } x_{n+1} < \pm \varepsilon < x_n \\ 0 & \text{outside this interval .} \end{cases} \quad (8)$$

The index p takes all integer values between $-\infty$ and $+\infty$, and the fundamental frequencies for each interval are given by $\omega_n = 2\pi/d_n$. The next step is to expand the conduction electron operators $a_{\varepsilon\sigma}$ in this basis, i.e.

$$a_{\varepsilon\sigma} = \sum_{np} \left[a_{np\sigma} \psi_{np}^+(\varepsilon) + b_{np\sigma} \psi_{np}^-(\varepsilon) \right] , \quad (9)$$

which corresponds to a Fourier expansion in each of the intervals. The inverse transformation reads

$$\begin{aligned} a_{np\sigma} &= \int_{-1}^1 d\varepsilon [\psi_{np}^+(\varepsilon)]^* a_{\varepsilon\sigma} , \\ b_{np\sigma} &= \int_{-1}^1 d\varepsilon [\psi_{np}^-(\varepsilon)]^* a_{\varepsilon\sigma} . \end{aligned} \quad (10)$$

The operators $a_{np\sigma}^{(\dagger)}$ and $b_{np\sigma}^{(\dagger)}$ defined in this way fulfill the usual fermionic commutation relations. The Hamiltonian Eq. (4) is now expressed in terms of these discrete operators.

In particular, the transformed hybridization term (first part only) is

$$\int_{-1}^1 d\varepsilon h(\varepsilon) f_{\sigma}^{\dagger} a_{\varepsilon\sigma} = f_{\sigma}^{\dagger} \sum_{np} \left[a_{np\sigma} \int^{+,n} d\varepsilon h(\varepsilon) \psi_{np}^{+}(\varepsilon) + b_{np\sigma} \int^{-,n} d\varepsilon h(\varepsilon) \psi_{np}^{-}(\varepsilon) \right], \quad (11)$$

where we have defined

$$\int^{+,n} d\varepsilon \equiv \int_{x_{n+1}}^{x_n} d\varepsilon, \quad \int^{-,n} d\varepsilon \equiv \int_{-x_n}^{-x_{n+1}} d\varepsilon. \quad (12)$$

For a constant $h(\varepsilon) = h$, the integrals in Eq. (11) filter out the $p = 0$ component only

$$\int^{\pm,n} d\varepsilon h \psi_{np}^{\pm}(\varepsilon) = \sqrt{d_n} h \delta_{p,0}. \quad (13)$$

In other words, the impurity couples only to the $p = 0$ components of the conduction band states. It will become clear soon, that this point was essential in Wilson's original line of arguments, so we would like to maintain this feature ($h(\varepsilon)$ being constant in each interval of the logarithmic discretization) also for a general, non-constant $\Delta(\omega)$. Note that this restriction for the function $h(\varepsilon)$ does not lead to additional approximations for a non-constant $\Delta(\omega)$ as one can shift all the remaining ε -dependence to the dispersion $g(\varepsilon)$, see Eq. (5).

As discussed in Chen and Jayaprakash (1995a) in the context of the soft-gap model (see also Chen and Jayaprakash (1995b)), one can even set $h(\varepsilon) = h$ for all ε . Here we follow the proposal of Bulla *et al.* (1997b), that is we introduce a step function for $h(\varepsilon)$

$$h(\varepsilon) = h_n^{\pm}, \quad x_{n+1} < \pm\varepsilon < x_n, \quad (14)$$

with h_n^{\pm} given by the average of the hybridization function $\Delta(\omega)$ within the respective intervals,

$$h_n^{\pm 2} = \frac{1}{d_n} \int^{\pm,n} d\varepsilon \frac{1}{\pi} \Delta(\varepsilon). \quad (15)$$

This leads to the following form of the hybridization term

$$\int_{-1}^1 d\varepsilon h(\varepsilon) f_{\sigma}^{\dagger} a_{\varepsilon\sigma} = \frac{1}{\sqrt{\pi}} f_{\sigma}^{\dagger} \sum_n [\gamma_n^{+} a_{n0\sigma} + \gamma_n^{-} b_{n0\sigma}], \quad (16)$$

with $\gamma_n^{\pm 2} = \int^{\pm,n} d\varepsilon \Delta(\varepsilon)$.

Next, we turn to the conduction electron term, which transforms into

$$\int_{-1}^1 d\varepsilon g(\varepsilon) a_{\varepsilon\sigma}^{\dagger} a_{\varepsilon\sigma} = \sum_{np} \left(\xi_n^{+} a_{np\sigma}^{\dagger} a_{np\sigma} + \xi_n^{-} b_{np\sigma}^{\dagger} b_{np\sigma} \right) + \sum_{n,p \neq p'} \left(\alpha_n^{+}(p, p') a_{np\sigma}^{\dagger} a_{np'\sigma} - \alpha_n^{-}(p, p') b_{np\sigma}^{\dagger} b_{np'\sigma} \right). \quad (17)$$

The first term on the right hand side of Eq. (17) is diagonal in the index p . The discrete set of energies ξ_n^{\pm} can be expressed as (Bulla *et al.*, 1997b)

$$\xi_n^{\pm} = \frac{\int^{\pm,n} d\varepsilon \Delta(\varepsilon) \varepsilon}{\int^{\pm,n} d\varepsilon \Delta(\varepsilon)} \left[= \frac{1}{2} \Lambda^{-n} (1 + \Lambda^{-1}) \right], \quad (18)$$

where we added the result for a constant $\Delta(\varepsilon)$ in brackets. The coupling of the conduction band states with different p, p' (the second term) recovers the continuum (no approximation has been made so far, Eq. (17) is still exact). For the case of a linear dispersion, $g(\varepsilon) = \varepsilon$, the prefactors $\alpha_n^{\pm}(p, p')$ are the same for both sides of the discretization and take the following form

$$\alpha_n^{\pm}(p, p') = \frac{1 - \Lambda^{-1}}{2\pi i} \frac{\Lambda^{-n}}{p' - p} \exp \left[\frac{2\pi i (p' - p)}{1 - \Lambda^{-1}} \right]. \quad (19)$$

The actual discretization of the Hamiltonian is now achieved by dropping the terms with $p \neq 0$ in the expression for the conduction band Eq. (17). This is, of course, an approximation, the quality of which is not clear from the outset. To motivate this step we can argue that (i) the $p \neq 0$ states couple only indirectly to the impurity (via their coupling to the $p = 0$ states in Eq. (17)) and (ii) the coupling between the $p = 0$ and $p \neq 0$ states has a prefactor $(1 - \Lambda^{-1})$ which vanishes in the limit $\Lambda \rightarrow 1$. In this sense one can view the couplings to the states with $p \neq 0$ as small parameters and consider the restriction to $p = 0$ as zeroth order step in a perturbation expansion with respect to the coefficients $a_n^{\pm}(p, p')$ (Wilson, 1975a). As it turns out, the accuracy of the results obtained from the $p = 0$ states only is surprisingly good even for values of Λ as large as $\Lambda = 2$, so that in all NRG calculations the $p \neq 0$ states have never been considered so far.

Finally, after dropping the $p \neq 0$ terms and relabeling the operators $a_{n0\sigma} \equiv a_{n\sigma}$, etc., we arrive at the discretized Hamiltonian as depicted by Fig. 1b

$$H = H_{\text{imp}} + \sum_{n\sigma} [\xi_n^{+} a_{n\sigma}^{\dagger} a_{n\sigma} + \xi_n^{-} b_{n\sigma}^{\dagger} b_{n\sigma}] + \frac{1}{\sqrt{\pi}} \sum_{\sigma} f_{\sigma}^{\dagger} \sum_n (\gamma_n^{+} a_{n\sigma} + \gamma_n^{-} b_{n\sigma}) + \frac{1}{\sqrt{\pi}} \sum_{\sigma} \left[\sum_n (\gamma_n^{+} a_{n\sigma}^{\dagger} + \gamma_n^{-} b_{n\sigma}^{\dagger}) \right] f_{\sigma}. \quad (20)$$

Before we continue with the mapping of the Hamiltonian Eq. (20) onto a semi-infinite chain, Fig. 1c, let us make a few remarks on alternative discretizations of the continuous bath spectral function.

The above procedure obviously applies for general asymmetric $\Delta(\omega)$, also for different upper and lower cut-offs, D_u and D_l . A special case is $D_l = 0$, which occurs for a bosonic bath, see Bulla *et al.* (2005); here the logarithmic discretization is performed for positive frequencies only, and the operators $b_{n\sigma}^{(\dagger)}$ in Eq. (20) are no longer present.

In Sec. III we shall discuss that the discreteness of the model Eq. (20) can be (in some cases) problematic for the calculation of physical quantities. As it is not possible in the actual calculations to recover the continuum by taking the limit $\Lambda \rightarrow 1$ (or by including the $p \neq 0$ terms), it has been suggested to average over various discretizations for fixed Λ (Frota and Oliveira, 1986; Oliveira and Oliveira, 1994; Yoshida *et al.*, 1990). The discretization points are then modified as

$$x_n = \begin{cases} 1 & : n = 0 \\ \Lambda^{-(n+Z)} & : n \geq 1, \end{cases} \quad (21)$$

where Z covers the interval $[0, 1)$. This ‘ Z -trick’ is, indeed, successful as it removes certain artificial oscillations (see Sec. III.A.4), but it should be stressed here that the continuum limit introduced by integrating over Z is not the same as the true continuum limit $\Lambda \rightarrow 1$.

Another shortcoming of the discretized model is that the hybridization function $\Delta(\omega)$ is systematically underestimated. It is therefore convenient to multiply $\Delta(\omega)$ with the correction factor

$$A_\Lambda = \frac{1}{2} \ln \Lambda \frac{\Lambda + 1}{\Lambda - 1}, \quad (22)$$

which accelerates the convergence to the continuum limit. For a recent derivation of this correction factor see Campo, Jr. and Oliveira (2005), where it was also shown that by a suitable modification of the discretization procedure, the factor A_Λ can be taken into account from the outset.

C. Mapping on a semi-infinite chain

According to Fig. 1b and c, the next step is to transform the discretized Hamiltonian Eq. (20) into a semi-infinite chain form with the first site of the chain (filled circle in Fig. 1c) representing the impurity degrees of freedom. In the chain Hamiltonian, the impurity directly couples only to one conduction electron degree of freedom with operators $c_{0\sigma}^{(\dagger)}$, the form of which can be directly read off from the second and third line in Eq. (20). With the definition

$$c_{0\sigma} = \frac{1}{\sqrt{\xi_0}} \sum_n [\gamma_n^+ a_{n\sigma} + \gamma_n^- b_{n\sigma}], \quad (23)$$

in which the normalization constant is given by

$$\xi_0 = \sum_n ((\gamma_n^+)^2 + (\gamma_n^-)^2) = \int_{-1}^1 d\varepsilon \Delta(\varepsilon), \quad (24)$$

the hybridization term can be written as

$$\frac{1}{\sqrt{\pi}} f_\sigma^\dagger \sum_n (\gamma_n^+ a_{n\sigma} + \gamma_n^- b_{n\sigma}) = \sqrt{\frac{\xi_0}{\pi}} f_\sigma^\dagger c_{0\sigma}, \quad (25)$$

(similarly for the hermitian conjugate term). Note that for a k -independent hybridization, $V_k = V$ in Eq. (2), the coupling in Eq. (25) reduces to $\sqrt{\xi_0/\pi} = V$.

The operators $c_{0\sigma}^{(\dagger)}$ represent the first site of the conduction electron part of the semi-infinite chain. These operators are of course not orthogonal to the operators $a_{n\sigma}^{(\dagger)}$, $b_{n\sigma}^{(\dagger)}$. Constructing a new set of mutually orthogonal operators $c_{n\sigma}^{(\dagger)}$ from $c_{0\sigma}^{(\dagger)}$ and $a_{n\sigma}^{(\dagger)}$, $b_{n\sigma}^{(\dagger)}$ by a standard Gram-Schmidt procedure leads to the desired chain Hamiltonian, which takes the form

$$H = H_{\text{imp}} + \sqrt{\frac{\xi_0}{\pi}} \sum_\sigma \left[f_\sigma^\dagger c_{0\sigma} + c_{0\sigma}^\dagger f_\sigma \right] + \sum_{\sigma n=0}^\infty \left[\varepsilon_n c_{n\sigma}^\dagger c_{n\sigma} + t_n \left(c_{n\sigma}^\dagger c_{n+1\sigma} + c_{n+1\sigma}^\dagger c_{n\sigma} \right) \right], \quad (26)$$

with the operators $c_{n\sigma}^{(\dagger)}$ corresponding to the n th site of the conduction electron part of the chain. The parameters of the chain are the on-site energies ε_n and the hopping matrix elements t_n . The operators $c_{n\sigma}^{(\dagger)}$ in Eq. (26) and the operators $\{a_{n\sigma}^{(\dagger)}, b_{n\sigma}^{(\dagger)}\}$ in Eq. (20) are related via an orthogonal transformation

$$a_{n\sigma} = \sum_{m=0}^\infty u_{mn} c_{m\sigma}, \quad b_{n\sigma} = \sum_{m=0}^\infty v_{mn} c_{m\sigma}, \quad c_{n\sigma} = \sum_{m=0}^\infty [u_{nm} a_{m\sigma} + v_{nm} b_{m\sigma}]. \quad (27)$$

From the definition of $c_{0\sigma}$ in Eq. (23) we can read off the coefficients u_{0m} and v_{0m}

$$u_{0m} = \frac{\gamma_m^+}{\sqrt{\xi_0}}, \quad v_{0m} = \frac{\gamma_m^-}{\sqrt{\xi_0}}. \quad (28)$$

For the remaining coefficients u_{nm} , v_{nm} , as well as for the parameters ε_n , t_n , one can derive recursion relations following the scheme described in detail in, for example, Appendix A of Bulla *et al.* (2005). The starting point here is the equivalence of the free conduction electron parts

$$\sum_{n\sigma} [\xi_n^+ a_{n\sigma}^\dagger a_{n\sigma} + \xi_n^- b_{n\sigma}^\dagger b_{n\sigma}] = \sum_{\sigma n=0}^\infty \left[\varepsilon_n c_{n\sigma}^\dagger c_{n\sigma} + t_n \left(c_{n\sigma}^\dagger c_{n+1\sigma} + c_{n+1\sigma}^\dagger c_{n\sigma} \right) \right]. \quad (29)$$

The recursion relations are initialized by the equations

$$\begin{aligned} \varepsilon_0 &= \frac{1}{\xi_0} \int_{-1}^1 d\varepsilon \Delta(\varepsilon) \varepsilon, \\ t_0^2 &= \frac{1}{\xi_0} \sum_m [(\xi_m^+ - \varepsilon_0)^2 (\gamma_m^+)^2 + (\xi_m^- - \varepsilon_0)^2 (\gamma_m^-)^2], \\ u_{1m} &= \frac{1}{t_0} (\xi_m^+ - \varepsilon_0) u_{0m}, \\ v_{1m} &= \frac{1}{t_0} (\xi_m^- - \varepsilon_0) v_{0m}. \end{aligned} \quad (30)$$

For $n \geq 1$, the recursion relations read

$$\begin{aligned}\varepsilon_n &= \sum_m (\xi_m^+ u_{nm}^2 + \xi_m^- v_{nm}^2) , \\ t_n^2 &= \sum_m [(\xi_m^+)^2 u_{nm}^2 + (\xi_m^-)^2 v_{nm}^2] - t_{n-1}^2 - \varepsilon_n^2 , \\ u_{n+1,m} &= \frac{1}{t_n} [(\xi_m^+ - \varepsilon_n) u_{nm} - t_{n-1} u_{n-1,m}] , \\ v_{n+1,m} &= \frac{1}{t_n} [(\xi_m^- - \varepsilon_n) v_{nm} - t_{n-1} v_{n-1,m}] .\end{aligned}\quad (31)$$

Note that for a particle-hole symmetric hybridization function, $\Delta(\omega) = \Delta(-\omega)$, the on-site energies ε_n are zero for all n .

For a general hybridization function, the recursion relations have to be solved numerically. Although these relations are fairly easy to implement, it turns out that the iterative solution breaks down typically after about 20-30 steps. The source of this instability is the wide range of values for the parameters entering the recursion relations (for instance for the discretized energies ξ_m^\pm). In most cases this problem can be overcome by using arbitrary precision routines for the numerical calculations. Furthermore, it is helpful to enforce the normalization of the vectors u_{nm} and v_{nm} after each step.

Analytical solutions for the recursion relations have so far been given only for few special cases. Wilson derived a formula for the t_n for a constant density of states of the conduction electrons in the Kondo version of the impurity model (Wilson, 1975a); this corresponds to a constant hybridization function $\Delta(\omega)$ in the interval $[-1, 1]$. Here we have $\varepsilon_n = 0$ for all n and the expression for the t_n reads

$$t_n = \frac{(1 + \Lambda^{-1})(1 - \Lambda^{-n-1})}{2\sqrt{1 - \Lambda^{-2n-1}}\sqrt{1 - \Lambda^{-2n-3}}} \Lambda^{-n/2} .\quad (32)$$

(Similar expressions have been given for the soft-gap model, see Bulla *et al.* (1997b).) In the limit of large n this reduces to

$$t_n \longrightarrow \frac{1}{2} (1 + \Lambda^{-1}) \Lambda^{-n/2} .\quad (33)$$

The fact that the t_n fall off exponentially with the distance from the impurity is essential for the following discussion, so let us briefly explain where this n -dependence comes from. Consider the discretized model Eq. (20) with a finite number $1 + M/2$ (M even) of conduction electron states for both positive and negative energies (the sum over n then goes from 0 to $M/2$). This corresponds to $2 + M$ degrees of freedom which result in $2 + M$ sites of the conduction electron part of the chain after the mapping to the chain Hamiltonian. The lowest energies in the discretized model Eq. (20) are the energies $\xi_{M/2}^\pm$ which, for a constant hybridization function, are given by $\xi_{M/2}^\pm = \pm \frac{1}{2} \Lambda^{-M/2} (1 + \Lambda^{-1})$, see Eq. (18). This energy shows up in the chain Hamiltonian as the last hopping matrix element t_M , so we have $t_M \sim \xi_{M/2}$ equivalent to Eq. (33).

Equation (26) is a specific one-dimensional representation of the single-impurity Anderson model Eq. (2) with the special feature that the hopping matrix elements t_n fall off exponentially. As mentioned above, this representation is not exact since in the course of its derivation, the $p \neq 0$ terms have been dropped. We should stress here that the dimensionality of the chain Hamiltonian is not related to that of the original model which describes, for example, an impurity in a three-dimensional host (apparently, this only holds for a non-interacting conduction band). Nevertheless, the conduction electron sites of the chain do have a physical meaning in the original model as they can be viewed as a sequence of shells centered around the impurity. The first site of the conduction electron chain corresponds to the shell with the maximum of its wavefunction closest to the impurity (Hewson, 1993; Wilson, 1975a); this shell is coupled to a shell further away from the impurity and so on.

D. Iterative diagonalization

The transformations described so far are necessary to map the problem onto a form (the semi-infinite chain, Eq. (26)) for which an iterative renormalization group (RG) procedure can be defined. This is the point at which, finally, the RG character of the approach enters.

The chain Hamiltonian Eq. (26) can be viewed as a series of Hamiltonians H_N ($N = 0, 1, 2, \dots$) which approaches H in the limit $N \rightarrow \infty$.

$$H = \lim_{N \rightarrow \infty} \Lambda^{-(N-1)/2} H_N ,\quad (34)$$

with

$$\begin{aligned}H_N &= \Lambda^{(N-1)/2} \left[H_{\text{imp}} + \sqrt{\frac{\xi_0}{\pi}} \sum_{\sigma} \left(f_{\sigma}^{\dagger} c_{0\sigma} + c_{0\sigma}^{\dagger} f_{\sigma} \right) \right. \\ &+ \left. \sum_{\sigma n=0}^N \varepsilon_n c_{n\sigma}^{\dagger} c_{n\sigma} + \sum_{\sigma n=0}^{N-1} t_n \left(c_{n\sigma}^{\dagger} c_{n+1\sigma} + c_{n+1\sigma}^{\dagger} c_{n\sigma} \right) \right] .\end{aligned}\quad (35)$$

The factor $\Lambda^{(N-1)/2}$ in Eq. (35) (and, consequently, the factor $\Lambda^{-(N-1)/2}$ in Eq. (34)) has been chosen to cancel the N -dependence of t_{N-1} , the hopping matrix element between the last two sites of H_N . Such a scaling is useful for the discussion of fixed points, as described below. For a different n -dependence of t_n , as for the spin-boson model (Bulla *et al.*, 2005), the scaling factor has to be changed accordingly. (The n -dependence of ε_n is, in most cases, irrelevant for the overall scaling of the many-particle spectra.)

Two successive Hamiltonians are related by

$$\begin{aligned}H_{N+1} &= \sqrt{\Lambda} H_N + \Lambda^{N/2} \sum_{\sigma} \varepsilon_{N+1} c_{N+1\sigma}^{\dagger} c_{N+1\sigma} \\ &+ \Lambda^{N/2} \sum_{\sigma} t_N \left(c_{N\sigma}^{\dagger} c_{N+1\sigma} + c_{N+1\sigma}^{\dagger} c_{N\sigma} \right) ,\end{aligned}\quad (36)$$

and the starting point of the sequence of Hamiltonians is given by

$$H_0 = \Lambda^{-1/2} \left[H_{\text{imp}} + \sum_{\sigma} \varepsilon_0 c_{0\sigma}^{\dagger} c_{0\sigma} + \sqrt{\frac{\xi_0}{\pi}} \sum_{\sigma} \left(f_{\sigma}^{\dagger} c_{0\sigma} + c_{0\sigma}^{\dagger} f_{\sigma} \right) \right]. \quad (37)$$

This Hamiltonian corresponds to a two-site cluster formed by the impurity and the first conduction electron site. Note that in the special case of the single-impurity Anderson model, one can also choose $H_{-1} = \Lambda^{-1} H_{\text{imp}}$ as the starting point (with a proper renaming of parameters and operators) since the hybridization term has the same structure as the hopping term between the conduction electron sites.

The recursion relation Eq. (36) can now be understood in terms of a renormalization group transformation R :

$$H_{N+1} = R(H_N). \quad (38)$$

In a standard RG transformation, the Hamiltonians are specified by a set of parameters \vec{K} and the mapping R transforms the Hamiltonian $H(\vec{K})$ into another Hamiltonian of the same form, $H(\vec{K}')$, with a new set of parameters \vec{K}' . Such a representation does not exist, in general, for the H_N which are obtained in the course of the iterative diagonalization to be described below. Instead, we characterize H_N , and thereby also the RG flow, directly by the many-particle energies $E_N(r)$

$$H_N |r\rangle_N = E_N(r) |r\rangle_N, \quad r = 1, \dots, N_s, \quad (39)$$

with the eigenstates $|r\rangle_N$ and N_s the dimension of H_N . This is particularly useful in the crossover regime between different fixed points, where a description in terms of an effective Hamiltonian with certain renormalized parameters is not possible. Only in the vicinity of the fixed points (except for certain quantum critical points) one can go back to an effective Hamiltonian description, as described below.

Our primary aim now is to set up an iterative scheme for the diagonalization of H_N , in order to discuss the flow of the many-particle energies $E_N(r)$. Let us assume that, for a given N , the Hamiltonian H_N has already been diagonalized, as in Eq. (39). We now construct a basis for H_{N+1} , as sketched in Fig. 2:

$$|r; s\rangle_{N+1} = |r\rangle_N \otimes |s(N+1)\rangle. \quad (40)$$

The states $|r; s\rangle_{N+1}$ are product states consisting of the eigenbasis of H_N and a suitable basis $|s(N+1)\rangle$ for the added site (the new degree of freedom). From the basis Eq. (40) we construct the Hamiltonian matrix for H_{N+1} :

$$H_{N+1}(rs, r's') = {}_{N+1}\langle r; s | H_{N+1} | r'; s' \rangle_{N+1}. \quad (41)$$

For the calculation of these matrix elements it is useful to decompose H_{N+1} into three parts

$$H_{N+1} = \sqrt{\Lambda} H_N + \hat{X}_{N,N+1} + \hat{Y}_{N+1}, \quad (42)$$

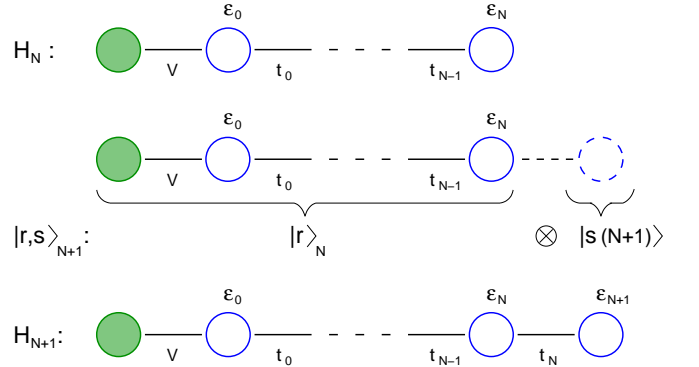


FIG. 2 In each step of the iterative diagonalization scheme one site of the chain (with operators $c_{N+1}^{(\dagger)}$ and on-site energy ε_{N+1}) is added to the Hamiltonian H_N . A basis $|r; s\rangle_{N+1}$ for the resulting Hamiltonian, H_{N+1} , is formed by the eigenstates of H_N , $|r\rangle_N$, and a basis of the added site, $|s(N+1)\rangle$.

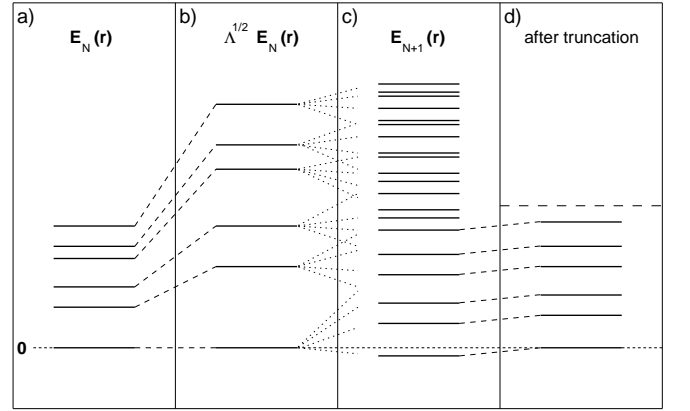


FIG. 3 (a): Many-particle spectrum $E_N(r)$ of the Hamiltonian H_N with the ground-state energy set to zero. (b): The relation between successive Hamiltonians, Eq. (36), includes a scaling factor $\sqrt{\Lambda}$. (c) Many-particle spectrum $E_{N+1}(r)$ of H_{N+1} , calculated by diagonalizing the Hamiltonian matrix Eq. (41). (d) The same spectrum after truncation where only the N_s lowest-lying states are retained; the ground-state energy has again been set to zero.

(see, for example, Eq. (36)) where the operator \hat{Y}_{N+1} only contains the degrees of freedom of the added site, while $\hat{X}_{N,N+1}$ mixes these with the ones contained in H_N . Apparently, the structure of the operators \hat{X} and \hat{Y} , as well as the equations for the calculation of their matrix elements, depend on the model under consideration.

The following steps are illustrated in Fig. 3: In Fig. 3a we show the many-particle spectrum of H_N , that is the sequence of many-particle energies $E_N(r)$. Note that, for convenience, the ground-state energy has been set to zero. Figure 3b shows the overall scaling of the energies by the factor $\sqrt{\Lambda}$, see the first term in Eq. (36).

Diagonalization of the matrix Eq. (41) gives the new eigenenergies $E_{N+1}(w)$ and eigenstates $|w\rangle_{N+1}$ which are

related to the basis $|r; s\rangle_{N+1}$ via the unitary matrix U :

$$|w\rangle_{N+1} = \sum_{rs} U(w, rs) |r; s\rangle_{N+1} . \quad (43)$$

The set of eigenenergies $E_{N+1}(w)$ of H_{N+1} is displayed in Fig. 3c (the label w can now be replaced by r). Apparently, the number of states increases by adding the new degree of freedom (when no symmetries are taken into account, the factor is just the dimension of the basis $|s(N+1)\rangle$). The ground-state energy is negative, but will be set to zero in the following step.

The increasing number of states is, of course, a problem for the numerical diagonalization; the dimension of H_{N+1} grows exponentially with N , even when we consider symmetries of the model so that the full matrix takes a block-diagonal form with smaller submatrices. This problem can be solved by a very simple truncation scheme: after diagonalization of the various submatrices of H_{N+1} one only keeps the N_s eigenstates with the lowest many-particle energies. In this way, the dimension of the Hilbert space is fixed to N_s and the computation time increases linearly with the length of the chain. Suitable values for the parameter N_s depend on the model; for the single-impurity Anderson model, N_s of the order of a few hundred is sufficient to get converged results for the many-particle spectra, but the accurate calculation of static and dynamic quantities usually requires larger values of N_s . The truncation of the high energy states is illustrated in Fig. 3d.

Such an ad-hoc truncation scheme needs further explanations. First of all, there is no guarantee that this scheme will work in practical applications and its quality should be checked for each individual application. Important here is the observation that the neglect of the high-energy states does not spoil the low-energy spectrum in subsequent iterations – this can be easily seen numerically by varying N_s . The influence of the high-energy on the low-energy states is small since the addition of a new site to the chain can be viewed as a perturbation of relative strength $\Lambda^{-1/2} < 1$. This perturbation is small for large values of Λ but for $\Lambda \rightarrow 1$ it is obvious that one has to keep more and more states to get reliable results. This also means that the accuracy of the NRG results is getting worse when N_s is kept fixed and Λ is reduced (vice versa, it is sometimes possible to improve the accuracy by *increasing* Λ for fixed N_s).

From this discussion we see that the success of the truncation scheme is intimately connected to the special structure of the chain Hamiltonian (that is $t_n \propto \Lambda^{-n/2}$) which in turn is due to the logarithmic discretization of the original model. A direct transformation of the single-impurity Anderson model to a one-dimensional chain results in $t_n \rightarrow \text{const}$ (Hewson, 1993), and the above truncation scheme fails. A similar observation is made when such a truncation is applied to the one-dimensional Hubbard model, see the brief discussion in Sec. V.

Let us now be a bit more specific on how to construct the basis $|r; s\rangle_{N+1}$. For this we have to decide, first of

all, which of the symmetries of the Hamiltonian should be used in the iterative diagonalization. In the original calculations of Wilson (1975a) and Krishna-murthy *et al.* (1980a,b) the following quantum numbers were used: total charge Q (particle number with respect to half-filling), total spin S and z -component of the total spin S_z . It has certainly been essential in the 1970's to reduce the size of the matrices and hence the computation time as much as possible by invoking as many symmetries as possible. This is no longer necessary to such an extent on the modern computer systems, i.e. one can, at least for single-band models, drop the total spin S and classify the subspaces with the quantum numbers (Q, S_z) only. This simplifies the program considerably as one no longer has to worry about reduced matrix elements and the corresponding Clebsch-Gordan coefficients, see, for example Krishna-murthy *et al.* (1980a). As we use this representation in Sec. III.A, let us here explicitly state the form of $|r; s\rangle_{N+1}$:

$$\begin{aligned} |Q, S_z, r; 1\rangle_{N+1} &= |Q+1, S_z, r\rangle_N , \\ |Q, S_z, r; 2\rangle_{N+1} &= c_{N+1\uparrow}^\dagger |Q, S_z - \frac{1}{2}, r\rangle_N , \\ |Q, S_z, r; 3\rangle_{N+1} &= c_{N+1\downarrow}^\dagger |Q, S_z + \frac{1}{2}, r\rangle_N , \\ |Q, S_z, r; 4\rangle_{N+1} &= c_{N+1\uparrow}^\dagger c_{N+1\downarrow}^\dagger |Q-1, S_z, r\rangle_N . \end{aligned} \quad (44)$$

Note that the quantum numbers (Q, S_z) on both sides of these equations refer to different systems, on the left-hand side they are for the system including the added site, and on the right-hand side without the added site. We do not go into the details of how to set up the Hamiltonian matrices Eq. (41), as this procedure is described in great detail in Appendix B in Krishna-murthy *et al.* (1980a).

For fermionic baths, the discretization parameter Λ and the number of states N_s kept in each iteration are the only parameters which govern the quality of the results of the NRG procedure. As discussed in more detail in Sec. IV.E, for the case of a bosonic bath the infinite dimensional basis $|s(N+1)\rangle$ for the added bosonic site requires an additional parameter N_b , which determines the dimension of $|s(N+1)\rangle$.

E. Renormalization group flow

The result of the iterative diagonalization scheme are the many-particle energies $E_N(r)$ with $r = 1, \dots, N_s$ (apparently, the number of states is less than N_s for the very first steps before the truncation sets in). The index N goes from 0 to a maximum number of iterations, N_{max} , which usually has to be chosen such that the system has approached its low-temperature fixed point.

As illustrated in Fig. 3, the set of many-particle energies cover roughly the same energy range independent of N , due to the scaling factor $\Lambda^{(N-1)/2}$ in Eq. (35). The energy of the first excited state of H_N is of the order of $\Lambda^{(N-1)/2} t_{N-1}$, a constant according to Eq. (33). The energy of the highest excited state kept after truncation

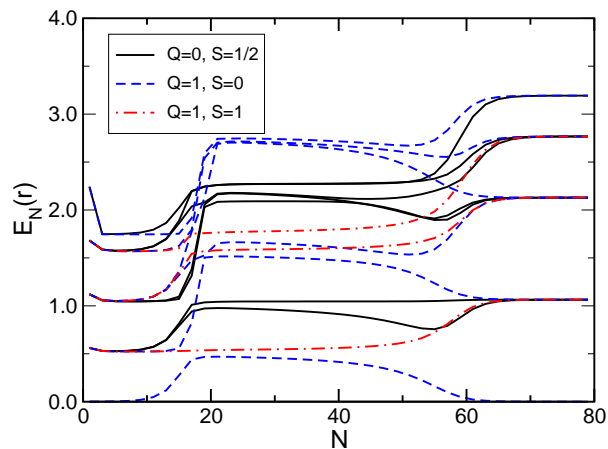


FIG. 4 Flow of the lowest-lying many-particle energies of the single-impurity Anderson model for parameters $\varepsilon_f = -0.5 \cdot 10^{-3}$, $U = 10^{-3}$, $V = 0.004$, and $\Lambda = 2.5$. The states are labeled by the quantum numbers total charge Q and total spin S . See the text for a discussion of the fixed points visible in this plot.

depends on N_s – for typical parameters this energy is approximately 5-10 times larger as the lowest energy.

Multiplied with the scaling factor $\Lambda^{-(N-1)/2}$, see Eq. (34), the energies $E_N(r)$ are an approximation to the many-particle spectrum of the chain Hamiltonian Eq. (26) within an energy window decreasing exponentially with increasing N . Note, that the energies for higher lying excitations obtained for early iterations are not altered in later iteration steps due to the truncation procedure. Nevertheless one can view the resulting set of many-particle energies and states from all NRG iterations N as approximation to the spectrum of the full Hamiltonian and use them to calculate physical properties in the whole energy range, see Sec. III.

Here we want to focus directly on the many-particle energies $E_N(r)$ and show how one can extract information about the physics of a given model by analyzing their flow, that is the dependence of $E_N(r)$ on N .

As a typical example for such an analysis, we show in Fig. 4 the flow of the many-particle energies for the symmetric single-impurity Anderson model, with parameters $\varepsilon_f = -0.5 \cdot 10^{-3}$, $U = 10^{-3}$, $V = 0.004$, and $\Lambda = 2.5$ (the same parameters as used in Fig. 5 in Krishna-murthy *et al.* (1980a); note that we show here a slightly different selection of the lowest-lying states). The energies are plotted for odd N only, that is an odd total number of sites (which is $N + 2$). This is necessary, because the many-particle spectra show the usual even-odd oscillations of a fermionic finite-size system (the patterns for even N look different but contain, of course, the same physics). The data points are connected by lines to visualize the flow. As in Krishna-murthy *et al.* (1980a), the many-particle energies are labeled by total charge Q and total spin S .

What is the information one can extract from such a flow diagram? First of all we note the appearance of

three different fixed points of the RG transformation for early iteration numbers $N < 10$, for intermediate values of N and for $N > 60$ (strictly speaking, because we look at N odd only, these are fixed points of R^2 , not of R). The physics of these fixed points cannot be extracted by just looking at the pattern of the many-particle energies. This needs some further analysis, in particular the direct diagonalization of fixed point Hamiltonians (which usually have a simple structure) and the comparison of their spectrum with the numerical data. An excellent account of this procedure for the symmetric and asymmetric single-impurity Anderson model has been given by Krishna-murthy *et al.* (1980a,b), and there is no need to repeat this discussion here. The analysis shows that for $N \approx 3 - 9$, the system is very close to the free-orbital fixed point, with the fixed point Hamiltonian given by Eq. (26) for $U = 0$ and $V = 0$. This fixed point is unstable and for $N \approx 11 - 17$, we observe a rapid crossover to the local-moment fixed point. This fixed point is characterized by a free spin decoupled from the conduction band. The local-moment fixed point is unstable as well and after a characteristic crossover (see the discussion below) the system approaches the stable strong-coupling fixed point of a screened spin. Note that the terminology ‘strong-coupling’ has been introduced originally because the fixed point Hamiltonian can be obtained from the limit $V \rightarrow \infty$, so ‘coupling’ here refers to the hybridization, not the Coulomb parameter U .

The NRG does not only allow to match the structure of the numerically calculated fixed points with those of certain fixed point Hamiltonians. One can in addition identify the deviations from the fixed points (and thereby part of the crossover) with appropriate perturbations of the fixed point Hamiltonians. Again, we refer the reader to Krishna-murthy *et al.* (1980a,b) for a detailed description of this analysis. The first step is to identify the leading perturbations around the fixed points. The leading operators can be determined by expressing them in terms of the operators which diagonalize the fixed point Hamiltonian; this tells us directly how these operators transform under the RG mapping R^2 . One then proceeds with the usual classification into relevant, marginal, and irrelevant perturbations. The final results of this analysis perfectly agree with the flow diagram of Fig. 4: There is a relevant perturbation which drives the system away from the free-orbital fixed point, but for the local-moment fixed point there is only a marginally relevant perturbation, therefore the system only moves very slowly away from this fixed point. Note that this marginal perturbation – which is the exchange interaction between the local moment and the spin of the first conduction electron site – gives rise to the logarithms observed in various physical quantities. Finally, there are only irrelevant operators which govern the flow to the strong-coupling fixed point. These are responsible for the Fermi-liquid properties at very low temperatures (Hewson, 1993).

Having identified the leading operators for each fixed point, it is possible to calculate physical properties

close to the fixed points perturbatively. We do not want to go into the calculational details here, see Krishna-murthy *et al.* (1980a) and also Sec. 4 in Hewson (1993). Recently, Hewson *et al.* (2004) and Hewson (2005) developed an alternative approach based on the renormalized perturbation theory. This approach is much easier to implement, has been used to describe the physics close to the strong-coupling fixed point and is, in principle, applicable also on all energy scales and for non-equilibrium (Hewson *et al.*, 2005).

Flow diagrams as in Fig. 4 also give information about the relevant energy scales for the crossover between the fixed points. For example, an estimate of the Kondo temperature T_K (the temperature scale which characterizes the flow to the strong-coupling fixed point) is given by $T_K \approx \omega_c \Lambda^{-\bar{N}/2}$, with $\bar{N} \approx 55$ for the parameters in Fig. 4.

The discussion of flow-diagrams as in Fig. 4 concludes our introduction to the basics of the NRG approach. An important part is still missing, of course, that is the calculation of physical quantities from the flow of the many-particle energies (and from certain additional matrix elements). This is the topic of the following section.

In Sec. IV we will come back to the discussion of flow diagrams and the structure of fixed points when studying various other quantum impurity systems, in particular the two-channel Kondo model which displays a non-Fermi liquid fixed point, see Sec. IV.B, and the soft-gap Anderson model which has a quantum critical point separating the strong-coupling and local-moment phase, see Sec. IV.C.2.

III. CALCULATION OF PHYSICAL PROPERTIES

In the previous section II we discussed the information that can be gained from the the low-lying energy levels during the RG flow. Apparently, a lot can already be learned on this level about the physical properties of the system. However, an obvious aim of any method is also to calculate thermodynamic quantities like specific heat, susceptibilities or even dynamical properties.

Let us start by reminding the reader that the coefficients t_n appearing in the transformed Hamiltonian Eq. (26) decay like $\Lambda^{-n/2}$ for large n . This aspect can be used in the following way (Krishna-murthy *et al.*, 1980a; Oliveira and Oliveira, 1994; Wilson, 1975a): Diagonalizing the Hamiltonian (35) for a given chain length N yields a set of eigenvalues $\eta_l^{(N)} \propto \pm \Lambda^l$. Obviously, eigenvalues $\Lambda^{-(N-1)/2} \eta_l^{(N)} \gg k_B T, \omega$ will not contribute significantly to the calculation of physical properties anyway. On the other hand, for those l where $\Lambda^{-(N-1)/2} \eta_l^{(N)} \ll k_B T, \omega$ one can safely approximate $\eta_l^{(N)} \approx 0$, which means that *for the calculation of impurity properties* these contributions will drop out. With $\beta = (k_B T)^{-1}$,

$$\beta \Lambda^{-(N-1)/2} =: \bar{\beta} \quad (45)$$

and $\bar{\beta}$ chosen properly, it will thus be sufficient to use

H_N instead of the full Hamiltonian (26).

Provided we can keep enough states in the truncation scheme introduced in Sec. II to ensure convergence of the partition function on the scale $k_B T$, it is thus permissible to use the truncated Hamiltonian on the level N obtained from the iterative diagonalization to calculate physical properties *for the impurity* on the temperature or energy scale $\Lambda^{-(N-1)/2}/\bar{\beta}$.

A. Thermodynamic and static properties

1. Entropy, specific heat and susceptibility

The simplest physical quantities related to the impurity degrees of freedom are the impurity contribution to the entropy, S_{imp} , specific heat, C_{imp} , and magnetic susceptibility, χ_{imp} .

The entropy and specific heat are the first derivative of the free energy $F = -k_B T \ln Z$ and internal energy $U = \langle H \rangle$ with respect to temperature, i.e.

$$S = - \frac{\partial F}{\partial T} ,$$

and

$$C = \frac{\partial U}{\partial T} .$$

From a numerical point of view, performing differentiations is something to avoid if possible. For the numerical implementation of the NRG another complication arises. To avoid an exponential increase of energies, it is necessary to subtract the ground state energy at each NRG-level N , i.e. one would have to keep track of these subtractions. Apparently, a much more convenient approach is to evaluate the derivative analytically, yielding

$$S/k_B = \beta \langle H \rangle + \ln Z ,$$

for the entropy and

$$C/k_B = \beta^2 [\langle H^2 \rangle - \langle H \rangle^2] ,$$

for the specific heat.

The prescription to calculate the impurity contribution to the magnetic susceptibility requires some more thought. The standard definition for the magnetic susceptibility is (we set $g\mu_B = 1$)

$$\chi(T) = \int_0^\beta \langle S_z[\tau] S_z \rangle d\tau - \beta \langle S_z \rangle^2 , \quad (46)$$

with

$$\langle S_z[\tau] S_z \rangle = \frac{1}{Z} \text{Tr} [e^{-\beta H} e^{\tau H} S_z e^{-\tau H} S_z] .$$

However, the evaluation of the latter expectation value is equivalent to the calculation of a *dynamical* correlation function. This is in general a much more complex

task and will be discussed in detail in the next section. Here, we employ a different approach, which in turn is also closer related to the experimental definition of this quantity.

In general, experiments address the susceptibility of the whole system. Since the total spin commutes with the Hamiltonian, the expression (46) simplifies to

$$\chi_{\text{tot}}(T) = \beta [\langle S_{\text{tot},z}^2 \rangle - \langle S_{\text{tot},z} \rangle^2] ,$$

in this case. From this, one subtracts the susceptibility of a reference system, i.e. without impurity, leading to Wilson's definition (Wilson, 1975a) of the impurity contribution to the susceptibility

$$\chi_{\text{imp}}(T) = \chi_{\text{tot}}(T) - \chi_{\text{tot}}^{(0)}(T) . \quad (47)$$

Since $S_{\text{tot},z}$ is a quantum number used to classify the states in the calculation, the expectation values in (47) can be evaluated straightforwardly.

Similarly, the impurity contributions to the entropy and specific heat can be calculated as

$$S_{\text{imp}}(T) = S_{\text{tot}}(T) - S_{\text{tot}}^{(0)}(T) , \quad (48)$$

and

$$C_{\text{imp}}(T) = C_{\text{tot}}(T) - C_{\text{tot}}^{(0)}(T) , \quad (49)$$

where $S_{\text{tot}}^{(0)}(T)$ and $C_{\text{tot}}^{(0)}(T)$ are again entropy and specific heat of a suitable reference system.

Let us discuss the details of the actual calculation for the entropy as specific example. Following the introductory remarks, we can – for a given temperature $k_B T$ – restrict the Hilbert space to the NRG iteration L fulfilling (45). If we denote the corresponding Hamiltonian by $H^{(N)}$, we can introduce the quantity

$$S^{(N)}/k_B := \beta \langle H^{(N)} \rangle^{(L)} + \ln Z^{(N)} , \quad (50)$$

where, using the notation of Sec. II (see, for example, Eq. (40)),

$$\langle \dots \rangle^{(N)} := \frac{1}{Z^{(N)}} \sum_{Q, S_z} \sum_r e^{-\beta E_L(Q, S_z, r)} \times_N \langle Q, S_z, r | \dots | Q, S_z, r \rangle_N , \quad (51)$$

and

$$Z^{(N)} := \sum_{Q, S_z} \sum_r e^{-\beta E_N(Q, S_z, r)} . \quad (52)$$

The impurity contribution to the entropy for a temperature $k_B T_N := \Lambda^{-(N-1)/2}/\bar{\beta}$ can then be obtained as

$$S_{\text{imp}}(T_N)/k_B \approx S^{(N)}/k_B - S_{\text{cb}}^{(N)}/k_B . \quad (53)$$

Here we introduced the “free entropy”

$$S_{\text{cb}}^{(N)}/k_B := \beta \langle H_{\text{cb}}^{(N)} \rangle^{(N)} + \ln Z_{\text{cb}}^{(N)} , \quad (54)$$

obtained from the bare conduction Hamiltonian

$$H_{\text{cb}}^{(N)} = \sum_{\sigma n=0}^N \left[\epsilon_n c_{n\sigma}^\dagger c_{n\sigma} + t_n \left(c_{n\sigma}^\dagger c_{n+1\sigma} + c_{n+1\sigma}^\dagger c_{n\sigma} \right) \right] . \quad (55)$$

Similarly, for $k_B T_N = \Lambda^{-(N-1)/2}/\bar{\beta}$ the specific heat and magnetic susceptibility are obtained as

$$C_{\text{imp}}(T_N)/k_B \approx C_{\text{tot}}^{(N)} - C_{\text{cb}}^{(N)} , \quad (56)$$

and

$$\chi_{\text{imp}}(T_N) \approx \chi_{\text{tot}}^{(N)} - \chi_{\text{cb}}^{(N)} . \quad (57)$$

Since the Hamiltonian (55) is a non-interacting system, these quantities $S_{\text{cb}}^{(N)}$ etc. can be expressed via the eigenenergies $\eta_{l\sigma}$ of (55) in standard fashion.

For $T \rightarrow 0$ the behavior of $S_{\text{imp}}(T)$ and $\chi_{\text{imp}}(T)$ given by Eqs. (56) and (57) can be obtained analytically from the fixed point spectra. We refer the reader interested in this derivation to Wilson (1975a) and concentrate here on the actual numerical calculations.

Another aspect is that the fixed points and the flow to them are different for N even and odd. This in turn means, that one in principle has to calculate thermodynamic properties either for N even or odd only and thus lose half of the temperature values. One can, however, use all information by properly averaging odd and even steps:

- For a given N , calculate the quantities $O^{(N-1)}$, $O^{(N)}$ and $O^{(N+1)}$.
- Approximate $O(T_N)$ as

$$O(T_N) \approx \frac{1}{2} \left[O^{(N)} + O^{(N-1)} + \frac{O^{(N+1)} - O^{(N-1)}}{T_{N+1} - T_{N-1}} (T_N - T_{N-1}) \right] .$$

The first term in the square bracket is the observable calculated at step N . The second and third term are a linear interpolation of the values at $N-1$ and $N+1$ to iteration N .

- Continue with $N+1$.

As a positive side effect, this averaging also improves the accuracy of the thermodynamic quantities calculated.

At this point some remarks about potential numerical problems one can encounter should be made. The arguments given in the introduction to this section rely on the assumption, that one can keep states with high enough energy to ensure (i) the accuracy of the states at medium and low energies and (ii) the convergence of the partition function and expectation values. Depending on the actual quantity to be calculated, the latter

point can in principle lead to problems. As an example, consider $\langle H \rangle$ and $\langle H^2 \rangle$. While for a given energy cut-off E_{cut} the contribution $\bar{\beta} E_{\text{cut}} e^{-\bar{\beta} E_{\text{cut}}}$ to $\langle H \rangle$ can already be small enough to use the sum up to E_{cut} as approximation to $\langle H \rangle$, this must not be necessarily true for $\langle H^2 \rangle$. Thus, the resulting values for the specific heat, $\bar{\beta} [\langle H^2 \rangle - \langle H \rangle^2]$, can be rather poor although entropy and susceptibility come out much more accurate.

2. Other local properties

While entropy, specific heat and impurity susceptibility can be obtained directly from the spectra of the Hamiltonian, other local quantities require the calculation of the corresponding local matrix elements. As an example, we want to discuss here the local occupancy $n_\sigma = \langle f_\sigma^\dagger f_\sigma \rangle$ and double occupancy $D = \langle f_\uparrow^\dagger f_\uparrow f_\downarrow^\dagger f_\downarrow \rangle$ for the single-impurity Anderson model Eq. (2). Both quantities are of interest in actual applications. Expectation values of other local operators can be calculated in a similar manner.

As before, on a given temperature scale $k_B T_N = \Lambda^{-(N-1)/2} / \bar{\beta}$, we approximate the expectation values by

$$n_\sigma(T_L) \approx \frac{1}{Z^{(N)}} \sum_{Q, S_z} \sum_r e^{-\beta E_N(Q, S_z, r)} \times \quad (58)$$

$${}_N \langle Q, S_z, r | f_\sigma^\dagger f_\sigma | Q, S_z, r \rangle_N ,$$

for the occupancy and a corresponding expression for the double occupancy. The matrix elements

$$n_\sigma(Q, S_z, r, r'; N) := {}_N \langle Q, S_z, r | f_\sigma^\dagger f_\sigma | Q, S_z, r' \rangle_N , \quad (59)$$

at a given step N can be calculated from those of the previous step $N - 1$ with the help of the basis transformation (43) for the step N . The same scheme works for the matrix elements of the double occupancy $D(Q, S_z, w, w'; -1)$ and the matrix elements of general local operators – like f_σ^\dagger needed in the calculation of the single-particle Green function (see Sec. III.B).

All we are left to specify are the initial values for $n_\sigma(Q, S_z, w, w'; -1)$ and $D(Q, S_z, w, w'; -1)$ on the level of the impurity. For the Anderson model Eq. (2) they are explicitly given as

$$\begin{aligned} n_\sigma(0, 0, 0, 0; -1) &= 0 , \\ n_\sigma(1, \sigma, 0, 0; -1) &= 1 , \\ n_\sigma(2, 0, 0, 0; -1) &= 2 , \\ D(0, 0, 0, 0; -1) &= 0 , \\ D(1, \sigma, 0, 0; -1) &= 0 , \\ D(2, 0, 0, 0; -1) &= 1 . \end{aligned} \quad (60)$$

With these prerequisites we are now in the position to do actual calculations for the thermodynamic properties of quantum impurity models using NRG.

3. Example: The Kondo model

As example for the method let us present results for the Kondo model Eq. (128). Depending on the number of bands coupling to the local spin, one observes a conventional Kondo effect with the formation of a local Fermi liquid or a non-Fermi liquid fixed point with anomalous temperature dependencies of specific heat and susceptibility as well as a residual entropy $S(0) = \frac{1}{2} \ln 2$ at $T = 0$ (Cragg *et al.*, 1980; Nozières and Blandin, 1980) (this will be discussed in more detail in Secs. IV.A and IV.B). In Fig. 5 we show the entropy $S_{\text{imp}}(T)$, suscepti-

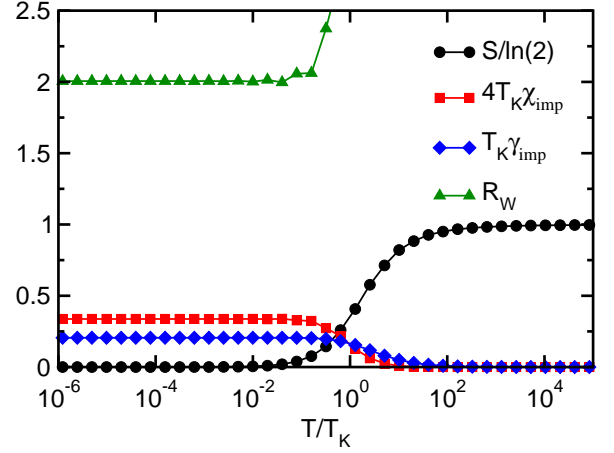


FIG. 5 Entropy $S_{\text{imp}}(T)$, susceptibility $\chi_{\text{imp}}(T)$, Sommerfeld coefficient $\gamma_{\text{imp}} = C_{\text{imp}}(T)/T$, and Wilson ratio R_W for the single-channel Kondo model. The Kondo temperature is defined by the Wilson relation $\chi_{\text{imp}}(0) = \frac{0.413}{4T_K}$.

bility $\chi_{\text{imp}}(T)$, Sommerfeld coefficient $\gamma_{\text{imp}} = C_{\text{imp}}(T)/T$ and Wilson ratio $R_W := 4\pi^2 \chi_{\text{imp}}(T) / (3\gamma_{\text{imp}}(T))$ as function of T/T_K for the single-channel Kondo model. As Kondo coupling we choose $J = 0.05D$, where D is the half-bandwidth of the conduction band, for which we assume a density of states $\rho_{\text{cb}}(\epsilon) = N_F \Theta(D - |\epsilon|)$. The value of T_K is obtained from Wilson's definition (Wilson, 1975a) $4T_K \chi_{\text{imp}}(0) = 0.413$. The calculations are performed with a discretization parameter $\Lambda = 4$, keeping 400 states at each NRG step. Although this value of Λ seems to be fairly large, experience tells that for static properties such large values of Λ are still permissible, considerably reducing the number of states one has to keep in the truncation procedure.

One nicely sees in Fig. 5 the quenching of the local moment by the Kondo effect for temperatures of the order of T_K . Also the high-temperature values for the entropy $S_{\text{imp}}(T \rightarrow \infty) = \ln 2$ and the Wilson ratio $R_W = 2$ (Wilson, 1975a) are obtained with high precision.

If one adds a second screening channel to the Kondo model, one arrives at the so-called two-channel Kondo model. The rather interesting physics of this model will be discussed in detail in Sec. IV.B. Here we merely want to demonstrate that NRG calculations for this model are

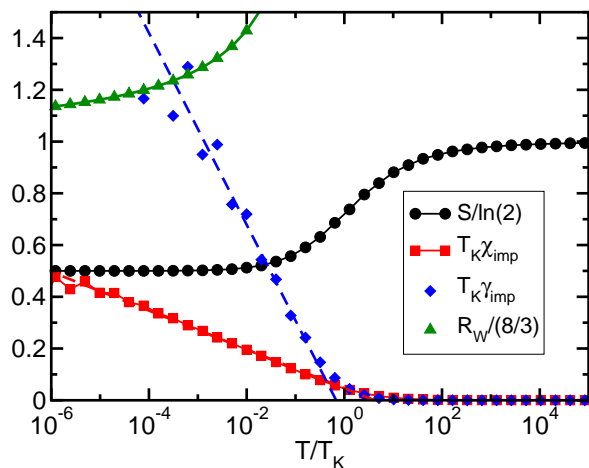


FIG. 6 Entropy $S_{\text{imp}}(T)$, susceptibility $\chi_{\text{imp}}(T)$, Sommerfeld coefficient $\gamma_{\text{imp}} = C_{\text{imp}}(T)/T$, and Wilson ratio R_W for the two-channel Kondo model. The value for the Kondo temperature is the same as in Fig. 5.

possible, too; however, the additional bath degrees of freedom, which lead to Hilbert spaces larger by a factor of four, make calculations more cumbersome and for some quantities also less accurate. In Fig. 6 we show as before the impurity contributions to the entropy, susceptibility and Sommerfeld coefficient as well as the Wilson ratio as function of T/T_K . The impurity parameters are the same as in Fig. 5; for the NRG we again choose $\Lambda = 4$ but keep 8100 states per iteration. The value of T_K is that of the corresponding single-channel model. As emphasized before, entropy and susceptibility come out quite accurately, in particular the residual entropy $S(0) = \frac{1}{2} \ln 2$ is obtained as well as the logarithmic increase of $\chi_{\text{imp}}(T) \propto \ln(T/T_K)$ for $T < T_K$ (Affleck *et al.*, 1992; Cragg *et al.*, 1980; Pang and Cox, 1991). The specific heat, however, is less accurate, but also shows the logarithmic increase as expected, although with strong oscillations superimposed. Fitting both quantities with a logarithmic form, one can recover the correct Wilson ratio $R_W = 8/3$ for $T \rightarrow 0$. Note, however, that the latter value is approached only logarithmically.

4. Improving the accuracy: The Z -averaging

For more complex quantum impurity models, like the two-channel Kondo model (discussed briefly in the previous section and in more detail in Sec. IV.B), or multi-orbital models, the Hilbert space per NRG step increases more strongly than for single-channel models. Consequently, the fraction of states kept in the truncation procedure has to be reduced. As has been pointed out by Oliveira and Oliveira (1994), this leads to an exponential decrease of accuracy, which can however be compensated by an increase of the discretization parameter Λ . However, the use of a large Λ , (i), takes one further away

from the continuum limit $\Lambda \rightarrow 1$ of interest, and, (ii), introduces oscillations into the thermodynamic expectation values. A way out of this dilemma, proposed by Oliveira and Oliveira (1994), is as follows:

- Instead of the discretization Eq. (6) choose

$$x_n = \Lambda^{-n+Z}, \quad n \geq 1, \quad Z \in [0, 1). \quad (61)$$

The mapping to a semi-infinite chain is done as before (see Sec. II.C) with the replacement $\Lambda^{-n} \rightarrow \Lambda^{-n+Z}$ for $n \geq 1$.

- For fixed $Z \in [0, 1)$ perform a NRG calculation for a fixed set of temperatures $T_L = \Lambda^{-(L-1)/2}/\bar{\beta}$ as before.
- Average over several calculations for different Z . This averaging is meant to reintroduce the continuum limit to some extent (Oliveira and Oliveira, 1994) and also can be shown to remove oscillations introduced by the use of a large $\Lambda \gg 1$.

Already for two different values of Z this procedure removes spurious oscillations in thermodynamic quantities and reproduces the exact result with good accuracy for Λ as large as $\Lambda = 10$. This technique can be incorporated straightforwardly into the NRG code (for applications, see Campo, Jr. and Oliveira (2003, 2004); Costa *et al.* (1997); Paula *et al.* (1999); Ramos *et al.* (2003); Silva *et al.* (1996)).

B. Dynamic properties

1. Equilibrium dynamics and transport

We consider now the application of the NRG to the calculation of dynamic and transport properties of quantum impurity models (Costi and Hewson, 1992b; Costi *et al.*, 1994a; Frota and Oliveira, 1986; Sakai *et al.*, 1989). For definiteness we shall consider the Anderson impurity model and illustrate the procedure for the impurity spectral density $A_\sigma(\omega, T) = -\frac{1}{\pi} \text{Im} G_\sigma(\omega, T)$, with

$$G_\sigma(\omega, T) = \int_{-\infty}^{+\infty} d(t-t') e^{i\omega(t-t')} G_\sigma(t-t'), \quad (62)$$

$$G_\sigma(t-t') = -i\theta(t-t') \langle [f_\sigma(t), f_\sigma^\dagger(t')] \rangle_\varrho, \quad (63)$$

with ϱ the density matrix of the system. Suppose, for the moment, that we have *all* the many-body eigenstates, $|r\rangle$, and eigenvalues, E_r , of the Anderson impurity Hamiltonian, H , exactly. Then the density matrix, $\varrho(T)$, and partition function, $Z(T)$, of the full system at temperature $k_B T = 1/\beta$ can be written

$$\varrho(T) = \frac{1}{Z(T)} \sum_r e^{-\beta E_r} |r\rangle \langle r|, \quad (64)$$

$$Z(T) = \sum_r e^{-\beta E_r}, \quad (65)$$

and the impurity spectral density, A_σ , can be written in the Lehmann representation as

$$A_\sigma(\omega, T) = \frac{1}{Z(T)} \sum_{r, r'} |M_{r, r'}|^2 (e^{-E_r/k_B T} + e^{-E_{r'}/k_B T}) \times \delta(\omega - (E_{r'} - E_r)). \quad (66)$$

with $M_{r, r'} = \langle r | f_\sigma | r' \rangle$ the relevant many-body matrix elements.

Consider first the $T = 0$ case ($T > 0$ is described below), then

$$A_\sigma(\omega, T = 0) = \frac{1}{Z(0)} \sum_r |M_{r, 0}|^2 \delta(\omega + (E_r - E_0)) + \frac{1}{Z(0)} \sum_{r'} |M_{0, r'}|^2 \delta(\omega - (E_{r'} - E_0)), \quad (67)$$

with $E_0 = 0$ the ground state energy. In order to evaluate this from the information which we actually obtain from an iterative diagonalization of H , we consider the impurity spectral densities corresponding to the sequence of Hamiltonians H_N , $N = 0, 1, \dots$, whose characteristic scale is $\omega_N = \frac{1}{2}(1 + \Lambda^{-1})\Lambda^{-(N-1)/2}$,

$$A_\sigma^N(\omega, T = 0) = \frac{1}{Z_N(0)} \sum_r |M_{r, 0}^N|^2 \delta(\omega + E_r^N) + \frac{1}{Z_N(0)} \sum_{r'} |M_{0, r'}^N|^2 \delta(\omega - E_{r'}^N). \quad (68)$$

Here, E_r^N and $|r\rangle_N$ are the eigenvalues and eigenstates of H_N , i.e.

$$H_N |r\rangle_N = E_r^N |r\rangle_N, \quad (69)$$

and,

$$M_{r, r'}^N = {}_N \langle r | f_\sigma | r' \rangle_N, \quad (70)$$

are the relevant many-body matrix elements, whose calculation will be outlined below. Since the spectrum of H_N is truncated, the range of excitations it describes is limited to $0 \leq \omega \leq K(\Lambda)\omega_N$, where $K(\Lambda)$ depends on both Λ and the actual number of states retained at each iteration and is typically 5 – 10 for $\Lambda = 1.5 - 2.0$ for $N_s = 500 - 1000$ retained states. Moreover, excitations and eigenstates below the characteristic scale ω_N of H_N will only be approximations to the excitations and eigenstates of the infinite system described by H . These excitations and eigenstates are refined in subsequent iterations. Hence, for each $N = 1, 2, \dots$ we can evaluate the spectral density from A_σ^N at a frequency ω chosen to lie in the window $\omega_N \leq \omega \leq K(\Lambda)\omega_N$,

$$A_\sigma(\omega, T = 0) \approx A_\sigma^N(\omega, T = 0). \quad (71)$$

A typical choice, for $\Lambda = 1.5 - 2.0$, is $\omega = 2\omega_N$.

The above procedure still only yields discrete spectra. For comparison with experiment, smooth spectra are required, so we replace the delta functions $\delta(\omega \pm E_r^N)$ appearing in (68) by smooth distributions $P(\omega \pm E_r^N)$. A

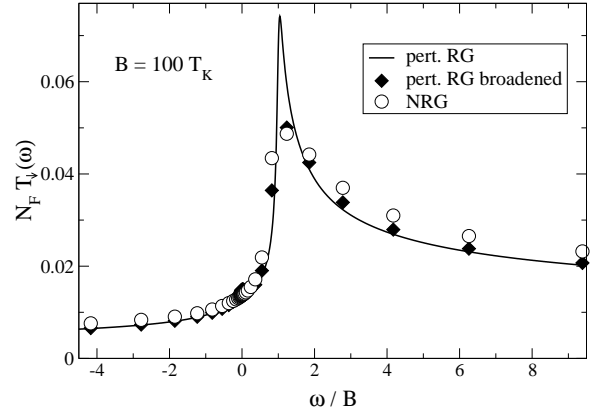


FIG. 7 The spin-resolved Kondo resonance at high magnetic fields calculated with NRG and perturbative RG. The large Gaussian broadening used at $\omega = g\mu_B B = 100T_K$ reduces the height of the sharp peak and overestimates its width, as is evident on applying the NRG broadening procedure to the analytic perturbative RG result (Rosch *et al.*, 2003).

natural choice for the width η_N of P is ω_N , the characteristic scale for the energy level structure of H_N . Two commonly used choices for P are the Gaussian, P_G , and the Logarithmic Gaussian, P_{LG} , distributions (Bulla *et al.*, 2001; Costi *et al.*, 1994a; Sakai *et al.*, 1989):

$$P_G(\omega \pm E_r^N) = \frac{1}{\eta_N \sqrt{\pi}} e^{-\left[\frac{(\omega \pm E_r^N)}{\eta_N}\right]^2}, \quad (72)$$

$$P_{LG}(\omega \pm E_r^N) = \frac{e^{-b^2/4}}{b E_r^N \sqrt{\pi}} e^{-\left[\frac{\ln(\omega/E_r^N)}{b}\right]^2}, \quad (73)$$

For the Gaussian, a width $\eta_N = 0.3\omega_N - 0.8\omega_N$ is typically used (Costi *et al.*, 1994a), whereas, for the logarithmic Gaussian, a typical width parameter $b = 0.3 - 0.7$ is used (Bulla *et al.*, 2001; Sakai *et al.*, 1989). Note that the logarithmic Gaussian gives little weight to excitations below ω_N and more weight to the higher energy excitations. Due to the logarithmic discretization, this might appear to be the better choice. In practice, the difference to using a Gaussian is small.

In general, spectra for even and odd N differ by a few % at most as a result of finite-size effects (see also the discussion of the reduced density matrix approach in Sec. III.B.2), so generally either even N or odd N spectra are calculated (as for thermodynamics). It is also possible to combine information from shell N and $N + 2$ by an appropriate weighting (Bulla *et al.*, 2001). We note also, that since the broadening is proportional to energy, a peak of intrinsic width Γ at frequency Ω_0 will be well resolved by the above procedure provided that $\Omega_0 \ll \Gamma$, which is the case for the Kondo resonance and other low energy resonances. In the opposite case, the low (logarithmic) resolution at higher frequencies may be insufficient to resolve the intrinsic widths and heights of such peaks, although their weights are correctly captured. In cases where the width of such high energy

peaks is due to single-particle effects, e.g. the resonant level in the empty orbital regime of the Anderson model, one can use the representation of the spectral density in terms of the correlation self-energy, as described in the next section, with the single-particle broadening being put in explicitly so that essentially the correct peak widths and heights is obtained. In other cases, when the width of such peaks is due to correlations, one inevitably has some over-broadening. An extreme example is the spin-resolved Kondo resonance at high magnetic fields, $B \gg T_K$, which is sharply peaked at $\omega = B$ and is highly asymmetrical, as shown in Fig. 7. The extent of the problem is quantified here by comparison with analytic perturbative results with and without the NRG broadening procedure.

A procedure for obtaining smooth spectra, which resolves finite frequency peaks without broadening the discrete spectra, involves an averaging over many different discretizations of the band (the Z-averaging discussed in the previous section on thermodynamics). We refer the reader to Yoshida *et al.* (1990) for details.

In calculating the impurity spectral density, one requires also the matrix elements $M_{r,r'}^N$ at each iteration. These are obtained recursively by using the unitary transformation Eq. (43) yielding

$$M_{r,r'}^N = \sum_{p,s_N} \sum_{p',s'_N} U_N(r,ps_N)U_N(r',p's'_N) \times \delta_{s_N,s'_N} M_{p,p'}^{N-1}. \quad (74)$$

Hence, the matrix elements $M_{r,r'}^N$ can be evaluated recursively from a knowledge of the eigenstates of all finite size Hamiltonians up to H_N starting from the initial matrix elements ${}_{-1}\langle r|f_\sigma|r'\rangle_{-1}$ of the isolated impurity $H_{\text{imp}} = \varepsilon_f \sum_\sigma f_\sigma^\dagger f_\sigma + U f_\uparrow^\dagger f_\uparrow f_\downarrow^\dagger f_\downarrow$. Similar considerations apply to other local dynamical quantities such as dynamical spin and charge susceptibilities. Figure 8 shows $T = 0$ spectral densities for single-particle, magnetic and charge excitations calculated using the above procedure. These NRG calculations have been shown to satisfy exact Fermi liquid relations, such as the Friedel sum rule for the single-particle spectral density and the Shiba relation for the magnetic excitation spectrum, to within a few percent irrespective of the interaction strength $U/\pi\Delta$ in the Anderson model or the value of the exchange J in the Kondo model, see Costi *et al.* (1994a) and Costi (1998) for a discussion.

The case of finite temperature dynamics is more complicated. Contributions to the spectral density at frequency $\omega \sim \omega_N$ now arise from excitations between arbitrary excited states, i.e. $\omega = E_r - E_0 = E_{r'} - E_{p'} = E_{r''} - E_{p''} = \dots$ with $E_0 = 0 < E_{p'} < E_{p''} < \dots$ see Fig. 9. Consequently, the finite-T spectral density at $\omega \sim \omega_N$ will have contributions from all energy shells $n = 1, \dots, N$. These need to be summed up, as in the calculation of transient quantities described in Sec. III.B.3. It is clear, however, that in the case of equilibrium spectral densities, the contributions from shells $n < N$ will

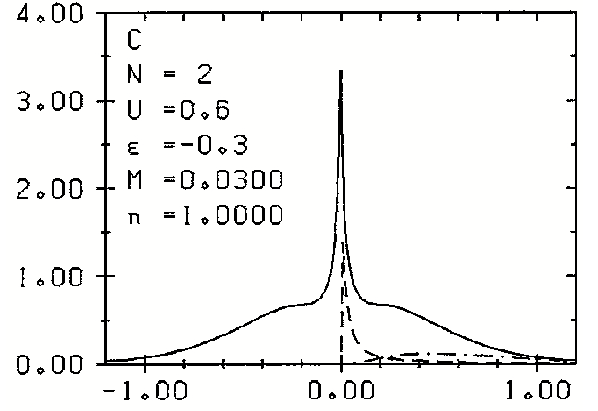


FIG. 8 $T = 0$ spectral densities for single-particle (solid line), magnetic (dashed line) and charge (dot-dashed line) excitations of the spin degenerate symmetric Anderson model versus energy ω/D for $U = 0.6D$, $D = 1.0$ and $\Delta/\pi = M = 0.03D$ (Sakai *et al.*, 1989).

be suppressed by Boltzmann factors. This motivates the following approximation: at $\omega = 2\omega_n > k_B T$ one can calculate $A_\sigma(\omega, T)$ as in the $T = 0$ case

$$A_\sigma(\omega_n, T) \approx A_\sigma^n(\omega_n, T) = \frac{1}{Z_n(T)} \sum_{r,r'} |M_{r,r'}^n|^2 (e^{-E_r^n/k_B T} + e^{-E_{r'}^n/k_B T}) \times \delta(\omega_n - (E_{r'}^n - E_r^n)). \quad (75)$$

In the other limit, $\omega = 2\omega_n \leq T$, there is no completely satisfactory procedure. One approach assumes that the main contribution to the spectral density for $\omega = 2\omega_n \leq T$ comes from the energy window containing thermal excitations $\mathcal{O}(k_B T)$ (Costi and Hewson, 1992b; Costi *et al.*, 1994a). In this case, the relevant shell, M , is determined by temperature via $\omega_M \approx \beta k_B T$, as in the evaluation of thermodynamic properties in the previous section, so that, for $\omega = 2\omega_n \leq k_B T$, we use

$$A_\sigma(\omega_n, T) \approx A_\sigma^M(\omega_n, T) = \frac{1}{Z_M(T)} \sum_{r,r'} |M_{r,r'}^M|^2 (e^{-E_r^M/k_B T} + e^{-E_{r'}^M/k_B T}) \times \delta(\omega_n - (E_{r'}^M - E_r^M)). \quad (76)$$

In practice, this procedure gives a smooth crossover as ω is lowered below $k_B T$ for temperatures comparable to the Kondo scale and higher, but becomes less reliable at $\omega < k_B T \ll T_K$.

Once the finite-T spectral density is known, one can also calculate transport properties, since the transport time, τ_{tr} , for electrons scattering from a small concentration, n_i , of magnetic impurities is given in terms of the spectral density by

$$\frac{1}{\tau_{\text{tr}}(\omega, T)} = \frac{2n_i}{N_F} \Delta A_\sigma(\omega, T), \quad (77)$$

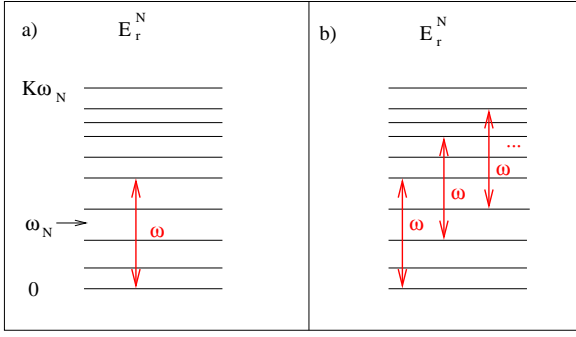


FIG. 9 Excitations of H_N contributing to the spectral function at frequency ω for, (a), $T = 0$, and, (b), $T > 0$.

where N_F is the conduction electron density of states and Δ is the hybridization strength. For example, the resistivity $R(T)$ due to Kondo impurities in a clean metal is given by

$$R(T) = \frac{1}{e^2 \int d\omega \left(-\frac{\partial f}{\partial \omega} \right) \tau_{\text{tr}}(\omega, T)}, \quad (78)$$

and the conductance through a quantum dot (or the resistivity of Kondo impurities in a dirty metal) modeled by an Anderson impurity model is given by

$$G(T)/G(0) = \sum_{\sigma} \int d\omega \left(-\frac{\partial f}{\partial \omega} \right) A_{\sigma}(\omega, T). \quad (79)$$

Figure 10 compares the scaled resistivity $R(T)/R(0)$ for the Kondo and Anderson models with the scaled conductance $G(T)/G(0)$ for the Kondo model. The conductance and resistivity are seen to be almost identical universal functions of T/T_K . At finite magnetic field, the two quantities deviate from each other in the region $T \approx B$ (Costi, 2000). The NRG results can be compared to analytic results at low and high temperature. The resistivity of the Anderson model in the low-temperature Fermi liquid regime is given by the result of Nozières (1974),

$$R(T)/R(0) = G(T)/G(0) = 1 - c \left(\frac{T}{T_K} \right)^2, \quad T \ll T_K, \quad (80)$$

where $c = \pi^4/16 = 6.088$ and T_K is the low-temperature Kondo scale defined from the static spin susceptibility via

$$\chi(T=0) = (g\mu_B)^2/4k_B T_K. \quad (81)$$

At high temperatures, $T > T_K$, Hamann used the Nagaoka-Suhl approximation (Hewson, 1993) to obtain for the resistivity of the Kondo model

$$R(T)/R(0) = \frac{1}{2} \left(1 - \frac{\ln(T/T_{\text{KH}})}{(\ln(T/T_{\text{KH}})^2 + \pi^2 S(S+1))^{1/2}} \right), \quad (82)$$

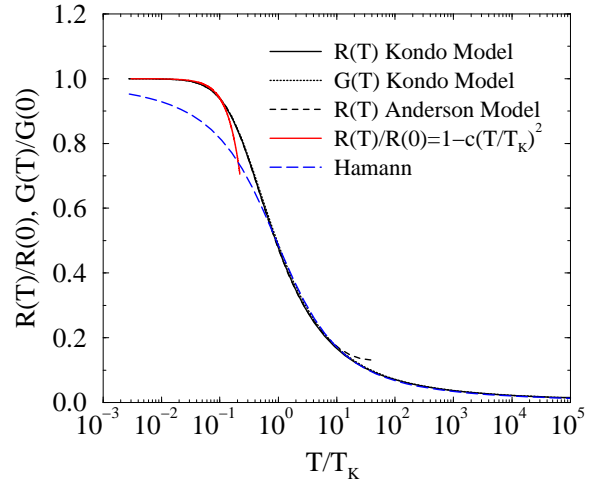


FIG. 10 Scaled resistivity and conductance of the $S = 1/2$ Kondo model. Adapted from Costi (2000). For comparison the resistivity of the symmetric Anderson model for $U/\pi\Delta = 4$ is also shown (Costi and Hewson, 1993) and is seen to be identical to that for the Kondo model, up to non-universal corrections arising from charge fluctuations at higher temperatures (for $U/\pi\Delta = 4$ these corrections occur for $T > 10T_K$).

where S is the impurity spin and T_{KH} is a Kondo scale defined by

$$R(T = T_{\text{KH}}) = R(0)/2. \quad (83)$$

Micklitz *et al.* (2006a) found numerically that $T_{\text{KH}} \approx 0.91T_K$. We see from Fig. 10 that the NRG result for the resistivity of the Kondo model agrees with the Hamann result for $T \geq T_K$. The T^2 Fermi liquid behavior at low-temperature $T \ll T_K$ is also recovered. In contrast, the Hamann result violates Fermi liquid behavior and cannot be trusted for $T < T_K$. A numerical determination of the coefficient c in Eq. (80) requires obtaining $\tau_{\text{tr}}(\omega, T)$ accurately up to second order in both ω and T (Costi *et al.*, 1994a). Typical errors for c can be as large as 10-30% so there is room for further improvement of the finite T dynamics in the Fermi liquid regime $T \ll T_K$. For a discussion of other transport properties of Kondo systems, such as thermopower and thermal conductivity, the reader is referred to Costi and Hewson (1993); Costi *et al.* (1994a); Zlatić *et al.* (1993).

2. Self-energy and reduced density matrix approach

We now describe two improvements to the calculation of dynamical quantities. The first of these, a direct calculation of the correlation part of the self-energy of the Anderson impurity model (Bulla *et al.*, 1998), is particularly important for applications to DMFT, where the impurity self-energy plays a central role. The second, the introduction of the reduced density matrix into the calculation of dynamics, is important, for example, in

correcting large finite-size errors in spin-resolved spectra of the Anderson and Kondo models when a magnetic field perturbs the ground state (Hofstetter, 2000).

The correlation part of the self-energy for the Anderson impurity model, Σ_σ , is defined via

$$G_\sigma(\omega, T) = \frac{1}{\omega - \varepsilon_f + i\Delta - \Sigma_\sigma(\omega, T)}, \quad (84)$$

and can be expressed, via the equation of motion for G_σ (Bulla *et al.*, 1998), as the ratio of a two-particle and a one-particle Green function

$$\Sigma_\sigma(\omega, T) = U \langle \langle f_\sigma f_{-\sigma}^\dagger f_{-\sigma}; f_\sigma^\dagger \rangle \rangle / \langle \langle f_\sigma; f_\sigma^\dagger \rangle \rangle. \quad (85)$$

Evaluating the spectral densities of the two Green functions in (85) as in the previous section, and calculating from these, via a Kramers-Kronig transformation, the corresponding real parts of the Green functions one obtains the self-energy. Using this in (84) one is able to obtain the impurity spectral density with improved resolution of high-energy peaks, since in this procedure, the single-particle broadening Δ is included exactly. In particular, this scheme recovers the limit $U \rightarrow 0$ exactly. It is also found to improve the spectral sum rule with typical errors as low as 0.1% or less.

The evaluation of spectral densities described in the previous section is subject to systematic errors due to neglect of high-energy states in constructing H_N . These are the same as for thermodynamic properties, and they can be controlled by increasing Λ and the number of retained states N_s . Another source of error, specific to the method used to calculate dynamics, is that while we chose the frequency ω in evaluating spectra from H_N carefully so that $\omega > \omega_N$, nevertheless the eigenstates in the range $0 \leq E_r^N \leq \omega_N$, which for small N are only crude approximations to the eigenstates of H , are also used in the evaluation. They enter the calculation directly, as can be seen from Fig. 9, and, also, via the density matrices (e.g. at $T = 0$ via $\varrho_N = |0\rangle_{NN}\langle 0|$) which are used to arrive at (68) and (75-76). As a result, the spectral density is subject to errors for small N , i.e. for high energies, due to the use of low-lying states which are not converged (Hofstetter, 2000). With increasing N , i.e. lower energies, this error will decrease. An improvement, due to Hofstetter (2000), is to use in place of ϱ_N the reduced density matrix, $\varrho^{N,\text{red}}$, of H_N , obtained from the density matrix of the largest finite size Hamiltonian diagonalized, $H_{N_{\text{max}}}$, i.e.,

$$\varrho^{N,\text{red}} = \text{Tr}_{s_{N+1}, \dots, s_{N_{\text{max}}}} [\varrho_{N_{\text{max}}}] \quad (86)$$

where $s_{N+1}, \dots, s_{N_{\text{max}}}$ are the extra degrees of freedom contained in $H_{N_{\text{max}}}$ but absent in H_N . As $\varrho^{N,\text{red}}$ is not diagonal in the eigenbasis of H_N , the resulting spectral function takes on a more complicated form

$$A_\sigma^N(\omega, 0) = \sum_{r', r} C_{r', r} M_{r', r}^N \delta(\omega - (E_{r'}^N - E_r^N)) \quad (87)$$

$$C_{r', r} = \sum_p \rho_{p, r}^{N,\text{red}} M_{r', p}^N + \sum_p \rho_{r', p}^{N,\text{red}} M_{p, r}^N. \quad (88)$$

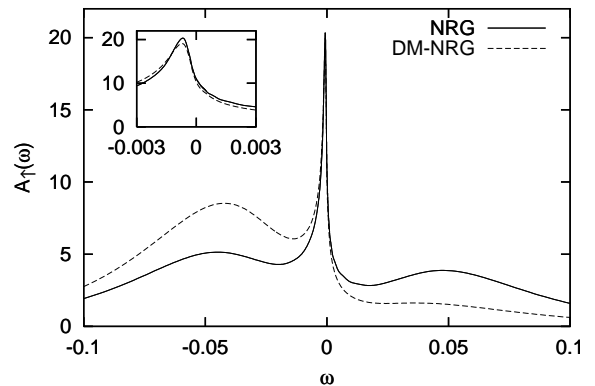


FIG. 11 Comparison of the spectral function for the Anderson impurity model calculated in a magnetic field with and without the reduced density matrix: $\Delta = 0.01, U = 0.1, \varepsilon_f = -0.05, B = 0.001$ from Hofstetter (2000).

The reduced density matrices $\varrho^{n,\text{red}}$ are calculated iteratively backwards starting from the density matrix of $H_{N_{\text{max}}}$. One situation where the reduced density matrix is important is in obtaining correctly the spin-resolved spectral density of the Anderson model in a magnetic field (Hofstetter, 2000). A magnetic field comparable to T_K changes the magnetization and therefore the occupation of up/down states by $\mathcal{O}(1)$ so large shifts in spectral weight occur at high energies in the impurity spectral density which are only captured correctly by using the reduced density matrix, see Fig. 11. Results for dynamical susceptibilities in a magnetic field using the reduced density matrix have been discussed by Hewson (2006). The reduced density matrix also eliminates to a large extent the difference between the spectra calculated for even/odd N and allows a correct description of the asymptotics of the Kondo resonance in high magnetic fields (Rosch *et al.*, 2003).

3. The x-ray problem and transient dynamics

We consider here the calculation of the response of a system to a sudden local perturbation, such as the excitation of an electron from a core-level to the conduction band of a metal in the x-ray problem, or, the time-dependent response of a spin in the spin-boson model following an initial-state preparation. The NRG approach to the x-ray problem (Oliveira and Wilkins, 1981) was the first application of the method to dynamical quantities. In common with previous treatments of the x-ray problem, for a review see (Mahan, 1975), the approach developed by Oliveira and Wilkins (1981) calculates the absorption spectrum within linear response theory, and, therefore, belongs logically to Sec. III.B.1. We include it here for two reasons, (i), because the response of the electrons to the appearance of the core-hole potential is a problem of transient dynamics, and, (ii), because it uses the idea of formulating the calculation of the absorption

spectrum in terms of initial and final state Hamiltonians (Nozières and De Dominicis, 1969), which is also inherent to the recent NRG approach to transient dynamics beyond linear response theory (Anders and Schiller, 2005; Costi, 1997a).

A simple model for describing the x-ray absorption spectra in metals, is given by the following spinless Hamiltonian

$$H = \sum_k \varepsilon_k c_k^\dagger c_k + E_d d^\dagger d + \sum_{k,k'} U_{dc} c_k^\dagger c_{k'} d d^\dagger, \quad (89)$$

where d^\dagger creates a core-electron with energy E_d and the attractive screening interaction, U_{dc} , acts only when the core-level is empty ($dd^\dagger = 1$). The core-level lifetime is assumed infinite, and the interaction with the x-ray field is taken to be of the form

$$H_x = w(c_0^\dagger d e^{-i\omega t} + H.c.), \quad (90)$$

where $c_0 = \sum_k c_k$. The x-ray absorption spectrum, $\mu(\omega)$, is obtained using linear response theory from the imaginary part of the optical conductivity, $\chi_{cd} = \langle\langle c_0^\dagger d; d^\dagger c_0 \rangle\rangle$. At zero temperature, one finds for the absorption spectrum a power law singularity of the form

$$\mu(\omega) \sim (\omega - E_T)^{-\alpha}, \quad (91)$$

where, E_T is the absorption threshold, and, α , is an exponent which depends on the strength of the core-hole potential. The exponent α has two contributions $\alpha = \alpha' - \varepsilon$, an excitonic part, α' , due to Mahan (1967) and an orthogonality part, ε , which follows from Anderson's orthogonality catastrophe theorem (Anderson, 1967). An exact solution of the 'x-ray problem' has been obtained by Nozières and De Dominicis (1969) by using the decomposition of (89) into single-particle initial-state, H_I , and final-state, H_F , Hamiltonians, corresponding to the situations before ($dd^\dagger = 0$) and after ($dd^\dagger = 1$) a core-electron is excited to the conduction band:

$$H_I = \sum_k \varepsilon_k c_k^\dagger c_k + E_d, \quad (92)$$

$$H_F = \sum_k \varepsilon_k c_k^\dagger c_k + \sum_{k,k'} U_{dc} c_k^\dagger c_{k'}. \quad (93)$$

For the spinless model, (89), Nozières and De Dominicis (1969) found the exponents

$$\alpha' = 2\delta/\pi, \quad \varepsilon = (\delta/\pi)^2, \quad (94)$$

where the phase-shift $\delta = \arctan(-\pi N_F U_{dc})$ is that for conduction electrons scattering from the additional potential created by the core-hole, and, N_F is the conduction electron density of states at the Fermi level. In addition to the absorption spectrum, the core-level photoemission spectrum, $A_d(\omega) = -\text{Im}[\langle\langle d; d^\dagger \rangle\rangle]/\pi$, is also of interest. In the core-level photoemission spectrum, only the orthogonality effect is operative and the core-electron spectral function, which has the quasiparticle

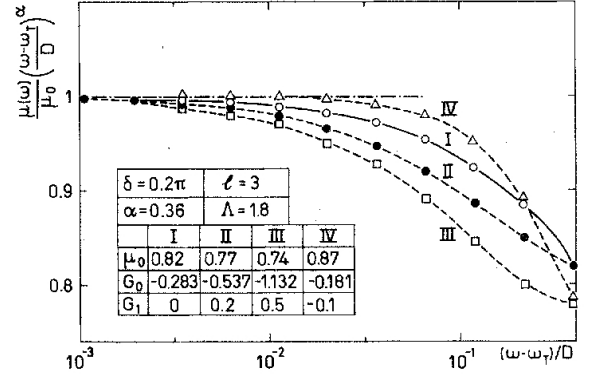


FIG. 12 Absorption spectrum normalized by the Nozières-De Dominicis result (Eq. (91)) for several screening potentials of the form $U_{dc}(k, k') = G_0 + G_1(k + k')$ (Oliveira and Wilkins, 1981).

form $A_d(\omega) = \delta(\omega - E_d)$ in the absence of screening, is replaced by an incoherent spectrum of the form

$$A_d(\omega) \sim \theta(\tilde{E}_d - \omega)(\tilde{E}_d - \omega)^{-(1-\varepsilon)}, \quad (95)$$

in the presence of screening (Doniach and Šunjić, 1970).

Oliveira and Wilkins (1981) applied the NRG to the initial-state and final-state Hamiltonians (92-93) and calculated the zero temperature linear response absorption spectrum,

$$\mu(\omega) = 2\pi w^2 \sum_{m_F} |\langle m_F | c_0^\dagger d | m_{I,GS} \rangle|^2 \times \delta(\omega - (E_{m_F} - E_{m_{I,GS}})), \quad (96)$$

with $H_{I,F} |m_{I,F}\rangle = E_{m_{I,F}} |m_{I,F}\rangle$ and $|m_{I,GS}\rangle$ the ground state of H_I . In evaluating $\mu(\omega)$, truncated Hamiltonians, $H_{I,F}^N$, were used and the spectrum was evaluated at an appropriate frequency $\omega = \omega_N$ as in Sec. III.B.1 but with a box broadening function on a logarithmic scale. They were able to recover the exact threshold exponent of Nozières and De Dominicis (1969) (see Líbero and Oliveira (1990a) for similar calculations of the photoemission spectra). They also extended the calculation of absorption spectra to core-hole potentials of finite range $U_{dc} \rightarrow U_{dc}(k, k')$, finding (see Fig. 12) that the threshold exponent remains universal, i.e. it depends only on the phase shift δ at the Fermi level, but that the asymptotic scale for the onset of power-law behavior depends on both the range (Oliveira and Wilkins, 1981) and the strength of the core-hole potential (Cox *et al.*, 1985). It also depends on any energy dependence in the density of states (Chen *et al.*, 1995). These results reflect the fact that the crossover scale to the low energy fixed point, determining universal properties, depends on details of the density of states and the core-hole potential.

X-ray singularities also play an important role in the dynamics of auxiliary particles in the slave-boson approach to the infinite U Anderson impurity model

(Coleman, 1984; Müller-Hartmann, 1984). A NRG calculation of the $T = 0$ photoemission spectra for slave-bosons, $A_b(\omega)$, and pseudo-fermions, $A_{f\sigma}(\omega)$, showed that these diverge with the exponents given above for the photoemission and absorption spectra respectively, generalized to include spin, (Costi *et al.*, 1996, 1994b):

$$A_{f\sigma}(\omega) \sim (\omega - E_T)^{-\alpha_f}, \quad (97)$$

$$A_b(\omega) \sim (\omega - E_T)^{-\alpha_b}, \quad (98)$$

$$\alpha_f = 2\frac{\delta_\sigma}{\pi} - \sum_\sigma \left(\frac{\delta_\sigma}{\pi}\right)^2, \quad (99)$$

$$\alpha_b = 1 - \sum_\sigma \left(\frac{\delta_\sigma}{\pi}\right)^2, \quad (100)$$

with the phase shift $\delta_\sigma = \pi n_{f\sigma}$ and $n_{f\sigma}$ the occupancy per spin of the local level. Here, also, the scale for the onset of power-law behavior is determined by the relevant low energy crossover scale, e.g., the Kondo scale in the Kondo regime.

We turn now to a problem which is formally similar to the x-ray problem, namely the dynamics of a spin subject to an initial state preparation, as in the case, for example, of the dynamics of the spin in the spin-boson model Eq. (139). Further discussion of the effects of screening on the spectra of impurity models is given in Sec. IV.A.1. In the spin-boson model one is interested in the dynamics of a spin, σ_z , described by $P(t) = \langle \sigma_z(t) \rangle_{\varrho_I}$, following an initial-state preparation of the system described by an initial density matrix ϱ_I (Leggett *et al.*, 1987). For example, the spin σ_z in (139) could be prepared in state $|\uparrow\rangle$ at $t < 0$ by an infinite bias $\varepsilon = \infty$ with the environment fully relaxed about this state, and the bias could subsequently be switched off at $t = 0$ allowing the spin to evolve. The time evolution of the spin for $t > 0$ is then described by

$$\langle \sigma_z(t) \rangle_{\varrho_I} = \frac{1}{Tr \varrho_I} Tr[\varrho_I e^{-iH_F t/\hbar} \sigma_z e^{iH_F t/\hbar}], \quad (101)$$

where $\varrho_I = Tr[e^{-\beta H_I}]$ and the initial and final state Hamiltonians are given by

$$H_I = H_{SB}(\varepsilon = \infty), \quad (102)$$

$$H_F = H_{SB}(\varepsilon = 0), \quad (103)$$

where H_{SB} is the spin-boson Hamiltonian (139).

This approach has been investigated within NRG by Costi (1997a) using, for the Ohmic case, in place of H_{SB} , the equivalent anisotropic Kondo model. Despite the formal similarity with the x-ray problem, the exact formulation indicates the difficulties that have to be overcome in calculating transient dynamical quantities beyond linear response. Consider the spectral function

$$P(\omega) = \frac{1}{Z_I} \sum_{m_I, m_F, m'_F} e^{-\beta E_{m_I}} \langle m_I | m_F \rangle \langle m'_F | m_I \rangle \times \langle m_F | \sigma_z | m'_F \rangle \delta(\omega - (E_{m_F} - E_{m'_F})), \quad (104)$$

with

$$P(t) = \int_0^{+\infty} P(\omega) \cos(\omega t) d\omega. \quad (105)$$

We see that even at $T = 0$, no ground state enters the delta functions in (104), in contrast to the linear-response expression (96) for $\mu(\omega)$ in the x-ray problem. This implies that in evaluating $P(\omega)$ at a frequency $\omega \sim \omega_N$, contributions will arise from all energy shells $n = 1, 2, \dots, N$ as discussed previously for finite- T dynamics. In the present situation, however, the contributions from higher energy shells (i.e. $n < N$) are not suppressed by Boltzmann factors, so it is not clear a priori that using a single shell approximation will give meaningful results. Such an approximation shows that the short-time dynamics of the spin-boson model can be recovered and that in order to obtain the long-time dynamics one has to sum up contributions from all shells (Costi, 1997a). Adding up such contributions using the retained states of successive Hamiltonians $H_{I,F}^N, H_{I,F}^{N+1}, \dots$ is problematical due to the overlap of the spectra at low energies. An elegant solution of this problem, allowing multiple-shell NRG calculations to be carried out, has recently been found by Anders and Schiller (2005). Their idea, was to recognize that the set of states discarded, $|r\rangle_{m,\text{disc}}$, at each NRG iteration m , supplemented with the degrees of freedom $|e; m\rangle = |s_{m+1}\rangle \otimes \dots \otimes |s_{N_{\text{max}}}\rangle$, for $m = 1, \dots, N_{\text{max}}$, with N_{max} the largest Hamiltonian diagonalized, forms a complete basis set

$$\sum_{m=1}^{N_{\text{max}}} \sum_{r \in \{\text{disc}\}} |r, e; m\rangle \langle r, e; m| = 1. \quad (106)$$

Using this identity, their result for $P(t)$ in the basis of final states is

$$P(t) = \sum_{m=1}^N \sum_{m_F, m'_F}^{\text{trun}} e^{i(E_{m_F}^m - E_{m'_F}^m)t/\hbar} \times \langle m_F | \sigma_z | m'_F \rangle \varrho_{m_F, m'_F}^{m, \text{red}}, \quad (107)$$

where $\varrho_{r_F, s_F}^{m, \text{red}}$ are the matrix elements of the reduced density matrix ϱ_I for H_I^m introduced in the previous section and the sum $\sum_{m_F, m'_F}^{\text{trun}}$ implies that at least one of the states m_F, m'_F is in the discarded sector for iteration m . Rotating $\varrho_{r_F, s_F}^{m, \text{red}}$ to the initial state basis gives overlap matrix elements $\langle m_I | m_F \rangle, \langle m_I | m'_F \rangle$ as in (104) above. Within this approach the time-dependent transient dynamics of a number of models has been investigated, including the Anderson and resonant level models (Anders and Schiller, 2005), the Kondo model (Anders and Schiller, 2006) and the sub-ohmic spin-boson model (Anders *et al.*, 2006).

The use of a complete basis set (106) has potential to improve also the finite- T calculation of spectral densities, particularly in the problematical range $\omega < T$ (Weichselbaum and von Delft, 2006). A further improvement in using a complete basis set is that

the sum rule for spectral densities $\int_{-\infty}^{\infty} d\omega A_{\sigma}(\omega, T) = 1$ is, by construction, fulfilled exactly (Peters *et al.*, 2006; Weichselbaum and von Delft, 2006).

IV. APPLICATION TO IMPURITY MODELS

In this section we review the application of the NRG to a range of quantum impurity models. Section IV.A reviews work on models with conduction electron screening (Sec. IV.A.1), underscreened and fully screened Kondo models (Sec. IV.A.2), and models exhibiting the Kondo effect in nanostructured devices (Sec. IV.A.3). Section IV.B deals with the prototypical overscreened Kondo model, the two-channel Kondo model, which is often encountered as an effective model describing the quantum critical point of more complex quantum impurity models, e.g. certain double quantum dot systems (Zaránd *et al.*, 2006) or two-impurity systems (Jones and Varma, 1987). Impurity quantum phase transitions are reviewed in Sec. IV.C in the contexts of multi-impurity systems (IV.C.1), soft-gap systems (IV.C.2) and in the context of magnetic impurities in superconductors (IV.C.3). Sec. IV.D reviews work on multi-orbital systems, including the effects of crystal-field splittings in Anderson impurity models. Finally, models with bosonic degrees of freedom are reviewed in Sec. IV.E. Note also, that a number of models of nanostructured devices, for example, the single-electron box, quantum dots with phonons, or multi-orbital quantum dots, are to be found in Sec. IV.B-IV.E.

A. Kondo effect and related phenomena

1. Screening and photoemission

Screening effects are important whenever an electron is excited from a localized core- or valence-state into the conduction band or removed completely, leaving behind a hole which attracts the conduction electrons. Such effects can have a drastic influence on the photoemission and absorption spectra of impurity systems. In this section we consider a number of extensions to the basic screening model (89) introduced in Sec. III.B.3,

$$H = \sum_k \varepsilon_k c_k^{\dagger} c_k + E_d d^{\dagger} d + \sum_{k, k'} U_{dc} c_k^{\dagger} c_{k'} d d^{\dagger}. \quad (108)$$

We consider first the generalization of (108) to a simplified model of an atom adsorbed on a metallic surface (Oliveira and Wilkins, 1985). In addition to a core-level, as in (108), the atom has a resonant level (created by b^{\dagger}) whose position, E_{bI} or E_{bF} , depends on the occupancy of the core-level according to the term

$$H_{db} = E_{bI} b^{\dagger} b d^{\dagger} d + E_{bF} b^{\dagger} b (1 - d^{\dagger} d), \quad (109)$$

and the level hybridizes with the conduction band via a term

$$H_{\text{mix}} = V \sum_k (c_k^{\dagger} b + H.c.). \quad (110)$$

Note that H_{db} just represents a screening of the core-hole by electrons in the resonant level. Excitation of an electron from the core-level by an x-ray can proceed either directly or via the resonant level, leading to a Fano anti-resonance in the x-ray absorption at finite energy (in addition to the usual edge singularity at $\omega = E_T$). This Fano anti-resonance, present also without the core-hole potential, is found to be significantly narrowed and shifted in the presence of the core-hole potential (Oliveira and Wilkins, 1985). It would be of interest to investigate also the core-level photoemission spectrum of this model using the NRG, as both this, and the absorption spectrum, are accessible in experiments. Brito and Frota (1990) have carried out such a calculation for an appropriately generalized spinfull version of the above model, i.e., the Anderson model (2) in the presence of both an interaction,

$$H_{dc} = U_{dc} d d^{\dagger} \sum_{kk'\sigma} c_{k\sigma}^{\dagger} c_{k'\sigma}, \quad (111)$$

between the core-hole and the conduction electrons, and, an interaction,

$$H_{df} = U_{df} d d^{\dagger} \sum_{\sigma} f_{\sigma}^{\dagger} f_{\sigma}, \quad (112)$$

between the core-hole and the valence level. Signatures of the valence states could be identified in the XPS spectra and their dependence on U_{dc} was investigated in the mixed valence and empty orbital regimes. A reduction of the hybridization between the valence level and the conduction band, arising from orthogonality effects, was found with increasing U_{dc} . The corresponding calculation in the Kondo regime is still lacking. The x-ray absorption spectrum of the same model has been investigated in (Helmes *et al.*, 2005) in the context of excitons in Kondo correlated quantum dots and the expected absorption exponent from the Nozières – De Domenicis theory was recovered.

In the models discussed so far, the core-level was assumed to have infinite lifetime. Consequently, the screening interaction gave rise to true singularities in the core-level absorption and photoemission spectra. These singularities are cut off as soon as the core-level lifetime is finite. Another situation where the singularities due to screening are cut off, but where screening effects may nevertheless be important, is in the valence band photoemission spectra of heavy fermions within a local impurity approach, which we now address.

It is often assumed that the effects of conduction electron screening on the f electron photoemission spectra of heavy fermions can be taken into account by renormalizing the bare parameters of an effective Anderson impurity

model. However, this is not a priori clear as the screening interaction in these systems can be an appreciable fraction of the local Coulomb repulsion. One of the merits of the NRG, which allows such questions to be investigated, is that it can deal with all local Coulomb interactions on an equal footing and in a non-perturbative manner, and some examples of this have already been given above. For the particle-hole symmetric Anderson model, (2), it was shown in Costi and Hewson (1991, 1992a) that the effect of a screening term of the form

$$H_{fc} = U_{fc} \sum_{kk'\sigma\sigma'} f_{\sigma}^{\dagger} f_{\sigma} c_{k\sigma}^{\dagger} c_{k'\sigma'} , \quad (113)$$

on the valence band photoemission spectrum could be well accounted for by a renormalization of the bare parameters of the Anderson model, both the local level position, $\varepsilon = -U/2$, and the hybridization. An excitonic like enhancement of the hybridization was found with increasing U_{fc} . Similar effects are reflected in the STM conductance of a magnetic adatom modeled by the screened Anderson model (Cornaglia and Balseiro, 2003). Calculations for the infinite U Anderson impurity model, for thermodynamics (Alascio *et al.*, 1986; Zhuravlev *et al.*, 2005), and, dynamics (Takayama and Sakai, 1993), are consistent with the above findings.

The above model for screening in heavy fermions assumes that the largest contribution to screening of f holes arises from conduction electrons in states that hybridize with the f states. These hybridizing states are usually the p levels from neighboring ligand ions, so the screening from these (denoted U_{fc} above) should be expected to be smaller than the onsite screening, U_{df} , from the d electrons of the rare-earth ion. By symmetry, the latter do not hybridize with the f states. Neglecting U_{fc} and representing the d electrons by a spinless s wave band, we may represent the screening of f holes by d electrons by adding to the Anderson model (2) the term

$$H_{scr} = \sum_k \varepsilon_k d_k^{\dagger} d_k + U_{df} \sum_{kk'} (n_f - 1) d_k^{\dagger} d_{k'} , \quad (114)$$

where $n_f = \sum_{\sigma} f_{\sigma}^{\dagger} f_{\sigma}$. The resulting model is a two-channel Anderson model, in which one channel screens, but, does not hybridize, and, the other channel hybridizes, but, does not screen. Assuming localized d electrons gives the model studied by Brito and Frota (1990) and discussed above. For the full model, Takayama and Sakai (1993, 1997) calculated the valence band photoemission spectrum and, surprisingly, found that the effect of U_{dc} in the Kondo regime could be absorbed into a renormalization of the Anderson model parameters. This result was for infinite U , but it should remain valid in the Kondo regime for any finite U provided U_{dc} remains smaller or comparable to U . In contrast to the model described above, where the screening occurs in the hybridizing channel, the effect of the screening interaction in the present model is to reduce the effective hybridization of the valence electrons to the conduction

band, which can be understood as an orthogonality effect. Nevertheless, we conclude from these NRG calculations that in the Kondo regime, and with realistic values of U_{df} (U_{fc}), the valence band photoemission spectra of both the above screening models can be well accounted for by an Anderson model with renormalized parameters.

The two-channel screening model above, has also been studied for finite U (Perakis and Varma, 1994; Perakis *et al.*, 1993). At particle-hole symmetry, increasing U_{dc} reduces both U and the effective hybridization, resulting, for sufficiently large U_{dc} , in an effective attractive local Coulomb interaction and a charge Kondo effect. For still larger U_{dc} , a Kosterlitz-Thouless transition to a non-Fermi liquid state occurs (Perakis and Varma, 1994; Perakis *et al.*, 1993) with a collapse of the Kondo resonance in the valence band photoemission spectrum (Costi, 1997b).

2. Kondo effect in the bulk and underscreened models

Real magnetic impurities in metals have both orbital and spin degrees of freedom and the resulting low-energy effective impurity models can be very complicated (Hewson, 1993). The NRG has been applied so far to models with at most three orbitals, see Sec. IV.D. In cases where the ground state is an orbital singlet, e.g. for dilute Mn ions in metals, Nozières and Blandin (1980) have given a useful classification of the resulting effective single-impurity Kondo models in terms of the size of the impurity spin S and the number of conduction channels, n , which couple to the spin via the Kondo exchange. These multi-channel Kondo models are described by

$$H = \sum_{k\sigma\alpha} \varepsilon_k c_{k\sigma\alpha}^{\dagger} c_{k\sigma\alpha} + J \sum_{\alpha} \mathbf{S} \cdot \mathbf{s}_{\alpha} , \quad (115)$$

where $\alpha = 1, \dots, n$ is the channel index, and the exchange constant, J , is antiferromagnetic. For $n = 2S$, complete screening of the impurity spin takes place leading to a local Fermi liquid at low temperatures. The overscreened case, $n > 2S$, exhibits non-Fermi liquid behavior and is reviewed in Sec. IV.B. In this section, we deal with some recent developments on the fully screened $S = 1/2$ Kondo model, relevant to bulk Kondo impurities, and also describe work on the the single-channel underscreened case, $n = 1 < 2S$.

One of the signatures of the Kondo effect is the appearance in the impurity spectral density of the Kondo resonance at the Fermi level. Point contact spectroscopy on Cu wires containing magnetic impurities, using the mechanically controllable brake junction technique, show a zero bias anomaly, which is attributed to the Kondo resonance (Yanson *et al.*, 1995). In addition, these experiments show that the Kondo resonance splits in a magnetic field. NRG calculations for the $S = 1/2$ Kondo model in a magnetic field do indeed show that the Kondo resonance splits in a magnetic field, B , provided the Zeeman splitting $g_i \mu_B B$ exceeds the Kondo scale T_K (Costi,

2000). Here g_i, μ_B are the impurity g -factor and Bohr magneton and T_K is the Kondo scale defined from the half-width at half-maximum of the $T = 0$ Kondo resonance. The latter is obtained from the imaginary part of the many-body T -matrix, $T_{kk'\sigma}$, for spin σ , defined by

$$G_{kk'\sigma}(\omega) = \delta_{kk'} G_{kk'\sigma}^0 + G_{kk\sigma}^0 T_{kk'\sigma} G_{k'k'\sigma}^0, \quad (116)$$

where $G_{kk'\sigma}(\omega) = \langle\langle c_{k\sigma}; c_{k'\sigma}^\dagger \rangle\rangle$ is the full conduction electron Green function and $G_{kk'}^0$ is the corresponding unperturbed Green function. From the equations of motion for $G_{kk'}$ one finds for the orbitally isotropic Kondo model

$$T_{kk'\sigma}(\omega) = \sigma \frac{J}{2} \langle S_z \rangle + \left(\frac{J}{2}\right)^2 \langle\langle O_\sigma; O_\sigma^\dagger \rangle\rangle, \quad (117)$$

$$O_\sigma = \sum_k \vec{S} \cdot \vec{\tau}_{\sigma\sigma'} c_{k\sigma'}, \quad (118)$$

with $\vec{\tau}$ the Pauli matrices. From the T -matrix one can also extract the transport time and thereby the magnetoresistivity. The latter is found to agree well with experimental data on diluted Ce impurities in LaAl_2 (Costi, 2000).

A recent development has been the realization by Zaránd *et al.* (2004) that one can use the NRG to extract from the many-body T -matrix both elastic and inelastic scattering rates and cross sections. The total scattering cross section, $\sigma_{\text{tot}}(\omega)$, is related to the imaginary part of the T -matrix by the optical theorem

$$\sigma_{\text{tot}}(\omega = \varepsilon_k) = -\frac{2}{v_k} \text{Im}[T_{kk\sigma}(\omega)], \quad (119)$$

with v_k the velocity of electrons with wavevector k . Consequently, by using the expression for the elastic scattering cross section

$$\sigma_{\text{el}}(\omega = \varepsilon_k) = \frac{2\pi}{v_k} \sum_{k'} \delta(\varepsilon_{k'} - \varepsilon_k) |T_{kk'\sigma}(\omega)|^2, \quad (120)$$

Zaránd *et al.* (2004) were able to calculate the inelastic scattering cross section $\sigma_{\text{inel}} = \sigma_{\text{tot}} - \sigma_{\text{el}}$ and the inelastic scattering time, $\tau_{\text{inel}} \sim \sigma_{\text{inel}}^{-1}$. In order to shed some light on the expression for σ_{inel} , consider the Anderson model for a flat band with density of states $N_F = \sum_{k'} \delta(\varepsilon_{k'} - \varepsilon_k)$ and resonant level width $\Delta = \pi N_F V^2$. We have, $T_{kk'} = V^2 G_d$, with $G_d = (\omega - \varepsilon_d + i\Delta - \Sigma(\omega))^{-1}$ and Σ the correlation part of the self-energy. The inelastic scattering cross section for $\omega = \varepsilon_k$ reduces to (Zaránd *et al.*, 2004)

$$\sigma_{\text{inel}} = -\frac{2}{v_k} \frac{V^2 \Sigma''(\omega)}{(\omega - \varepsilon_d - \Sigma'(\omega))^2 + (\Delta - \Sigma''(\omega))^2}, \quad (121)$$

which shows that the inelastic scattering rate vanishes for electrons at the Fermi level due to the Fermi liquid properties of the self-energy. Zaránd *et al.* (2004) evaluated σ_{inel} for the $S = 1/2$ Kondo model via the NRG using the T -matrix in (117) at $T = 0$ and for both zero and finite magnetic fields. The maximum in the inelastic scattering rate occurs close to the $\omega \approx T_K$ (see Fig. 13).

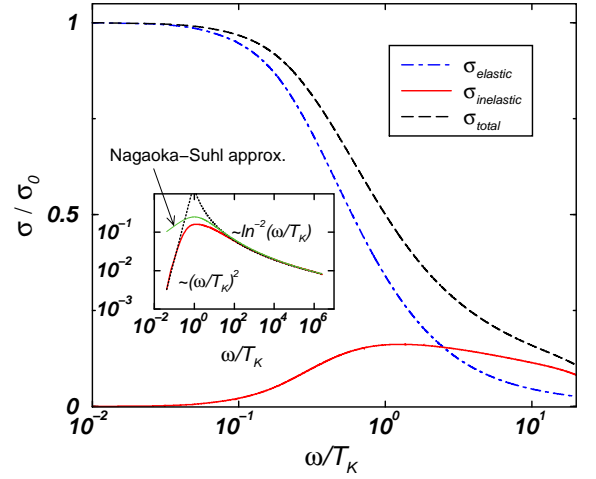


FIG. 13 Elastic, inelastic and total scattering rates for the $S = 1/2$ fully screened Kondo model at $T = 0$ (from Zaránd *et al.* (2004)). The Kondo scale T_K is that from the half-width at half-maximum of the Kondo resonance and is approximately twice that from the $T = 0$ susceptibility defined in (81).

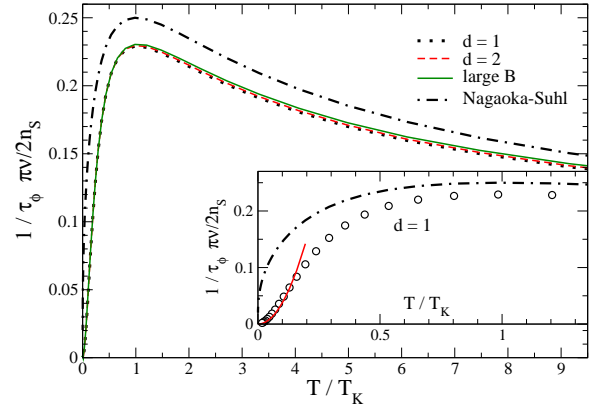


FIG. 14 Universal dephasing rate for the $S = 1/2$ fully screened Kondo model calculated via NRG for Kondo impurities in $d = 1, 2$ dimensional conductors (from Micklitz *et al.* (2006a)). The solid line in the inset is the analytic T^2 result from Fermi liquid theory valid for $T \ll T_K$, where T_K is the scale defined in (81).

A quantity closely related to the inelastic scattering time, $\tau_{\text{inel}} \sim \sigma_{\text{inel}}^{-1}$, is the dephasing time, τ_ϕ , for electrons scattering from magnetic impurities and measured in weak-localization experiments on diffusive conductors (Bäuerle *et al.*, 2005; Mohanty *et al.*, 1997; Pierre *et al.*, 2003; Schopfer *et al.*, 2003). The two quantities are, however, not identical. An exact expression for the dephasing rate of electrons scattering from a dilute concentration of Kondo impurities in a weakly disordered metal has recently been derived (Micklitz *et al.*, 2006a). Fig. 14 shows the dephasing rate as a universal function of T/T_K for the $S = 1/2$ Kondo model, obtained by using the NRG for finite temperature dynamics. The maximum

dephasing rate occurs at $T \approx T_K$ and decreases at first linearly with temperature below T_K and eventually as T^2 in the Fermi liquid region $T \ll T_K$. The magnetic field dependence of the dephasing time, $\tau_\phi(B, T)$, has also been calculated and the expression for the dephasing rate has been generalized to arbitrary dynamical scatterers (Micklitz *et al.*, 2006b). Recent experiments on Fe impurities in Ag wires show better than expected agreement with the theoretical predictions for the dephasing rate of the $S = 1/2$ Kondo model (Alzoubi and Birge, 2006; Mallet *et al.*, 2006). Fe impurities in Ag will have both an orbital moment and a spin $S = 2$ in the absence of crystal field and spin-orbit interactions. Inclusion of the latter, may, however, result in an effective $S = 1/2$ single-channel Kondo model at the low temperatures $T \approx 1K$ of the experiments, thereby helping to explain the good agreement with the $S = 1/2$ theory. At the very lowest temperatures, $T < 0.1T_K$, a slower decay of the dephasing rate has been reported in these experiments, as compared to that expected from a fully screened model. One possible explanation for this is that a small fraction of Fe impurities is only partially screened. Underscreened Kondo models, to which we now turn, are known to give a much slower decay of the dephasing rate below the Kondo scale, see below and Vavilov and Glazman (2003).

Cragg and Lloyd (1979) investigated the single-channel $S = 1$ underscreened Kondo model and showed that its low-energy fixed point corresponds to the spectrum of the ferromagnetic $S' = 1/2$ Kondo model. The deviations from the fixed point at iteration N are of the form $\tilde{J}(N)\vec{S}' \cdot \vec{s}_0$ with $\tilde{J}(N)$ being $\mathcal{O}(-A/(N + C(J)))$ with A being a constant and $C(J)$ depending on J , i.e. the deviations are marginally irrelevant. These calculations were extended by Koller *et al.* (2005b) to models with $S = 1, \dots, 5/2$. They also determined $C(J)$ explicitly for the different cases. Using the relation of N to energy $\omega \sim \Lambda^{-N/2}$, the effective coupling can be written as $\tilde{J}(\omega) \sim 1/\ln(\omega/T_0)$ with T_0 an appropriate Kondo scale (Koller *et al.*, 2005b). Consequently, there are logarithmic corrections to thermodynamic quantities at low temperature, instead of the power-law corrections characteristic of fully screened Kondo models. Non-analytic corrections are also found in dynamical quantities (Koller *et al.*, 2005b; Mehta *et al.*, 2005), so underscreened Kondo models have been termed ‘‘singular Fermi-liquids’’ (Mehta *et al.*, 2005). For, example, the spectral density, $\rho_t(\omega)$, obtained from the T-matrix (117) takes a finite value at the Fermi level, but the approach to this value is non-analytic (Koller *et al.*, 2005b):

$$\rho_t(\omega) = \rho_t(0) - b/\ln(\omega/T_0)^2, \quad (122)$$

Similarly, the $T = 0$ inelastic cross section, also calculated by Koller *et al.* (2005b), decays as $1/\ln(\omega/T_0)^2$, at low energies, and consequently, the dephasing rate decays as $\tau_\phi^{-1}(T) \sim 1/\ln(T/T_0)^2$. As mentioned above, a small fraction of underscreened Fe impurities may explain the excess dephasing observed at the lowest temperatures in the experiments of Mallet *et al.* (2006) and

Alzoubi and Birge (2006). Calculations for the temperature dependence of the resistivity and dephasing rates of the spin $S > 1/2$ underscreened Kondo models and their relevance to Fe impurities in Ag can be found in (Mallet *et al.*, 2006). It is also interesting to note, that calculations for ferromagnetic Kondo models (Koller *et al.*, 2005b) show that all cross sections vanish at the Fermi level with the inelastic part contributing nearly all the scattering in this limit and with the elastic part being negligibly small.

Finally we mention recent work on calculating spatial correlations such as spin-density correlations, $C(x) = \langle \vec{S} \cdot \vec{s}_x \rangle$, around Kondo impurities, where \vec{s}_x is the electron spin density at distance x from the impurity (for earlier work involving perturbative aspects combined with NRG see (Chen *et al.*, 1987, 1992)). Borda (2006) works with Wannier states centered at both the impurity and at x , thereby reducing the problem to a two-impurity type calculation (Sec. IV.C.1). At $T = 0$ and in one dimension, the decay of $C(x)$ is found to change from $1/x$ to $1/x^2$ around $x = \xi_K = \hbar v_F/T_K$, where the coherence length, ξ_K , describes the size of the Kondo screening cloud. At finite temperature, the expected exponential decay of $C(x)$ for $x > \xi_T = \hbar v_F/k_B T$ is recovered.

3. Kondo effect in nanostructures

Recent experimental work has demonstrated the importance of the Kondo effect in determining the low-temperature transport properties of nanoscale size devices such as quantum dots (Cronenwett *et al.*, 1998; Goldhaber-Gordon *et al.*, 1998; van der Wiel *et al.*, 2000). An example of such a device, a quantum dot, is shown in Fig. 15. More complicated devices, such as capacitively coupled double-dots or dots contained in one or two arms of an Aharonov-Bohm interferometer can be built up from this basic unit. A quantum dot consists of a confined region of electrons coupled to leads via tunnel barriers. It may be viewed as an artificial multi-electron atom, in which the different levels (filled, partially filled or empty) couple to electron reservoirs via one or more channels. A quantum dot can be described, in general, by the following multi-level Anderson impurity model

$$\begin{aligned} H &= H_{\text{dot}} + H_c + H_{\text{tun}}, \quad (123) \\ H_{\text{dot}} &= \sum_{i\sigma} \epsilon_{i\sigma} d_{i\sigma}^\dagger d_{i\sigma} + E_C (\hat{N} - \mathcal{N})^2 - J_H \vec{S}^2, \\ H_c &= \sum_{k\alpha\sigma} \epsilon_{k\sigma} c_{k\alpha\sigma}^\dagger c_{k\alpha\sigma}, \\ H_{\text{tun}} &= \sum_{k\alpha i\sigma} t_{\alpha i} \left(d_{i\sigma}^\dagger c_{k\alpha\sigma} + c_{k\alpha\sigma}^\dagger d_{i,\sigma} \right), \end{aligned}$$

where $\epsilon_{i\sigma}$, $i = 1, 2, \dots$, are the dot level energies for spin σ electrons, $\mathcal{N} = \langle \hat{N} \rangle = \sum_{i\sigma} \langle d_{i\sigma}^\dagger d_{i\sigma} \rangle$, is the dot occupancy, E_C is the charging energy, $\vec{S} = \frac{1}{2} \sum_{i\mu\nu} d_{i\mu}^\dagger \vec{\sigma}_{\mu\nu} d_{i\nu}$ is the total spin of the dot and $J_H > 0$ is the Hund’s exchange

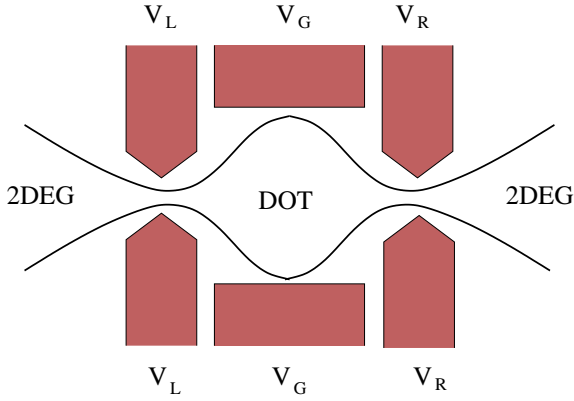


FIG. 15 Schematic top view of a lateral quantum dot, consisting of a confined region of typical size 10-100nm defined in the two-dimensional electron gas (2DEG) of a GaAs/AlGaAs heterostructure. The dot is connected to left and right electron reservoirs. Gate voltages $V_{L,R}$ control the tunnel barriers into and out of the dot, while V_G controls the dot level positions.

coupling. In the above, $\alpha = L, R$ labels left/right lead degrees of freedom and k labels the wavevector of a single transverse channel propagating through the constriction between the 2DEG and the quantum dot. Electrons tunnel into and out of the dot with amplitudes $t_{\alpha i}$ and give rise to a single-particle broadening Γ_i of the levels.

The model above is essentially the same model as the multi-orbital model of Sec. IV.D, used to describe bulk Kondo systems. The novel situation in quantum dots is that parameters such as the tunnel couplings and level positions can be controlled by gate voltages. This allows such models to be experimentally investigated in all physically interesting regimes, such as spin and charge fluctuation regimes, and in principle also to be tuned through quantum phase transitions. In addition, different realizations of quantum dots (nanotubes, vertical dots) may have level degeneracies or near level degeneracies, allowing the effects of Hund's exchange to be investigated. Finally, the devices described by (123) can be driven out of equilibrium by a finite transport voltage, allowing the study of non-equilibrium effects in relatively "simple" quantum many-body systems. This would be one motivation to further develop the NRG to steady-state non-equilibrium situations.

a. Single-level quantum dots In the low-temperature limit, only one or two partially filled levels close to the Fermi level of the leads will be important for transport. The remaining levels will be either filled or empty, and, at the low temperatures of interest for quantum transport, they may be neglected. The simplest model, therefore, to describe low-temperature transport through a quantum dot, is the single-level Anderson impurity model (2) with level position $\varepsilon_1 = \varepsilon_f = -eV_G$ controlled by gate voltage and Coulomb repulsion U given by the charging energy $E_C = U/2$. Only one conduction channel, the

even combination of left and right electron states, $a_{k\sigma}$, below, couples to the local level, as can be seen by using the canonical transformation

$$a_{k\sigma} = (t_L c_{kL\sigma} + t_R c_{kR\sigma}) / \sqrt{t_L^2 + t_R^2}, \quad (124)$$

$$b_{k\sigma} = (-t_R c_{kL\sigma} + t_L c_{kR\sigma}) / \sqrt{t_L^2 + t_R^2}, \quad (125)$$

with $t_\alpha = t_{\alpha i} \delta_{i,1}$. We note that treating the Coulomb interaction classically implies that, for an integer number of electrons on the dot, transport is blocked for large U , since transferring electrons through the dot requires overcoming the large Coulomb repulsion. Glazman and Raikh (1988) and Ng and Lee (1988) pointed out, however, that in the situation where the total spin on the dot is finite, as happens for an odd number of electrons (i.e. for $\mathcal{N} = 1$ in the effective single-level model), one should expect, on the basis of (2), an enhancement of the conductance to its maximum possible value of $G = 2e^2/h$ via the Kondo effect in the limit of zero temperature. A device, representing a tunable Anderson impurity model, was realized (Cronenwett *et al.*, 1998; Goldhaber-Gordon *et al.*, 1998) and the predicted enhancement of the low-temperature conductance for dots with an odd number of electrons was measured and compared (Goldhaber-Gordon *et al.*, 1998) to quantitative NRG calculations (Costi *et al.*, 1994b) such as those shown in Fig. 10 for the conductance in the Kondo regime (see also Izumida *et al.* (2001a)). Tuning the quantum dot to the mixed valence and empty orbital regimes, has enabled also comparisons with theory in those regimes (Costi, 2003; Schoeller and König, 2000).

The frequency dependence of the linear conductance, $G'(\omega)$, of a single-level quantum dot described by (2) has been considered by several authors (Campo, Jr. and Oliveira, 2003; Izumida *et al.*, 1997; Sindel *et al.*, 2005). Sindel *et al.* (2005) calculated $G'(\omega)$, in the Kondo regime at $T = 0$, and extracted also the current noise

$$C(\omega) = \int_{-\infty}^{+\infty} dt e^{i\omega t} [\langle I(0)I(t) \rangle - \langle I \rangle^2], \quad (126)$$

by making use of the fluctuation-dissipation theorem

$$C(\omega) = \frac{2\hbar\omega}{e^{\hbar\omega/k_B T} - 1} G'(\omega). \quad (127)$$

The conductance and spin-resolved conductances of single-level quantum dots in a magnetic field have also been calculated and a strong spin-filtering effect has been observed in the mixed valence regime (Costi, 2001). For spin-filtering effects in quantum dots with ferromagnetic leads see Martinek *et al.* (2003); Simon *et al.* (2006).

One of the hallmarks of the $S = 1/2$ single-channel Kondo effect is the flow of the exchange coupling to strong coupling (Wilson, 1975a). This can be interpreted as resulting in a phase shift of the conduction electrons at the Fermi level, at $T = 0$, of $\delta_\sigma = \pi/2$ (Nozières, 1974).

A direct measurement of this phase shift is possible if one embeds a quantum dot in one arm of an Aharonov-Bohm interferometer. Assuming a single-level Anderson model for the quantum dot and a multi-terminal open geometry, Gerland *et al.* (2000) carried out NRG calculations for the interference term, G_{AB} , whose measurement can be used to extract δ_σ . A similar set-up has been investigated by Hofstetter *et al.* (2001) for the flux dependence $G(\phi)$ of the conductance at $T = 0$ and by Kang *et al.* (2005) for the complex transmission. Izumida *et al.* (1997) calculated $G(\phi)$ for two single-level quantum dots embedded in the arms of an Aharonov-Bohm interferometer. This model, reduces, in general, to a two-channel two-orbital Anderson model, which we discuss next.

b. Two-level quantum dots A quantum dot with two active levels for transport introduces some new physics due to the competition between the level spacing $\delta = \varepsilon_2 - \varepsilon_1$, the charging energy E_C and the Hund's exchange J_H . In particular, a Kondo effect with an even number of electrons on the dot can be realized. This can occur when the dot is occupied with two electrons and $\delta < 2J_H$ so that the ground state of the dot has $S = 1$. Such a two-level dot will, in general, couple to two channels so a $S = 1$ Kondo effect will result, leading to a singlet ground state and an enhanced conductance $G(T)$ at low temperatures. In the opposite case $\delta > 2J_H$ the dot will have $S = 0$, the Kondo effect is absent and the conductance will be low. This behavior is believed to have been measured in the experiments of Sasaki *et al.* (2000) on vertical quantum dots, where a magnetic field was used to decrease the energy splitting, $\Delta_{TS} = \delta - 2J_H$, between the triplet and singlet states, thereby leading to the above mentioned crossover behavior in the conductance at $\mathcal{N} = 2$. Theoretical calculations by Izumida *et al.* (2001b), shown in Fig. 16, are consistent with the experimental results.

The singlet-triplet crossover behavior in a two-level quantum dot can become a quantum phase transition for the special case where only one conduction channel couples to the leads, e.g. when all lead couplings are equal (Hofstetter and Schoeller, 2002; Pustilnik and Glazman, 2001). In this case, for large Hund's exchange, an effective single-channel $S = 1$ underscreened Kondo model results which has a doubly degenerate many-body ground state. For small Hund's exchange, a model with $S = 0$ results having a non-degenerate many-body ground state. A sharp transition separates these two different ground states. As discussed above, however, two channels will, in general, couple to the dot and this will result in perfect screening of the $S = 1$ so that the ground state is always a singlet. Nevertheless, proximity to the singlet-triplet transition can still be seen as signatures in various quantities, such as a non-monotonic dependence of the conductance as a function of magnetic field on the triplet side of the crossover (Hofstetter and Zaránd, 2004). Experiments on lateral quantum dots at the singlet-triplet crossover point (van der Wiel *et al.*, 2002) show behavior

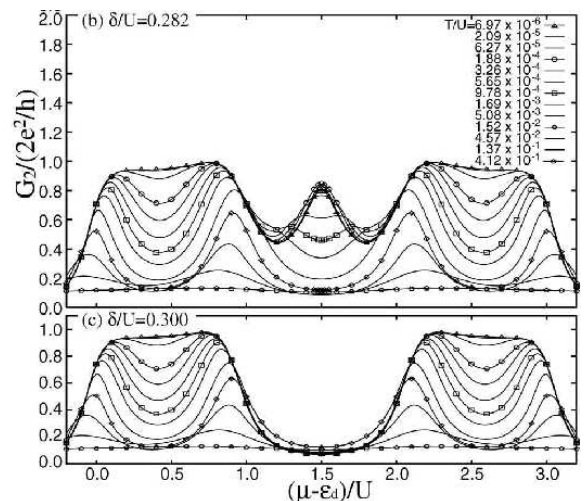


FIG. 16 The singlet-triplet crossover in the linear conductance of the two-channel two-orbital Anderson model including a Hund's exchange J_H , intra- and inter-orbital Coulomb energy, U , levels $\varepsilon_d \pm \delta/2$ and temperature T . Top/bottom panels shows $G(T)$ on the triplet/singlet side of the crossover and $(\mu - \varepsilon_d)/U = 0.5, 1.5, 2.5$ correspond to $\mathcal{N} = 1.0, 2.0, 3.0$ electrons on the dot. Adapted from Sakai and Izumida (2003).

in the differential conductance similar to predictions for the spectral density (Hofstetter and Schoeller, 2002).

The above is only a brief account of the simplest nanostructured devices studied using the NRG. Further applications include numerous studies of double-dot systems, including realizing an $SU(4)$ Kondo state (Borda *et al.*, 2003) and quantum critical points of two-impurity Kondo models (Garst *et al.*, 2004; Zaránd *et al.*, 2006; Zhu and Varma, 2006) (see Sec. IV.C.1), static and dynamics of double-dots (Galpin *et al.*, 2006a,b), double dots with only one dot coupled to the leads (Cornaglia and Grepel, 2005b), applications to quantum tunneling in molecular magnets (Romeike *et al.*, 2006a,b), a novel Kondo effect in a $\nu = 1$ integer quantum Hall system (Choi *et al.*, 2003b) and the conductance of ultrasmall tunnel junctions (Frota, 2004; Frota and Flensberg, 1992).

B. Two-channel Kondo physics

Nozières and Blandin (1980) have proposed a variation of the Kondo model in which the localized spin couples to *two* conduction bands. The Hamiltonian of this two-channel Kondo model is given by

$$H = \sum_{k\sigma\alpha} \varepsilon_k c_{k\sigma\alpha}^\dagger c_{k\sigma\alpha} + J \sum_{\alpha} \mathbf{S} \cdot \mathbf{s}_{\alpha}, \quad (128)$$

with $\alpha = 1, 2$ the channel index and \mathbf{S} (\mathbf{s}_{α}) the spin operators of the impurity (the conduction band electrons at the impurity site with channel index α).

An important feature of this model is the overscreening of the impurity spin: in the strong-coupling limit, the spins of both conduction bands try to screen the impurity spin, so that again a net spin 1/2 object is formed. In other words, the strong-coupling fixed point at $J = \infty$ (which gives rise to the Fermi-liquid fixed point in the single-channel case) is unstable and an intermediate-coupling fixed point is realized. This new fixed point shows a variety of non-Fermi liquid properties such as

- a divergence of the specific heat ratio $C/T = \gamma \propto \ln T$ and of the spin susceptibility $\chi \propto \ln T$ for $T \rightarrow 0$;
- an anomalous Wilson ratio $R = \chi/\gamma = 8/3$, in contrast to the result for the standard Kondo model $R = 8/4 = 2$;
- a zero-point entropy of $\frac{1}{2} \ln 2$, indicating that ‘half’-fermionic excitations (Majorana fermions) play a crucial role for the structure of the fixed point.

We have discussed these features already in the section on the calculation of thermodynamic and static quantities, see Fig. 6. An extensive review of the two-channel Kondo model, its physical properties and its relevance for non-Fermi liquid behavior in real materials has been given in Cox and Zawadowski (1998). This paper also reviews the earlier NRG-calculations for this model.

Historically, the two-channel Kondo model has been the first application of the NRG to a quantum impurity model in which the physics is not governed by the Fermi liquid fixed point of the standard Kondo model. In this sense, the early work of Cragg *et al.* (1980) on the two-channel Kondo model opened the way for a variety of investigations of more complex impurity models, displaying both Fermi liquid and non-Fermi liquid fixed points. Due to the importance of this and following work, we want to focus this section purely on two-channel Kondo physics and shift the discussion of other multi-band models to the section on orbital effects (Sec. IV.D).

As discussed already in Sec. II, the truncation of states within the iterative diagonalization scheme severely limits the applicability of the NRG to multi-band models. In the calculations of Cragg *et al.* (1980), the iterations were observed to break down only after a few (approximately twelve) steps. The source of this problem is mainly the small number of states ($N_s \approx 400$) used in this work, which would correspond to keeping $N_s \approx \sqrt{400} = 20$ states in a one-channel calculation. Specific symmetries of the two-channel Kondo model, such as the total axial charge, have been used to reduce the matrix sizes in the diagonalization (Pang and Cox, 1991), but later calculations showed that by simply increasing the number of states, the iterations can be stabilized sufficiently. Independent of the value of N_s , it is important to avoid any symmetry breaking due to the truncation of states.

In order to approach the non-Fermi liquid fixed point within only a few iterations, Cragg *et al.* (1980) and Pang and Cox (1991) used large values of the exchange

coupling J or large values of the discretization parameter (up to $\Lambda = 9.0$). Nevertheless, these calculations give the correct fixed point spectrum of the (isotropic) two-channel Kondo model with the characteristic structure of excitations at energies $1/8, 1/2, 5/8, 1$, etc., at least for the lowest-lying excited states. Figure 17 shows a typical flow diagram for parameters $J = -0.05D$, where $2D$ is the bandwidth of the featureless conduction band density of states, $\Lambda = 4$, and $N_s = 4900$, for both even (dashed curves) and odd NRG iterations (full curves) (for similar plots, see Fig. 1 in Cragg *et al.* (1980) and Figs. 1 and 2 in Pang and Cox (1991)). After some initial even-odd oscillations, the flow reaches the non-Fermi liquid fixed point which does not show any even-odd effect. Note that this feature is by no means related to the non-Fermi liquid properties of the model; it just reflects the fact that in each iteration, two sites are added to the chain so that (for particle-hole symmetry) the number of electrons in the ground state is always even.

Comparison with conformal field theory calculations (Affleck *et al.*, 1992) gave an excellent agreement with the NRG for both the excitation spectrum and the corresponding degeneracies. Such a comparison, however, requires the extrapolation of the NRG fixed point spectra for $\Lambda \rightarrow 1$ (see Fig. 9 in Affleck *et al.* (1992); the analysis is not quite satisfactory for $\Lambda < 2$ and it would be interesting to repeat these calculations using larger values of N_s). This work, and the previous paper by Pang and Cox (1991), also focussed on the stability of the non-Fermi liquid fixed point against various perturbations. As it turns out, the non-Fermi liquid fixed point is stable against anisotropy in the exchange interaction ($J_z \neq J_\perp$) but unstable against both the presence of a magnetic field and the lifting of the exchange symmetry between the two channels ($J_a \neq J_b$). In the latter case, a temperature scale $T^* \propto (J_a - J_b)^2$ for the crossover between the non-Fermi liquid fixed point at intermediate temperatures and the stable Fermi liquid fixed point at $T \rightarrow 0$ has been found. These instabilities have been later

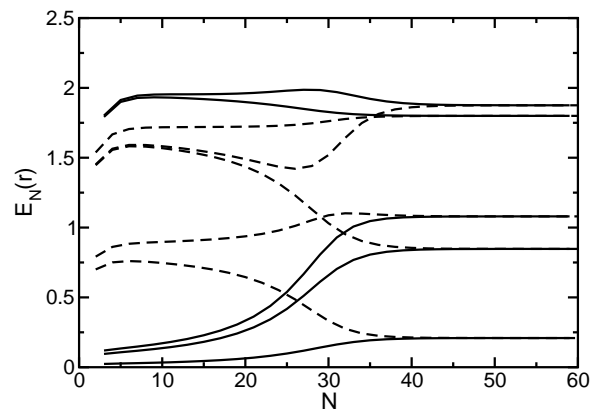


FIG. 17 Flow diagram of the lowest lying many-particle levels for the isotropic two-channel Kondo model (even iterations dashed curves, odd iterations full curves).

investigated in more detail in Yotsuhashi and Maebashi (2002), via the calculation of the impurity entropy and the crossover temperature.

Further investigations concerning the stability of the non-Fermi liquid fixed point have been performed in Pang (1994) (flavor exchange coupling) and Kusunose and Kuramoto (1999); Kusunose *et al.* (1996) (effect of repulsion among conduction electrons and potential scattering).

A ‘pedestrian’ approach for the understanding of the two-channel Kondo model was introduced by Coleman *et al.* (1995). The authors of this work argued that the two conduction bands in the two-channel Kondo model can be replaced by a *single* conduction band, with a coupling between impurity spin \mathbf{S} to both spin σ and isospin τ of the conduction band. The isospin τ takes into account the charge degrees of freedom of the conduction band and the compactified ‘ σ - τ ’ model takes the form

$$H = \sum_{k\sigma} \varepsilon_k c_{k\sigma}^\dagger c_{k\sigma} + J (\mathbf{S} \cdot \sigma + \mathbf{S} \cdot \tau) . \quad (129)$$

This model can be related to an Anderson-type model (the ‘O(3)-symmetric’ Anderson model) via a Schrieffer-Wolff transformation (Coleman and Schofield, 1995).

It has been later verified with the NRG approach (Bulla and Hewson, 1997) that these compactified models indeed show many of the anomalous non-Fermi liquid properties of the two-channel Kondo model, although these models do not allow for an overscreening of the impurity spin. Furthermore, the structure of the non-Fermi liquid fixed point has been studied in detail. It turns out that the many-particle spectrum of this fixed point is composed of single Majorana fermion excitations (Bulla *et al.*, 1997a). This information can then be extended to the fixed point structure of the two-channel Kondo model which can be described by two towers of excitations which are both composed of Majorana fermions, see Sec. VIII in Bulla *et al.* (1997a).

Naturally, we expect that the non-Fermi liquid properties of the two-channel Kondo model are also visible in its dynamic properties, but, unfortunately, detailed and comprehensive NRG calculations for the dynamics have not been performed so far. Apart from a brief sketch of the results for the T -matrix and the magnetic susceptibility in Sakai *et al.* (1993a), the published data are only for models equivalent to the two-channel Kondo model in certain limits.

It has been argued in Bradley *et al.* (1999) that the dynamical spin-susceptibility $\chi(\omega)$ of the compactified models introduced above is exactly equivalent to that of the two-channel Kondo model, and that this equivalence holds for the *full* frequency range. The NRG-results show, for example, a $\ln(\omega)$ -divergence of $\chi'(\omega)$ for $\omega \rightarrow 0$, in agreement with the results of Sakai *et al.* (1993a). On the other hand, there is no counterpart of the single-particle dynamics calculated by Bradley *et al.* (1999) in the two-channel Kondo model.

The two-channel Anderson model investigated in Anders (2005) is connected to the two-channel Kondo model via a Schrieffer-Wolff transformation (note that this only holds when the impurity degrees of freedom in the Anderson model are written in terms of Hubbard operators which include the channel index). This connection is clearly visible in thermodynamic properties, such as the zero-point entropy of $\frac{1}{2} \ln 2$. Again, the single-particle dynamics (spectral function and self-energy) do not have a counterpart in the two-channel Kondo model. Concerning the results for the dynamic susceptibility $\chi(\omega)$ presented in Anders (2005), a comparison to the corresponding results of the two-channel Kondo model has not yet been done.

There is an ongoing discussion about the observability of two-channel Kondo physics in experiments for a variety of systems. Let us stress here that the instability of the non-Fermi liquid fixed point itself does not exclude its observation. As for any system with a quantum critical point, the corresponding anomalous properties dominate a significant fraction of the finite-temperature phase diagram (determined by the critical exponent) so that a precise tuning of the Hamiltonian parameters is not required. Nevertheless, two-channel Kondo physics is now mainly discussed within systems in which alternative degrees of freedom (such as orbital quantum numbers) take the role of spin or channel in the Hamiltonian Eq. (128); one example is the quadrupolar Kondo model which is discussed in detail in Cox and Zawadowski (1998).

Here we want to briefly discuss NRG calculations for two-channel Kondo physics in quantum dot systems (Anders *et al.*, 2004, 2005; Lebanon *et al.*, 2003a,b). Within a model of a quantum box coupled to the leads via a single-mode point contact (see Fig. 1 in Lebanon *et al.* (2003b)), the physics at the degeneracy points of the Coulomb blockade staircase can be directly connected to that of the two-channel Kondo model. Here the two charge configurations in the box play the role of the impurity spin and the physical spin of the conduction electrons corresponds to the channel index. For such a system, the NRG allows the non-perturbative calculation of the charge inside the box and the capacitance in the whole parameter regime. The results show, for example, that the shape of the charge steps is governed by the non-Fermi liquid fixed point of the two-channel Kondo model.

To conclude this section let us mention that there are models involving a more complicated orbital structure of the impurity – including, for example, excited crystalline electric field levels – which reduce to the two-channel Kondo model in certain limits or which display non-Fermi liquid fixed points of the two-channel Kondo type. NRG-studies of such models can be found in Hattori (2005); Koga and Cox (1999); Koga and Shiba (1995, 1996); Sakai *et al.* (1997). Overscreening can also be realized in single-channel models when the conduction electron spin exceeds the impurity spin, for a discussion of this issue see for example Kim *et al.* (1997). We note also

a recent study (Kolf and Kroha, 2006) showing an exponential dependence of the Kondo scale on $-1/JN_F$ and $-JN_F$, for small and large coupling cases respectively, which may explain the absence of a broad distribution of Kondo scales in nanoconstrictions with two-channel Kondo impurities.

C. Impurity quantum phase transitions

In this section, we focus on models which, as a function of one or more couplings in the model, give rise to a phase transition in the ground state. Typically, this is due to a competition between the Kondo effect on the one hand, which tends to favor a strong-coupling ground state with a screened or partially screened local moment, and some competing mechanism, which leads to a ground state with a free or almost free local moment. In general, such phase transitions are termed ‘impurity quantum phase transitions’ (for recent reviews, see Bulla and Vojta (2003); Vojta (2006)), as they are only observable in the *impurity* contribution to physical properties and not connected to possible phase transitions in the bulk to which the impurity couples.

As impurity quantum phase transitions are usually associated with a vanishing low-energy scale, the NRG method is ideally suited to their investigation, allowing their detection and characterization with very high accuracy. This is most evident for continuous transitions where the critical exponents connected to the quantum critical point can only be calculated when a large range of energy or temperature scales is accessible. In this section we give an overview on NRG-results for multi-impurity models (Sec. IV.C.1), models with locally critical behavior (Sec. IV.C.2), and models with magnetic impurities in superconductors (Sec. IV.C.3). Note that impurity quantum phase transitions are also observed in models which are discussed in other sections of this review: the non-Fermi liquid fixed point of the two-channel Kondo model Sec. IV.B can be viewed as a quantum critical point when the control parameter ‘channel anisotropy’ is tuned through zero; locally critical behavior is also connected to models with coupling to a bosonic bath as discussed in Sec. IV.E.

1. Multi-impurity physics

An early extension of the NRG to more complex systems was the study of the two-impurity $S = 1/2$ Kondo model (Jones and Varma, 1987; Jones *et al.*, 1988), whose Hamiltonian is given by

$$H = \sum_{k\sigma} \varepsilon_k c_{k\sigma}^\dagger c_{k\sigma} + J_K \sum_{l=1}^2 \mathbf{S}(\mathbf{R}_l) \cdot \mathbf{s}(\mathbf{R}_l) + I_D \mathbf{S}(\mathbf{R}_1) \cdot \mathbf{S}(\mathbf{R}_2). \quad (130)$$

Here, $\mathbf{s}(\mathbf{R}_l)$ is the conduction electron spin density at the impurity site \mathbf{R}_l and $J_K > 0$ is the antiferromagnetic Kondo exchange. The first two terms in Eq. (130) are sufficient to generate an indirect RKKY interaction I_{RKKY} between the impurity spins. In some contexts a direct exchange interaction among the impurity spins of strength I_D can arise (Jones and Varma, 1987), so the last term has been added. The net effective exchange interaction between the spins is given by $I_{\text{eff}} = I_D + I_{\text{RKKY}}$ and can be either ferromagnetic $I_{\text{eff}} < 0$ or antiferromagnetic $I_{\text{eff}} > 0$. The properties of the model then depend solely on the ratio I_{eff}/T_K , where T_K is the single-ion Kondo scale, and the details of the dispersion relation ε_k . The model in Eq. (130) also arises in the Schrieffer-Wolff limit (Schrieffer and Wolff, 1966) of the two-impurity Anderson model, which in the notation introduced in Eq. (2) reads

$$H = \sum_{k\sigma} \varepsilon_k c_{k\sigma}^\dagger c_{k\sigma} + \sum_{l=1}^2 \sum_{\sigma} \varepsilon_{l\sigma} f_{l\sigma}^\dagger f_{l\sigma} + U \sum_{l=1}^2 f_{l\uparrow}^\dagger f_{l\uparrow} f_{l\downarrow}^\dagger f_{l\downarrow} + \frac{1}{\sqrt{N}} \sum_{l=1}^2 \sum_{k\sigma} V_k \left(e^{i\mathbf{R}_l \cdot \mathbf{k}} f_{l\sigma}^\dagger c_{k\sigma} + \text{h.c.} \right) + I_D \mathbf{S}(\mathbf{R}_1) \cdot \mathbf{S}(\mathbf{R}_2). \quad (131)$$

The motivation to study such two-impurity models originally arose in the context of heavy fermions. In these systems, the competition between the local Kondo exchange and the intersite RKKY interaction is expected to lead to a phase transition between non-magnetic and magnetically ordered ground states as a function of I_{eff}/T_K (Doniach, 1977). The nature of this quantum phase transition remains an open question in heavy fermion physics (v. Löhneysen *et al.*, 2006). It is therefore of some interest to investigate the possibility of a transition in the two-impurity problem as this might shed light on the physics of heavy fermions.

Jones *et al.* (1988) have established that such a phase transition can occur under certain conditions, see below, in the particle-hole symmetric two-impurity Kondo model. This can be seen by considering the strong-coupling limits $I_{\text{eff}} \rightarrow \pm\infty$ (Affleck *et al.*, 1995). For $I_{\text{eff}} \rightarrow -\infty$ the two spins combine to form a spin $S = 1$ interacting antiferromagnetically with two conduction channels (characterized by even/odd parity) with, in general, energy dependent coupling strengths $J_e(k), J_o(k)$ replaced in (Jones *et al.*, 1988) by constants (see below). The resulting two-stage Kondo effect progressively screens the $S = 1$ spin down to a singlet and leads to a Fermi-liquid ground state characterized by phase shifts $\delta_{e,o}$ for electrons in the even/odd parity channels. The assumed particle-hole symmetry and the nature of the strong-coupling ground state ensures that these phase shifts will be exactly $\pi/2$ (Millis *et al.*, 1990). In the other limit, $I_{\text{eff}} \rightarrow \infty$, the spins form an intersite sin-

glet $S = 0$ and the Kondo effect is absent so that the phase shifts are exactly zero. Since the fixed points at $I_{\text{eff}} = \pm\infty$ are both stable and characterized by different (constant) phase-shifts, it follows that there can be an unstable fixed point at some critical intermediate value of the intersite exchange, I_c , at which the phase shifts change discontinuously. This phase transition has also been found in the particle-hole symmetric two-impurity Anderson model (Paula *et al.*, 1999; Sakai and Shimizu, 1992a). Jones *et al.* (1988) estimates $I_c/T_K \approx 2.2$. The associated critical point has been characterized using conformal field theory (Affleck and Ludwig, 1992; Affleck *et al.*, 1995) and bosonization (Gan, 1995), and the physics is found to be similar to that of the two-channel Kondo model. In particular, the staggered susceptibility, $\chi_s(T)$, diverges logarithmically at low temperature and the residual entropy has the same value as in the two-channel Kondo model $S(T=0) = \ln\sqrt{2}$ (Gan, 1995). In contrast $C(T)/T = \gamma$ is predicted to remain finite exactly at the critical point, in contrast to the behavior in the two-channel Kondo model. Close to the critical point, conformal field theory predicts $\gamma \sim (I_{\text{eff}} - I_c)^{-2}$, in agreement with numerical results (Jones, 1990). The level structure of the fixed point at quantum criticality agrees well with NRG calculations and is rather complex, exhibiting a hidden $SO(7)$ symmetry (Affleck *et al.*, 1995).

For generic situations, the natural energy dependence of $J_{e/o}$ obtained from transforming the Kondo model (130) or Anderson model (131) as described below in Eq. (132), as well as a charge transfer term of the form $t \sum_{\sigma} (f_{1\sigma}^{\dagger} f_{2\sigma} + h.c.)$ in the two-impurity Anderson model, breaks particle-hole symmetry and destroys the critical point (Affleck *et al.*, 1995; Sakai *et al.*, 1990). A similar charge transfer term involving conduction electrons has the same effect in the two-impurity Kondo model (Zaránd *et al.*, 2006; Zhu and Varma, 2006). Potential scattering, if it does not induce charge transfer, breaks particle-hole symmetry but may not affect the critical point, for a discussion see Affleck *et al.* (1995); Zaránd *et al.* (2006); Zhu and Varma (2006). Thus, in general the quantum phase transition discussed above will be absent in the two-impurity models (130) and (131), although signatures of it might still be observable as crossover behavior in various properties. We note briefly here the case of Ising coupled spins $IS_z(\mathbf{R}_1)S_z(\mathbf{R}_2)$. In this case, the ground state for large I will be doubly degenerate as compared to that for small I where the Kondo effect screens the individual spins to singlets, so a quantum phase transition separating these two different ground states arises and is found to be of the Kosteritz-Thouless type (Garst *et al.*, 2004).

In order to formulate Eq. (130) or (131) as a linear chain problem for treatment with the NRG, one needs an orthonormal basis set. The local conduction electron states on the impurity sites in Eq. (130) are not orthogonal. Following Jones and Varma (1987), the Kondo exchange part of Eq. (130) is rewritten in terms of orthonor-

mal even (e) and odd (o) parity states for the conduction electrons. This results in more complicated interaction terms; in particular, one will obtain two exchange couplings $J_{e/o}(k)$, with $J_e(k) \neq J_o(k)$ in general, which will depend on momentum or energy (Jones and Varma, 1987). The precise form of $J_{e/o}(k)$ will depend on the details of the band-structure of the conduction electrons. For free electrons in $D = 3$ it can be approximated as (Jones and Varma, 1987; Sakai *et al.*, 1990)

$$J_{e/o}(k) \approx J_K \left[1 \pm \frac{\sin kR}{kR} \right],$$

where $R = |\mathbf{R}_1 - \mathbf{R}_2|$. Jones and Varma (1987) used constant couplings $J_{e/o}(k) \approx J_{e/o}(k_F)$ to obtain for the interaction part of the Hamiltonian (130)

$$\begin{aligned} H_{\text{int}} = & \mathbf{S}^{(e)} \cdot \sum_{\alpha\beta} \left[J_e c_{e\alpha}^{\dagger} \sigma_{\alpha\beta} c_{e\beta} + J_o c_{o\alpha}^{\dagger} \sigma_{\alpha\beta} c_{o\beta} \right] + \\ & \mathbf{S}^{(o)} \cdot \sum_{\alpha\beta} \left[i\sqrt{J_e J_o} c_{e\alpha}^{\dagger} \sigma_{\alpha\beta} c_{o\beta} + h.c. \right] + \\ & I_D \mathbf{S}(\mathbf{R}_1) \cdot \mathbf{S}(\mathbf{R}_2), \end{aligned} \quad (132)$$

where $\mathbf{S}^{(e/o)} := \mathbf{S}(\mathbf{R}_1) \pm \mathbf{S}(\mathbf{R}_2)$. The conduction electron Hamiltonian now consists of two decoupled linear chains with even and odd parity symmetry. By neglecting the energy dependence of the couplings a particle-hole symmetric model results. This is the form used by Jones *et al.* (1988) to investigate the phase transition discussed above. The results of retaining the full energy dependence of the couplings, using for example the formulation of Sec. II, will be described below. We note here that from the NRG point of view the two-impurity models (131) and (130) present a challenging task because, as in the case of the two-channel Kondo model (128), the ‘‘impurity’’ now couples to *two semi-infinite chains*. Consequently, the Hilbert space grows by a factor 16 in each NRG step. While this is still manageable with modern computer resources, it is apparent that larger clusters or more complex situations quickly become too expensive to be treated with NRG with sufficient accuracy, although the flow of the many-body eigenstates can still be used to identify fixed points and thus qualitatively describe the physics of more complicated systems, like the two-channel two-impurity Kondo model (Ingersent *et al.*, 1992) and the three-impurity Kondo model (Ingersent *et al.*, 2005). In high-symmetry situations even a calculation of thermodynamical quantities has been performed recently for three-impurity models (Žitko and Bonča, 2006a). However, for a reliable calculation of *dynamics* or in situations with less symmetries in the system – e.g. in an external magnetic field – additional tools like the ones described in section III.A.4 allowing one to work with large $\Lambda \gg 1$ and so maintain low truncation errors should be useful.

The generic two-impurity Anderson model (131), including a charge transfer term, has been studied by Sakai and coworkers (Sakai and Shimizu, 1992a,b; Sakai *et al.*,

1990) using the NRG. Single particle and magnetic excitation spectra were calculated and in the case of particle-hole symmetry, Sakai *et al.* (1993a) showed that on passing through the transition, a peak in the impurity single-particle spectra sharpened at $I_{\text{eff}} = I_c$ into a cusp and turned into a dip for $I_{\text{eff}} > I_c$. In the generic case, the regime with Kondo screening, $|I_{\text{eff}}| \ll T_K$, and the non-local singlet regime, $I_{\text{eff}} \gg T_K$, are connected via a smooth crossover (Campo, Jr. and Oliveira, 2004; Sakai and Shimizu, 1992a,b; Sakai *et al.*, 1990; Silva *et al.*, 1996).

Results from thermodynamic calculations are shown in Fig. 18 for the squared effective magnetic moment taken from Silva *et al.* (1996) for the two-impurity Kondo model with $I_D = 0$. In these calculations $I_{\text{eff}} = I_{\text{RKKY}}$ and the energy dependence of $J_{e/o}(k)$ is crucial to generate the intrinsic RKKY exchange interaction I_{RKKY} . Using the result for free electrons in three dimensions (Sakai *et al.*, 1990), an approximate formula for the energy dependence of the coupling constants is (Silva *et al.*, 1996)

$$J_{e/o}(\epsilon) = J_K \left(1 \pm \frac{\sin[k_F R(1 + \epsilon)]}{k_F R(1 + \epsilon)} \right) \quad (133)$$

with $\epsilon \in [-1, 1]$, k_F the Fermi momentum of the conduction states. For the derivation of Eq. (133) a linearized dispersion relation $\epsilon_k \approx \frac{D}{k_F}(k - k_F)$ was assumed and $D = 1$ used as energy scale.

Dependent on the value of $k_F R$, different regimes can then be identified (see, for example, Fig. 18): For $k_F R \rightarrow$

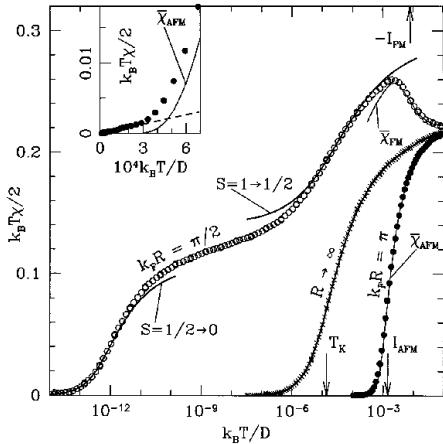


FIG. 18 Effective local moment $\mu^2(T) := T \cdot \chi_{\text{imp}}(T)$ for the two-impurity Kondo model (131) for the three regimes described in the text. Figure taken from Silva *et al.* (1996). The arrows indicate the Kondo scale $T_K = 1.4 \times 10^{-4}$, and the RKKY interactions for ferromagnetic ($I_{\text{FM}} = -8 \times 10^{-3}$) and antiferromagnetic cases ($I_{\text{AFM}} = 3 \times 10^{-3}$).

∞ we have $I_{\text{RKKY}} = 0$, single-impurity physics dominates and no non-local magnetic exchange is generated, as expected (Jones and Varma, 1987). For $k_F R = \pi/2$,

the RKKY exchange $I_{\text{RKKY}} = I_{\text{FM}}$ is ferromagnetic, with $|I_{\text{RKKY}}|/T_K \gg 1$ and a two-stage screening scenario arises: First, the system locks into an $S = 1$ state at high temperatures due to the RKKY interaction. In the intermediate temperature regime this triplet is screened to a doublet via the even channel, which then is further screened to a singlet by the odd channel. Finally, for $k_F R = \pi$, the RKKY exchange $I_{\text{RKKY}} = I_{\text{AFM}}$ is antiferromagnetic with $I_{\text{RKKY}}/T_K \gg 1$ and a non-local singlet is formed eventually. Similar results for entropy and specific heat of the two-impurity Kondo model, exhibiting a smooth change of physical properties with changing I_{RKKY} , can be found in Campo, Jr. and Oliveira (2004).

We note, here, that while two-impurity models with energy independent coupling constants are crude approximations in the context of bulk Kondo impurities and heavy fermions, these can, however, be realized in quantum dots. Correspondingly, they have been proposed to describe various extensions of single quantum dots and studied in this context with NRG by several groups (Boese *et al.*, 2002; Borda *et al.*, 2003; Hofstetter and Schoeller, 2002; Vojta *et al.*, 2002a; Zaránd *et al.*, 2006; Žitko and Bonča, 2006b) over the past years. Since modern nanostructure technology permits a rather broad tailoring of such mesoscopic objects, the models discussed typically introduce additional interactions as compared to the conventional two-impurity Anderson model (131) like capacitive couplings (Boese *et al.*, 2002; Borda *et al.*, 2003; Hofstetter and Schoeller, 2002) or direct hopping (Dias da Silva *et al.*, 2006; Žitko and Bonča, 2006b). Consequently, these extended models show a much larger variety in intermediate- and low-temperature fixed points than the bare model (131), ranging from conventional Kondo effect over a two-stage Kondo effect (Jayaprakash *et al.*, 1981; Vojta *et al.*, 2002a), two-channel physics as intermediate fixed-point (Žitko and Bonča, 2006a,b) to quantum-phase transitions (Vojta *et al.*, 2002a; Zaránd *et al.*, 2006; Zhu and Varma, 2006; Žitko and Bonča, 2006b).

2. Local criticality

The term ‘local criticality’ has been first used in the context of phase transitions in certain heavy fermion systems, such as $\text{CeCu}_{6-x}\text{Au}_x$ (Si *et al.*, 2001, 1999; v. Löhneysen *et al.*, 2006). It has been argued that the quantum critical point separating the magnetically ordered and the paramagnetic phases at $T = 0$ is characterized by critical excitations which are local. This observation raised a considerable interest in models which show such locally critical behavior: these are either lattice models studied within certain extensions of DMFT (see also Sec. V.B) or impurity models as discussed in this section. Such impurity models might not be directly connected to the locally critical behavior in heavy fermion systems, nevertheless, the insights gained in studying im-

purity models might be helpful in constructing theories for lattice systems (for a general discussion of the relation between quantum impurity physics and the physics of lattice systems, see Bulla (2006)).

Let us focus here on the soft-gap Anderson model, originally proposed by Withoff and Fradkin (1990). The Hamiltonian is the same as the one for the standard single-impurity Anderson model Eq. (2), but the hybridization function is assumed to have a power-law form

$$\Delta(\omega) = \Delta_0 |\omega|^r \quad \text{with } r > -1, \quad (134)$$

either valid over the whole frequency range or restricted to some low-frequency region. The competing mechanisms leading to a quantum phase transition in this model are local moment formation (favored by increasing U) and screening of the local moments. For values of the exponent $r > 0$, corresponding to a soft-gap in $\Delta(\omega)$, there are less degrees of freedom available to screen the moment and a quantum phase transition occurs at some finite value of Δ_0 .

This quantum phase transition and the physical properties in the whole parameter regime have been studied in detail with a variety of techniques (for an overview, see Bulla and Vojta (2003); Vojta (2006) and the introductory parts in Lee *et al.* (2005)). The NRG method has been particularly helpful to clarify the physics of the soft-gap Anderson model (and the related Kondo version of the model) as we shall briefly discuss in the following. The technical details necessary to apply the NRG to the soft-gap Anderson model have already been introduced in Sec. II, see also Bulla *et al.* (1997b).

Thermodynamic and static properties of the various phases of the soft-gap Anderson and Kondo models have been presented in Chen and Jayaprakash (1995a), Ingersent (1996), Bulla *et al.* (1997b), and Gonzalez-Buxton and Ingersent (1998). The most comprehensive review of these results is given in Gonzalez-Buxton and Ingersent (1998). This paper covers the discussion of thermodynamic properties and the analysis of the various fixed points also for the under-screened spin-1 Kondo model and the (overscreened) two-channel Kondo model (both with a soft-gap in the conduction electron density of states).

The key role of particle-hole symmetry has been identified in Ingersent (1996) and investigated in more detail in Gonzalez-Buxton and Ingersent (1998). As shown, for example, in Fig. 5 in this work, the line of quantum critical points separating the local moment (LM) and strong-coupling (SC) phases is restricted to $0 < r < 1/2$ in the particle-hole symmetric case (for $r > 1/2$, only the LM phase exists). This is different in the asymmetric case where transition line extends up to $r \rightarrow \infty$. Particle-hole symmetry also influences the physical properties of the various fixed points. The symmetric SC fixed point, for example, shows a residual magnetic moment of $\chi_{\text{imp}} = r/(8k_B T)$ and a residual entropy of $S_{\text{imp}} = 2rk_B \ln 2$, whereas both values are zero in the asymmetric SC fixed point. The appearance of unstable

fixed points is particularly complex in the asymmetric case, see, for example, the schematic flow diagrams of Fig. 16 in Gonzalez-Buxton and Ingersent (1998).

The impurity spectral function of the symmetric soft-gap Anderson model was first investigated in Bulla *et al.* (1997b): the spectral function shows a divergence $A(\omega) \propto |\omega|^{-r}$ for both the SC and quantum critical phases whereas it goes as $A(\omega) \propto |\omega|^r$ in the LM phase (for the behavior in the asymmetric case, see the discussion in Sec. IV.C.3).

In the symmetric SC phase, the product $F(\omega) = c|\omega|^r A(\omega)$ (where the prefactor cancels the divergence in the spectral function) contains a generalized Kondo resonance at the Fermi level with a pinning of $F(\omega = 0)$ (for a properly chosen constant c) and a width that goes to zero upon approaching the quantum critical point. This feature, together with the scaling properties and the low-energy asymptotics has been discussed in detail in Bulla *et al.* (2000), based on both the results from NRG and from the local moment approach (also described earlier in Logan and Glossop (2000)).

Dynamical properties at the quantum critical point are particularly interesting: Ingersent and Si (2002) have shown that the dynamical susceptibility at the critical point exhibits ω/T -scaling with a fractional exponent, similar to the locally critical behavior in the heavy fermion systems mentioned above. This result also implies that the critical fixed point is interacting, in contrast to the stable fixed points (SC and LM) which both can be composed of non-interacting single-particle excitations.

The interacting fixed point of the symmetric soft-gap model has been further analyzed in Lee *et al.* (2005). The general idea of this work can be best explained with Fig. 19 which shows the dependence of the many-particle spectra for the various fixed points on the exponent r .

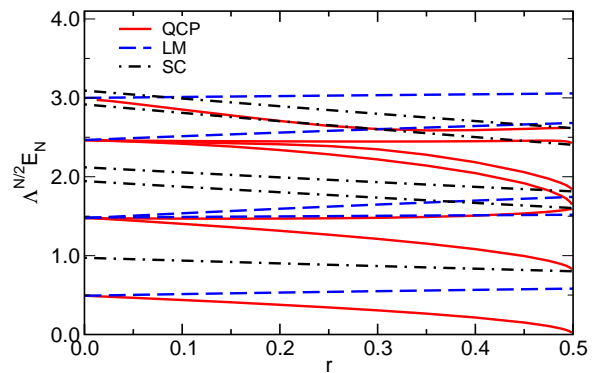


FIG. 19 Dependence of the many-particle spectra for the three fixed points of the particle-hole symmetric soft-gap Anderson model on the exponent r : SC (dot-dashed lines), LM (dashed lines), and the (symmetric) quantum critical point (solid lines). (Figure adapted from Lee *et al.* (2005)).

For the limits $r \rightarrow 0$ and $r \rightarrow 1/2$, the many-particle spectra of the quantum critical point approach those of the LM and SC fixed points, respectively. The deviations and splittings of the spectra at the quantum critical

point close to these limits can then be understood from a proper perturbational analysis using suitable marginal operators. Information on these operators can be extracted from epsilon-expansion techniques, as shown in Lee *et al.* (2005).

The case of negative exponents in the hybridization function, $\Delta(\omega) \propto |\omega|^r$ with $-1 < r < 0$, where the soft-gap turns into a divergence at the Fermi level, has been analyzed in Vojta and Bulla (2002a) in the context of the Kondo model with both ferromagnetic and antiferromagnetic values of J . The behavior of this class of models turns out to be rather complex, see the schematic flow diagrams of Fig. 1 in this work. A remarkable feature here is the appearance of a *stable* intermediate coupling fixed point with universal properties corresponding to a fractional ground-state spin.

The case of a hard gap in the hybridization function, that is $\Delta(\omega) = 0$ within a certain gap region around the Fermi level, can be viewed as the $r \rightarrow \infty$ -limit of the soft-gap case, provided the powerlaw is restricted to the gap region $|\omega| \leq E_g/2$, with E_g the width of the gap.

From a technical point of view, two different strategies have been developed to apply the NRG to the hard-gap case. Takegahara *et al.* (1992) and Takegahara *et al.* (1993) considered the case of a small but finite value of $\Delta(\omega)$ in the gap region, $\Delta(\omega) = \bar{\Delta}$ for $|\omega| \leq E_g/2$, and based their conclusions on the extrapolation $\bar{\Delta} \rightarrow 0$. In this approach, the standard NRG for non-constant hybridization functions as described in Sec. II can be applied.

If, on the other hand, the value of $\bar{\Delta}$ is set to zero from the outset, the NRG approach has to be modified. As discussed in Chen and Jayaprakash (1998), the logarithmic discretization of a $\Delta(\omega)$ with a hard gap results in a discretized model which maps onto a chain with a *finite* number of sites, M , with E_g of the order of Λ^{-M} . The iterative diagonalization then has to be terminated at site M . Thermodynamic properties at temperatures $T < E_g$ can nevertheless be computed using the Hamiltonian of the final iteration (see Chen and Jayaprakash (1998) where also a variety of correlations functions have been calculated for both the Kondo and the Anderson model with a hard gap).

Certain features of the soft-gap case with finite r are also visible in the fully gapped case. As expected from the discussion above, there is no transition in the particle-hole symmetric case, but a transition exists as soon as one is moving away from particle-hole symmetry (Chen and Jayaprakash, 1998; Ingersent, 1996; Takegahara *et al.*, 1992). This transition turns out to be of first order.

3. Kondo effect in superconductors

Let us now consider magnetic impurities in superconducting hosts. In this case, the screening of the magnetic moments competes with Cooper pair formation of

the conduction electrons. We therefore expect a quantum phase transition from a screened phase to a local moment phase upon increasing the value of the superconducting gap, Δ , similar to the phase transitions in the soft-gap (and hard-gap) impurity models discussed in Sec. IV.C.2. In fact, a relation between impurity models in superconductors and those in metallic hosts with a soft or hard gap can be established as discussed below.

The first applications of the NRG to magnetic impurities in superconductors focused on the *s*-wave case (Sakai *et al.*, 1993b; Satori *et al.*, 1992), with the standard Kondo Hamiltonian Eq. (115) supplemented by the BCS pairing interaction

$$-\Delta \sum_k \left(c_{k\uparrow}^\dagger c_{-k\downarrow}^\dagger + c_{-k\downarrow} c_{k\uparrow} \right) .$$

Several strategies have been developed to transform the Hamiltonian including the BCS-term onto a semi-infinite chain which can then be diagonalized iteratively in the usual way. Satori *et al.* (1992) performed a sequence of transformations, including a Bogoliubov and a particular particle-hole transformation, to map the original model onto a Hamiltonian which conserves particle number (this is somewhat easier for the numerical implementation though not absolutely necessary). The approach in Sakai *et al.* (1993b) leads to the same Hamiltonian, the difference here is that the Bogoliubov transformation is performed *before* the logarithmic discretization. In both cases, the semi-infinite chain contains a staggered potential of the form

$$-\Delta \sum_{n=0}^{\infty} (-1)^n \left(c_{n\uparrow}^\dagger c_{n\uparrow} + c_{n\downarrow}^\dagger c_{n\downarrow} \right) .$$

This term does not fall off exponentially as the other terms in the chain-Hamiltonian so that the NRG-iterations should be terminated a few steps after the characteristic scale ω_N of the chain Hamiltonian H_N has reached the superconducting gap Δ . This procedure still allows to access the properties of the localized excited state within the energy gap whose position and weight can now be determined in the full parameter space (in contrast to previous investigations, see the references in Satori *et al.* (1992)). Figure 20 shows position and weight of the localized excited state as a function of T_K/Δ (T_K is determined from the corresponding Kondo model with $\Delta = 0$). The position changes its sign when T_K is of the order of Δ (the precise value depends on the model), corresponding to a change of the ground state from doublet for small T_K/Δ to singlet for large T_K/Δ . This quantum phase transition can be characterized as a level crossing transition (see Fig. 5 in Satori *et al.* (1992)) and is not connected to quantum critical behavior.

These studies of impurities in *s*-wave superconductors have been later extended to more complex impurity models. Yoshioka and Ohashi (1998) investigated the case of an anisotropic interaction between impurity and conduction electron spin, with basically the same NRG approach

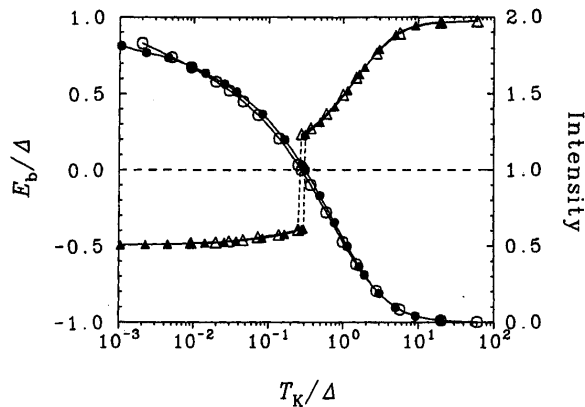


FIG. 20 Position E_b and weight (intensity) of the localized excited state as a function of T_K/Δ for the Kondo model in an s -wave superconductor. At $T_K/\Delta \approx 0.2$, the position changes its sign and the weight jumps by a factor of 2, see also Fig. 2A in Sakai *et al.* (1993b).

as in Sakai *et al.* (1993b). The phase diagram of this model turns out to be much more complex than the one for the isotropic case. For example, *two* localized excited states with different energies appear in certain regions of the parameter space.

Yoshioka and Ohashi (2000) considered the Anderson version of the impurity model with coupling to an s -wave superconductor. From a technical point of view, this case is different to the corresponding Kondo model since the sequence of transformations used in, for example, Sakai *et al.* (1993b) now produce an extra impurity term of the form $\delta(f_{\uparrow}^{\dagger}f_{\downarrow}^{\dagger} + h.c.)$, so that the whole Hamiltonian does no longer conserve charge (note that the parameter δ is zero for the particle-hole symmetric case). The results for the Kondo regime of this model are, as expected, the same as those obtained previously, but the approach of Yoshioka and Ohashi (2000) also allows to study other parameter ranges of the model, such as the mixed valent regime.

It is important to note here that the final Hamiltonian used in Satori *et al.* (1992) and Sakai *et al.* (1993b) for the NRG iteration is the same as the one for an impurity in a non-superconducting host with a gapped density of states (which corresponds to the quasiparticle density of states of the superconductor). In addition, the sequence of transformations also generates a potential scattering term. In the light of the results for the hard-gap impurity models (Sec. IV.C.2) this potential scattering term is essential to observe the quantum phase transition from a screened to an unscreened phase.

The question now arises, whether the quasiparticle density of states can be used as the sole bath characteristic (possibly supplemented by a potential scattering term) in more general situations, such as impurities in unconventional superconductors. Before we address this issue, let us have a look at what happens when a simi-

lar sequence of transformations as in the s -wave case is applied to impurity models in p - or d -wave superconductors.

Matsumoto and Koga (2001, 2002) considered the Kondo model with a coupling of the impurity spin to superconductors with $p_x + ip_y$ and $d_{x^2-y^2} + id_{xy}$ symmetry (with extensions to spin-polarized superconducting states investigated in Koga and Matsumoto (2002a) and to $S = 1$ impurities in Koga and Matsumoto (2002b)). The quasiparticle density of states in these cases also shows a full gap, as for s -wave superconductors, but the sequence of transformations now results in a model with a coupling of the impurity to *two* angular momenta of the conduction electrons. NRG calculations for this two-channel model give a ground state which is always a spin doublet for arbitrary values of T_K/Δ , in contrast to the s -wave case, and no level crossing is observed. This is supported by calculations of the impurity susceptibility which show that the effective magnetic moment is always finite, although strongly reduced with increasing T_K/Δ (Matsumoto and Koga, 2002). The authors of this work argued that the orbital dynamics of the Cooper pairs is responsible for the ground state spin.

This interpretation has been questioned in Fritz and Vojta (2005), where it was shown that, indeed, the local quasiparticle density of states of the superconductor is the only necessary ingredient in a number of cases, in particular for unconventional superconductors. Applied to the model studied in Matsumoto and Koga (2001), this means that the results of the NRG calculations for the effective two-channel model can also be understood from a single-band calculation where screening is absent for a hard-gap density of states and particle-hole symmetry.

The results of Fritz and Vojta (2005) also have important consequences for the study of impurities in unconventional superconductors with $d_{x^2-y^2}$ symmetry. In this case, the mappings which have been used for the models discussed above result in an impurity model with coupling to infinitely many bands to which the NRG clearly cannot be applied. For certain geometries, however, it is sufficient to consider only the quasiparticle density of states which, for a point-like impurity, shows a soft-gap with exponent $r = 1$.

This simplification has already been used earlier in Vojta and Bulla (2002b) (at that time it has been argued to be a reasonable approximation). The results of this work are therefore both valid for the soft-gap Kondo model and for impurities in d -wave superconductors. Vojta and Bulla (2002b) have motivated their investigations with experimental results for non-magnetic impurities in cuprate superconductors which have been seen to generate magnetic moments. As discussed in this work, an effective model for this problem then takes the form of a Kondo model in a d -wave superconductor. Connections to experimental results can indeed be made within this framework. For example, the T -matrix $T(\omega)$ displays a very narrow peak at finite frequencies with the

peak energy corresponding to the energy scale which vanishes at the quantum phase transition from a screened to an unscreened moment. A very similar peak has been observed in STM-experiments.

This work has been later extended in Vojta *et al.* (2002b), where the effects of local and global magnetic fields have been investigated. For the case of a local field h_{loc} , the quantum phase transition for zero field persists for $h_{\text{loc}} \neq 0$, but for a global field, the quantum phase transition turns into a sharp crossover since the global field induces a finite spectral weight at the Fermi level.

The investigations described so far are mainly applicable to impurities in the bulk or on the surface of a superconducting host. A different geometry is realized in quantum dot systems (see Sec. IV.A.3). For superconducting leads, such a setup introduces a new control parameter to the problem, that is the phase difference, $\Phi = \Phi_L - \Phi_R$, between the phases of the two superconducting leads. The resulting Josephson current, in particular the transition from 0- to π -junction behavior, has been studied in detail in Choi *et al.* (2004a) and Oguri *et al.* (2004).

Choi *et al.* (2004a) investigated various static and dynamic properties for this geometry with identical s -wave superconductors as the two leads. For zero phase difference, $\Phi = 0$, the local pairing correlation shows a sign change at $T_K/\Delta \approx 0.42$. Physically, this is connected to the same quantum phase transition as described above since for $\Phi = 0$ and identical leads the model can be mapped onto the same model as discussed in Satori *et al.* (1992). For finite phase difference (or for non-identical leads) the system remains a two-channel problem and the NRG analysis is more complicated. Nevertheless, detailed information on ground state properties such as the single-particle excitation spectrum have been obtained in Choi *et al.* (2004a) and interpreted as a phase-dependent formation of Andreev bound states.

In Oguri *et al.* (2004), the Hamiltonian of an Anderson impurity coupling to two superconducting leads has been considerably simplified by studying the limit $|\Delta_L| \gg |\Delta_R|$ in which the model can be mapped exactly onto a single-channel one with an extra superconducting gap on the impurity. Results for this limit show that the phase difference changes both the energy and the wave function of the bound state. In particular, the phase difference appears to work against the screening of the local moment.

D. Orbital effects

1. Multi-orbital Anderson model

The physics of the Kondo effect requires the existence of local magnetic moments, as realized, for example, in systems with open d or f shells, such as transition metal or rare-earth impurities in non-magnetic host metals. For such systems, the local Coulomb correlations and Hund's exchange determine the electronic structure of the impu-

rity and they usually give rise to finite spin and orbital magnetic moments. Thus, a realistic description of such impurities in solids, requires taking both spin and orbital magnetic moments into account. The same is true for the compounds of transition metal, rare-earth and actinide elements, where the interplay of orbital and spin degrees of freedom gives rise to very rich phase diagrams (Imada *et al.*, 1998). Among the methods to theoretically study the properties of these materials, the dynamical mean-field theory (see Sec. V) has become a standard approach. Since in this approach one ends up with an effective quantum impurity problem which retains the full local orbital and spin structure of the original lattice system, the development of a reliable method to solve quantum impurity models with orbital and spin degrees of freedom is of crucial importance.

In this section we, therefore, discuss the application of the NRG to situations where orbital and spin degrees of freedom are both present. Some orbital effects in quantum dots have been discussed in Sec. IV.A.3 and will be discussed further below. The appropriate model is again a suitable extension of the single-impurity Anderson model (2) and is given by

$$\begin{aligned}
H = & \sum_k \sum_{mm'\sigma} \epsilon_{k\sigma}^{mm'} c_{km\sigma}^\dagger c_{km'\sigma} \\
& + \sum_{m\sigma} \varepsilon_{m\sigma} n_{m\sigma}^f + \frac{U}{2} \sum_{m\sigma} n_{m\sigma}^f n_{m\bar{\sigma}}^f \\
& + \frac{2U' - J}{4} \sum_{m \neq m'} \sum_{\sigma\sigma'} n_{im\sigma}^f n_{im'\sigma'}^f \\
& - J \sum_{m \neq m'} \vec{S}_m^f \cdot \vec{S}_{m'}^f \\
& - \frac{J}{2} \sum_{m \neq m'} \sum_{\sigma} f_{m\sigma}^\dagger f_{m\bar{\sigma}}^\dagger f_{m'\bar{\sigma}} f_{m'\sigma} \\
& + \frac{1}{\sqrt{N}} \sum_k \sum_{mm'\sigma} \left(V_{k\sigma}^{mm'} c_{km\sigma}^\dagger f_{m'\sigma} + \text{h.c.} \right), \tag{135}
\end{aligned}$$

where m labels the orbital degrees of freedom, and $n_{m\sigma}^f = f_{m\sigma}^\dagger f_{m\sigma}$, with $\vec{S}_m^f = \frac{1}{2} \sum_{\alpha\beta} f_{m\alpha}^\dagger \vec{\sigma}_{\alpha\beta} f_{m\beta}$. In addition to the intra-orbital Coulomb term U also occurring in (2), the following interaction terms are present now: An inter-orbital Coulomb repulsion U' and an exchange term J . The exchange term we have split in accordance with standard notation (Imada *et al.*, 1998) into a Heisenberg-like spin-exchange term (Hund's coupling) and an orbital exchange term. To account for the proper combination of operators in the general exchange contribution, an additional part proportional to J appears in the inter-orbital Coulomb term. For free atoms, rotational invariance usually imposes $U' = U - 2J$ as constraint for the different Coulomb parameters (Imada *et al.*, 1998). Further modifications to the model (135) can be made, to take into account, for example, spin-orbit and crystal-field effects.

The mapping of (135) onto a linear-chain model, see Eq. (26) of Sec. II, clearly leads to m semi-infinite conduction chains coupled to the local Hamiltonian, which in turn means that at each step of the iterative diagonalization, the Hilbert space increases by a factor 4^m . For large m , this exponential increase in the number of states makes the NRG truncation scheme useless, because the number of states one can keep is way too small to allow for a reasonable accuracy. Thus, calculations for the model (135) involving a full d shell ($m = 5$), or even a full f shell ($m = 7$), and taking into account all interactions seem to be impossible.

In practice, however, one is typically not interested in rotationally invariant situations, as described by (135), but in situations where the impurity is embedded in the crystalline environment of a solid. The reduced point-group symmetry due to the crystalline electric field, then leads to a splitting of the orbital degeneracy. The energy associated with this crystal-field splitting can be much larger than the temperatures one is interested in experiments, for example in $3d$ transition metals. Furthermore, the local Coulomb interaction can lead to a localization of electrons in the lower crystal-field multiplets, as happens, for example, in the case of manganese in a cubic environment (Imada *et al.*, 1998). In this case, these states form a localized spin according to Hund's rules. For manganese, for example, this results in a high-spin state ($S = 3/2$) of the threefold degenerate t_{2g} orbitals, which couples ferromagnetically to the twofold degenerate e_g electrons. Thus, the actual number of relevant orbitals, and thus the number of semi-infinite chains coupling to the local Hamiltonian, may be considerably reduced. Similar effects can be observed in the higher rare-earth elements, for example in gadolinium.

In case the local point-group symmetry is reduced sufficiently, one may, in fact, be left with a localized spin S coupled to a single spin-degenerate, correlated orbital hybridizing with conduction states. This Kondo-Anderson model is given by (2) supplemented with the ferromagnetic exchange term $-J_H \vec{S} \cdot \vec{s}_d$, with \vec{s}_d the spin-density of the correlated level in the Anderson model. Such a Kondo-Anderson model was studied by Sakai *et al.* (1996) and Peters and Pruschke (2006) and shown to exhibit different types of screening, ranging from conventional Kondo screening to two-stage screening and local singlet formation or two-channel Kondo effect.

2. NRG calculations – an overview

A first serious attempt to study effects of true orbital degeneracy with NRG can be found in Sakai *et al.* (1989). However, the authors did not study the full Hamiltonian (135), but a $SU(N)$ version of it, using values of N ranging from two (i.e. the standard single-impurity Anderson model (2)) to five, representative for rare-earth ions like samarium or thulium in solids under the influence of a crystalline field (Allub and Aligia, 1995; Shimizu *et al.*,

1990). Since the $SU(N)$ model has a large degeneracy of the individual levels, it allows for a considerable reduction of the sizes of the individual Hilbert spaces in the diagonalization. This enabled the authors to use the NRG to calculate physical properties including dynamical quantities and to study, for example, the development of the Kondo temperature or the behavior of the Abrikosov-Suhl resonance as function of degeneracy (Sakai *et al.*, 1989; Shimizu *et al.*, 1990). Similar investigations for the model (135) with fixed orbital degeneracy $m = 2$ in the presence of a magnetic field were presented in the work by Zhuravlev *et al.* (2004), a comparison with STM experiments for Cr(001) surface states by (Kolesnychenko *et al.*, 2005), and a detailed study of the dependence of the low-energy properties of the multi-orbital Anderson model for $m = 2$ with $J > 0$ by Pruschke and Bulla (2005). Furthermore, from the fixed-point level structure, interesting information about quantities like “residual interactions” in the heavy Fermi liquid state can be extracted (Hattori *et al.*, 2005). In particular for an f^2 ground state – as possibly realized in uranium compounds – a subtle enhancement of interorbital interactions can be observed (Hattori *et al.*, 2005), which can lead to superconducting correlations in a triplet channel when used as effective interaction in a model for heavy-fermion superconductivity.

While these studies deal with the conventional Kondo effect in multi-orbital models, it was noted (Cox and Zawadowski, 1998) that for higher rare-earth and actinide elements the orbital structure in connection with spin-orbit coupling and crystal-field effects can result in an orbital multiplet structure that leads to the two-channel Kondo effect (see Sec. IV.B). Multi-orbital models of that type were studied by Sakai *et al.* (1996), Shimizu *et al.* (1998), Shimizu *et al.* (1999a,b), Koga (2000) and Hattori and Miyake (2005), covering a wide range of aspects possibly realized in actinide heavy-fermion systems. The authors could identify parameter regimes where non-Fermi liquid properties related to the two-channel Kondo effect can be observed and could, in addition, identify relevant symmetry breakings like crystal-field splittings or external fields that eventually lead to conventional Kondo physics below a temperature scale connected to the energy scale of the symmetry breaking.

As mentioned in the introductory remarks of this section, the crystal-field splitting is usually much larger than the relevant low-energy scales. However, this does not need to be true in general. Besides uranium-based compounds (Kusunose, 2005), a possible example where the crystal-field splitting can actually be of the order of the Kondo scale is $\text{Ce}_{1-x}\text{La}_x\text{Ni}_9\text{Ge}_4$ (Scheidt *et al.*, 2005). For higher temperatures, the ground state seems to be a quadruplet, i.e. it can be described by a multi-orbital Anderson model with $m = 2$. The states building this quadruplet are obtained from spin-orbit coupled f states, which results in different g -factors for its members. Interestingly, these different g -factors in connection with the

small crystal-field splitting can lead to a behavior, where specific heat and susceptibility seem to have different low-energy scales (Scheidt *et al.*, 2005). However, this discrepancy can be resolved by observing that the difference in g -factors leads to a “protracted” screening behavior for the specific heat in NRG calculations, while the system as a whole has only one, but strongly reduced Kondo temperature. In addition, NRG results for the low-energy spin dynamics show an anomalous energy dependence, which again is related to the difference in the g -factors entering the local susceptibility (Anders and Pruschke, 2006).

Conventionally, the Hund’s exchange J appearing in (135) is positive, i.e. mediating a ferromagnetic interaction leading to Hund’s first rule. However, there may be circumstances, for example a coupling to vibrational modes, Jahn-Teller distortions or crystal-field induced anisotropies (De Leo and Fabrizio, 2004), which can lead to an effective $J < 0$, i.e. *antiferromagnetic* exchange. In this case we encounter a situation similar to the multi-impurity problem (see section IV.C.1), where the exchange was generated by the RKKY effect. Under special conditions, an antiferromagnetic exchange then could lead to a quantum phase transition between Kondo screening and non-local singlet formation. Consequently, one may expect a similar transition for the multi-orbital model, too, when one varies J from the ferromagnetic to the antiferromagnetic regime. Such a model was studied by Fabrizio *et al.* (2003) and, with an additional single-ion anisotropy, by De Leo and Fabrizio (2004) for two orbitals, i.e. $m = 2$. The model indeed shows the anticipated quantum phase transition, which in this case is driven by the competition between the local antiferromagnetic exchange coupling and the hybridization to the band states. Furthermore, one can study the development of the spectral function across this transition (De Leo and Fabrizio, 2004). One finds that the impurity spectral function on the Kondo screened side of this transition shows a narrow Kondo peak on top of a broader resonance. As has also been observed by Pruschke and Bulla (2005) and Peters and Pruschke (2006) this broad resonance is related to the exchange splitting J . The narrow peak transforms into a pseudogap on the unscreened side of the transition.

De Leo and Fabrizio (2005) have demonstrated that NRG calculations are possible even for $m = 3$, using the symmetries of the model to reduce the size of the Hilbert space blocks. They studied a realistic model for a doped C_{60} molecule, taking into account the orbitally threefold degenerate t_{2u} lowest unoccupied molecular orbitals. Again, coupling to vibrational modes can lead to Hund’s coupling with negative sign. In this regime, one observes non-Fermi liquid behavior for half-filling $n = 3$, associated with a three-channel, $S = 1$ overscreened Kondo model. Interestingly, the critical susceptibilities associated with this non-Fermi liquid appear to be a pairing in the spin and orbital singlet channel (De Leo and Fabrizio, 2005). Using conformal field the-

ory, the authors could deduce the residual entropy as

$$S(T = 0) = \frac{1}{2} \ln \left[\frac{\sqrt{5} + 1}{\sqrt{5} - 1} \right],$$

and also corresponding fractional values for the local spectral function $\rho_f(0)$ at the Fermi energy, which leads to non-unitary values in the conductance, and a non-integer power law for $\rho_f(\omega) - \rho_f(0)$. Away from half filling a quantum phase transition between Kondo screening and local singlet formation as function of filling occurs (De Leo and Fabrizio, 2005). Multi-orbital models also arise in the context of quantum dots as described in Sec. IV.A.3 and Sec. IV.C.1.

3. Selected results on low-energy properties

In the following we shall present some selected results for the properties of the multi-orbital Anderson model (135) with orbital degeneracy $m = 2$.

a. Effect of Hund’s coupling As a first example we want to discuss the influence of Hund’s exchange J on the low-energy properties of the model Eq. (135). We consider only $J \geq 0$, i.e. the usual atomic ferromagnetic exchange, and in addition use the constraint $U' = U - 2J$. For the conduction electrons we assume a band with a flat density of states $\rho_c^{(0)}(\epsilon) = N_F \Theta(D - |\epsilon|)$ and use $\Delta_0 = \pi V^2 N_F$ as energy scale. Results for thermodynamic quantities are shown in Fig. 21. The calculations are for $U/\Delta_0 = 16\pi$

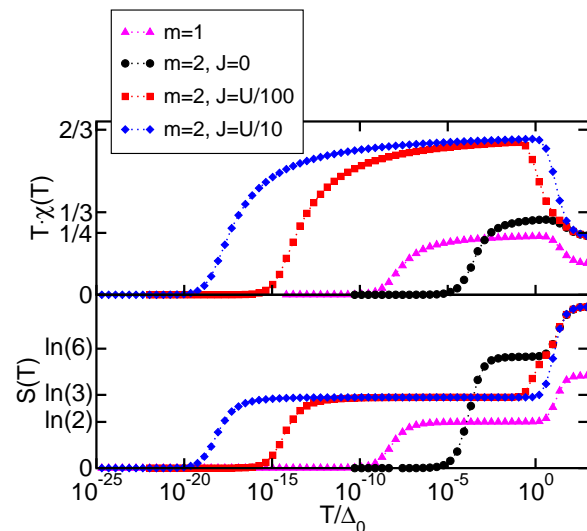


FIG. 21 Effective local moment $T \cdot \chi(T)$ (upper panel) and entropy (lower panel) for a two-orbital impurity Anderson model. Model parameters are $U/\Delta_0 = 16\pi$ at particle-hole symmetry. For comparison the results for one orbital are included (triangles).

and particle-hole symmetry. NRG parameters are $\Lambda = 5$

and 2500 retained states per iteration. The triangles are results from a calculation with $m = 1$ for the same parameters. For $J = 0$ (circles) we find the behavior expected for a $SU(4)$ symmetry, i.e. an energy scale, T_K^m , that is related to the Kondo scale at $m = 1$, $T_K^{m=1}$, by $T_K^m = (T_K^1)^{1/m}$. However, even a small Hund coupling $J = U/100$ leads to a dramatic reduction of T_K , which increases with increasing J . Let us note here, that for $J > 0$ the effect of the orbital exchange term in (135) is negligible, i.e. the results are indistinguishable if one does the calculation with and without this contribution. Very often, the orbital exchange term is neglected in theoretical studies of transition metal compounds (Imada *et al.*, 1998), an approximation which is supported by the above result.

b. Crystal-field effects Recently, experiments showing unusual specific heat, magnetic susceptibility and resistivity data for $Ce_{1-x}La_xNi_9Ge_4$ have drawn a lot of attention, because this material has the “largest ever recorded value of the electronic specific heat at low temperature” (Killer *et al.*, 2004) of $\gamma(T) = \Delta C/T \approx 5JK^{-2}mol^{-1}$. While the γ coefficient continues to rise at the lowest experimentally accessible temperature, the magnetic susceptibility tends to saturate at low temperatures.

One possible scenario (Anders and Pruschke, 2006; Scheidt *et al.*, 2005) to account for the behavior of $Ce_{1-x}La_xNi_9Ge_4$ is a competition of Kondo and crystal-field effects which leads to a crossover regime connecting incoherent spin scattering at high temperatures and a conventional strong-coupling Fermi liquid regime at temperatures much lower than the experimentally accessible 30mK. The Hund’s rule ground state of Ce^{3+} with $j = 5/2$ is split in a tetragonal symmetry (Killer *et al.*, 2004) in three Kramers doublets. If the crystalline electric field (CEF) parameters are close to those of cubic symmetry, the two low-lying doublets $\Gamma_7^{(1)}$ and $\Gamma_7^{(2)}$, originating from the splitting of the lowest Γ_8 quartet, are well separated from the higher lying Γ_6 doublet. Ignoring this Γ_6 doublet, we can discuss two extreme limits. In a cubic environment, the CEF splitting vanishes and the low-temperature physics is determined by an $SU(4)$ Anderson model. In a strongly tetragonally distorted crystal, on the other hand, the crystal-field splitting of the quartets is expected to be large. In this case, the low-temperature properties are determined by an $SU(2)$ Anderson model. If, however, the material parameters lie in the crossover regime where the effective low-temperature scale T^* is of the order of the crystal-field splitting $\delta_{CEF} = E_{\Gamma_7^{(2)}} - E_{\Gamma_7^{(1)}}$, then the excited doublet will have significant weight in the ground state so that the total magnetic response differs from a simple $SU(4)$ Anderson model.

Such a situation can be captured by a $SU(4)$ Anderson model with infinite U whose Hamiltonian is given by

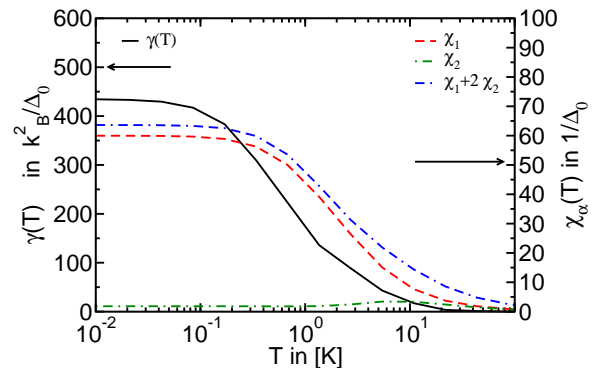


FIG. 22 Comparison between $\gamma(T) = C(T)/T$ versus T and the susceptibility contributions of the two doublets versus T for $E_{\Gamma_7^{(1)}}/\Delta_0 = -8.5$, $\delta_{CEF}/\Delta_0 = 0.015$ and $g_2^2/g_1^2 = 2$. The contribution of the lower doublet, χ_1 is much larger than the one of the upper doublet, χ_2 . NRG parameters are $\Lambda = 4$ and 1500 states kept in each step.

(Scheidt *et al.*, 2005)

$$H = \sum_{k\alpha\sigma} \epsilon_{k\alpha\sigma} c_{k\alpha\sigma}^\dagger c_{k\alpha\sigma} + \sum_{\alpha\sigma} E_{\alpha\sigma} |\alpha\sigma\rangle \langle \alpha\sigma| \quad (136)$$

$$+ \sum_{k\alpha\sigma} V_{\alpha\sigma} \left(|\alpha\sigma\rangle \langle 0| c_{k\alpha\sigma} + c_{k\alpha\sigma}^\dagger |0\rangle \langle \alpha\sigma| \right),$$

where $|\alpha\sigma\rangle$ represents the state $\Gamma_7^{(\alpha)}$ with spin σ and energy $E_{\alpha\sigma}$ on the Ce 4*f* shell, and $c_{k\alpha\sigma}$ annihilates a corresponding conduction electron state with energy $\epsilon_{k\alpha\sigma}$. Note that locally only fluctuations between an empty and a singly occupied Ce 4*f* shell are allowed.

While the entropy and specific heat for the model (136) can be calculated in the usual way, the Ce contribution to the susceptibility requires some more thought, because the spin-orbit coupled states $\Gamma_7^{(\alpha)}$ have different g -factors, which we label by g_α . Thus, the total susceptibility is given by (Scheidt *et al.*, 2005)

$$\chi_{\text{imp}} = \mu_B^2 \sum_{\alpha} g_\alpha^2 \chi_{\text{imp}}^{(\alpha)}. \quad (137)$$

While the g -factors are, in principle, determined by the CEF states of the multiplets, we view them as adjustable parameters and fix them together with $E_{\Gamma_7^{(\alpha)}}$ by comparing with experiment (Scheidt *et al.*, 2005).

The comparison between the temperature dependence of $\gamma(T)$ and $\chi(T)$ is shown in Fig. 22 assuming a ratio of $g_2^2/g_1^2 = 2$ for a good fit to the experimental data (Scheidt *et al.*, 2005). The ground state doublet dominates the magnetic response at low temperature and tends to saturate at temperatures higher than the γ -coefficient, consistent with the experiments (Killer *et al.*, 2004). We find this behavior only for CEF-splittings $\delta_{CEF} \approx T^*$ (δ_{CEF}) while for much larger or much smaller values $\chi(T)$ and $\gamma(T)$ saturate simultaneously.

E. Bosonic degrees of freedom and dissipation

In the models discussed so far, the bath consists of non-interacting fermionic degrees of freedom while the impurity is either represented by a fermion or a spin. This section deals with quantum impurity systems involving *bosonic* degrees of freedom. We distinguish between models in which only a small number of bosonic degrees of freedom couples to the impurity and models where the impurity couples to a bosonic bath (corresponding to an infinite number of bosonic degrees of freedom).

As we will see below, the first case can be dealt with in the usual scheme, provided the subsystem consisting of impurity and bosons can be treated as a large impurity which is then coupled to the fermions. The second class, however, requires a different set-up for the NRG-procedure.

Let us first consider the so-called Anderson-Holstein model (Hewson and Meyer, 2002) in which the impurity is linearly coupled to a single bosonic degree of freedom (typically a phonon mode):

$$H = H_{\text{SIAM}} + \lambda(b^\dagger + b) \sum_{\sigma} f_{\sigma}^{\dagger} f_{\sigma} + \omega_0 b^\dagger b, \quad (138)$$

with H_{SIAM} the Hamiltonian of the single-impurity Anderson model as in Eq. (2). The coupling to the bosonic operators (b^\dagger and b) does not influence the mapping of the conduction electron part of the Hamiltonian to a semi-infinite chain. This means that the bosons enter the iterative diagonalization only in the very first step in which the coupled impurity-boson subsystem has to be diagonalized. The fact that only a limited number of bosonic states n_b can be taken into account in this diagonalization imposes some restrictions on the parameters λ (the electron-phonon coupling strength) and ω_0 (the frequency of the phonon mode). As discussed in Hewson and Meyer (2002), it should be sufficient to include a number of $n_b \approx 4\lambda^2/\omega_0^2$ bosonic states for the initial diagonalization. With an upper limit of $n_b \approx 1000$ this means that the limit $\omega_0 \rightarrow 0$ (with fixed λ) cannot be treated within this setup.

Apart from this minor restriction, Hewson and Meyer (2002) showed that the NRG (which is non-perturbative in both λ and U) works very well for such type of impurity models. In particular, both electron and phonon spectral functions as well as dynamic charge and spin susceptibilities can be calculated with a high accuracy.

As discussed in detail in Jeon *et al.* (2003) and Choi *et al.* (2003a), the calculation of the phonon spectral function needs some extra care and the authors introduced an improved method (as compared to Hewson and Meyer (2002)). The proper calculation of the phonon spectral function is important to discuss the softening of the phonon mode, see also the discussion in Sec. V.C in the context of lattice models with coupling to phonons.

The low-energy features of the model Eq. (138) can

be partly explained by an effective single-impurity Anderson model in which the coupling to the phonons is included in an effective interaction U_{eff} . An explicit form of this interaction can only be given in the limit $\omega_0 \rightarrow \infty$: $U_{\text{eff}} = U - 2\lambda^2/\omega_0$. Interestingly, Hewson *et al.* (2004) have shown that an effective quasiparticle interaction can be defined for *any* value of ω_0 . This can be accomplished with the renormalized perturbation theory by fitting the lowest lying energy levels obtained in the NRG calculations to those from a renormalized Anderson model.

These investigations represent a starting point for various applications of the NRG to coupled electron-phonon system. For the investigation of transport properties of single molecule devices, for which the coupling to local phonons is a natural ingredient, similar models as Eq. (138) have been investigated in Cornaglia *et al.* (2004) and Cornaglia and Grepel (2005a). Not only the coupling to the electron density as in Eq. (138), but also the change of the hybridization between molecule and leads due to the phonons has been shown to be important for the conductance properties (Cornaglia *et al.*, 2005).

Different physical phenomena can be expected in multi-orbital systems when the impurity degrees of freedom couple to Jahn-Teller phonons. Such a model has been investigated in Hotta (2006) and it was argued that within this model a new mechanism of Kondo phenomena with non-magnetic origin can be established.

Two different strategies have been developed to study impurity models with a coupling to a bosonic bath, i.e. a bosonic environment with a continuous spectral density $J(\omega)$. Let us discuss these strategies in the context of the spin-boson model

$$H = -\frac{\Delta}{2}\sigma_x + \frac{\epsilon}{2}\sigma_z + \sum_i \omega_i a_i^\dagger a_i + \frac{\sigma_z}{2} \sum_i \lambda_i (a_i + a_i^\dagger). \quad (139)$$

This model naturally arises in the description of quantum dissipative systems (Leggett *et al.*, 1987). The dynamics of the two-state system, represented by the Pauli matrices $\sigma_{x,z}$, is governed by the competition between the tunneling term Δ and the friction term $\lambda_i(a_i + a_i^\dagger)$. The a_i constitute a bath of harmonic oscillators responsible for the damping, characterized by the bath spectral function

$$J(\omega) = \pi \sum_i \lambda_i^2 \delta(\omega - \omega_i). \quad (140)$$

A standard parametrization of this spectral density is

$$J(\omega) = 2\pi \alpha \omega_c^{1-s} \omega^s, \quad 0 < \omega < \omega_c, \quad s > -1. \quad (141)$$

The case $s = 1$, known as Ohmic dissipation, allows a mapping of the spin-boson model onto the anisotropic Kondo model (for the definition of the Hamiltonian and the relation of its parameters to those of the spin-boson model, see Costi and Kieffer (1996)). The first strategy is then to apply the NRG to the anisotropic Kondo

model and to treat the fermionic conduction band in the usual way. Though restricted to the Ohmic case, such calculations have been shown to give very accurate results for dynamic and thermodynamic quantities of the corresponding spin-boson and related models, as briefly discussed in the following.

The focus of Costi and Kieffer (1996) has been the equilibrium dynamics of the spin-boson model, in particular the spin-spin correlation function, $\chi(\omega) = \langle\langle\sigma_z; \sigma_z\rangle\rangle$, at temperature $T = 0$. An interesting finding of this study, is that the spin relaxation function, $\chi''(\omega)/\omega$, exhibits a crossover from inelastic to quasielastic behavior as α exceeds the value $1/3$ signalling the onset to incoherent dynamics which occurs at $\alpha \geq 1/2$ (Leggett *et al.*, 1987). The accuracy of this approach has been shown via the comparison to exactly solvable limiting cases, such as the Toulouse point $\alpha = 0.5$, and via the generalized Shiba relation. The issue of scaling and universality, concepts which are quite naturally connected to renormalization group treatments of the Kondo problem, have been discussed in the context of the spin-boson model in Costi (1998). Universal scaling functions have been calculated for thermodynamic quantities (the specific heat), the static susceptibility and the spin-relaxation function. Scaling as a function of temperature or frequency has been observed in the limit $\Delta \rightarrow 0$ for *fixed* coupling strength α , this means that the scaling functions turn out to depend on the value of α . This is illustrated, for example, in Fig. 2 in Costi (1998) which shows the temperature dependence of the specific heat for different α . In particular, a signature distinguishing weakly dissipative from strongly dissipative systems is found in $\gamma(T) = C(T)/T$, which is found to exhibit a peak for $\alpha < 1/3$ but is monotonic in temperature for $\alpha \geq 1/3$. This, together with the above mentioned behavior in the spin-relaxation function, is reminiscent of measurements on $\text{Ce}_{1-x}\text{La}_x\text{Al}_3$ (Goremychkin *et al.*, 2002), but the applicability of an anisotropic Kondo model here is controversial (Pietri *et al.*, 2001). Specific heats have also been calculated for more complicated tunneling models, such as the ionic tunneling model with a spinless fermionic bath (Ferreira and Líbero, 2000), which shows similar behavior to the Ohmic spin boson model for $\alpha \leq 1/4$, and to an extension of this including an assisted tunneling term (Ramos and Líbero, 2006). The spectral density of the former has also been investigated (Líbero and Oliveira, 1990b).

The mapping of a bosonic bath to a fermionic one has been also exploited for various other problems. Costi and McKenzie (2003) have used the NRG to calculate the entropy of entanglement for the spin-boson model, a quantity which measures the entanglement between the spin and the environment. Interestingly, the entanglement appears to be highest for $\alpha \rightarrow 1^-$, where the system undergoes a quantum phase transition from a delocalized to a localized phase.

The case of *two* bosonic baths which couple to different components of the impurity spin operator, has been

discussed in Castro Neto *et al.* (2003) and Novais *et al.* (2005). The bosonic baths in these models can be mapped onto two independent fermionic baths, and a generalization of the anisotropic Kondo model is obtained. These models are of interest to study the effect of quantum frustration of decoherence.

The second strategy to investigate impurity models with a coupling to a bosonic bath does not rely on a mapping to a fermionic impurity model. This approach – which has been termed “bosonic” NRG – was introduced in Bulla *et al.* (2003) in the context of the spin-boson model (for full details see (Bulla *et al.*, 2005)). Let us just mention briefly the main differences to the standard (fermionic) NRG: the logarithmic discretization is now directly performed for the bosonic bath (for the spin-boson model, the bath spectral function $J(\omega)$ Eq. (140) is discretized); the subsequent mapping onto a semi-infinite chain is technically very similar to the fermionic case but the resulting tight-binding chain is built up of bosonic sites. This gives rise to additional difficulties in setting up the iterative diagonalization scheme because only a finite number of bosonic states N_b can be taken into account when adding one site to the chain. Furthermore, the set of N_b states should in general be optimized to give the best description of the lowest lying many-particle states, see the discussion in Bulla *et al.* (2005).

The first applications of the bosonic NRG focused on the spin-boson model Eq. (139), in particular the sub-Ohmic case with exponents $0 < s < 1$ in the parametrization of the bath spectral function $J(\omega)$ Eq. (141). The sub-Ohmic case does not allow for the mapping to a fermionic impurity model, in contrast to the Ohmic case. Furthermore, the bosonic NRG turns out to have certain advantages over other approaches usually applied to the spin-boson model (Leggett *et al.*, 1987) as it is non-perturbative in both α and Δ . As an example of the success of the bosonic NRG we show in Fig. 23 the $T = 0$ phase diagram of the spin-boson model with bias $\epsilon = 0$ in the α - s plane for different values of the tunneling amplitude Δ .

The most remarkable feature of the phase diagram is the line of quantum critical points for $0 < s < 1$ which terminates for $s \rightarrow 1^-$ in the Kosterlitz-Thouless transition of the Ohmic case. The critical exponents along this line have been discussed in detail in Vojta *et al.* (2005) where it was shown that the exponents fulfill certain hyperscaling relations.

There are still quite a number of open issues and possible applications in the context of the sub-Ohmic spin-boson model which can be investigated with the bosonic NRG, see for example Tong and Vojta (2006). In addition, the NRG can be generalized to more complex impurity models with a coupling to a bosonic bath. Two recent examples are the investigations of the Bose-Fermi Kondo model (Glossop and Ingersent, 2005) and of models which are connected to electron and exciton transfer phenomena (Tornow *et al.*, 2006a,b).

Technically the most challenging of these extensions

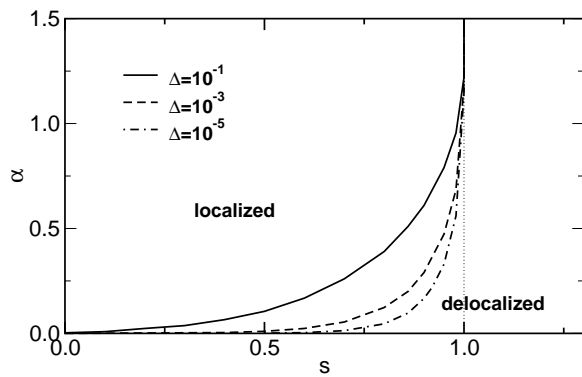


FIG. 23 Phase diagram of the spin-boson model for $T = 0$ calculated with the bosonic NRG for various values of Δ . A line of quantum critical points separates the delocalized from the localized phase. (Figure adapted from Bulla *et al.* (2003)).

is the study of impurity models which couple to both fermionic and bosonic baths. The first successful treatment of such a model, the Bose-Fermi Kondo model with Ising-type coupling between spin and bosonic bath, has been discussed in Glossop and Ingersent (2005, 2006a). Here the two baths are mapped on two semi-infinite chains, one for the bosonic and one for the fermionic degrees of freedom. Due to the competition between dissipation and screening, quantum phase transitions occur which turn out to be in the same universality classes as the transitions in the spin-boson model. This can be understood through a mapping between the (Ising-)Bose-Fermi Kondo model and the spin-boson model where the bath spectral function has both an Ohmic and a sub-Ohmic component (the Ohmic part represents the coupling to the fermionic bath, while the sub-Ohmic part is the same as the one in the original model, see also Li *et al.* (2005)). On the other hand, the (Ising-)Bose-Fermi Kondo model with an Ohmic bosonic bath can also be mapped onto the anisotropic Kondo model, see for example Borda *et al.* (2005).

V. APPLICATION TO LATTICE MODELS WITHIN DMFT

The application of the NRG is restricted to quantum impurity systems with the impurity degree of freedom coupled to a *non-interacting* bath. Therefore, the NRG cannot be directly applied to lattice models of interacting particles, such as the Hubbard model (see Eq. (142) in Sec. V.A). Early attempts to extend Wilson’s concepts to such models failed (Bray and Chui, 1979; Chui and Bray, 1978; Lee, 1979). The reason for this failure was later found to be connected with boundary conditions between “system” and “environment” (Noack and Manmana, 2005; White and Noack, 1992), and led to a novel scheme nowadays known as *density-matrix renormalization group* (Hallberg, 2006;

Schollwöck, 2005), which today is a standard technique to study one-dimensional interacting quantum models.

There exists, however, an approximation for correlated lattice models, where the interacting lattice problem is mapped onto an effective quantum impurity model, for which the NRG can be applied. Underlying this approach is the dynamical mean-field theory (DMFT). The DMFT has its origin in the investigation of correlated lattice models in the limit of infinite spatial dimensionality (Metzner and Vollhardt, 1989). A proper scaling of the hopping matrix element t in models such as the Hubbard model (142) leads to a vanishing of all non-local self-energy skeleton diagrams. The resulting purely local self-energy $\Sigma(z)$ can be identified with the self-energy of an effective single-impurity Anderson model. In this sense we speak of a mapping of a lattice model onto an effective quantum impurity model, typically the single-impurity Anderson model as introduced in Eq. (2), supplemented by a self-consistency condition, which determines the bath degrees of freedom of the effective quantum-impurity. Since the technical details of the DMFT are not the subject of this review, we refer the reader to the review by Georges *et al.* (1996).

To investigate lattice models in the DMFT we therefore need a technique (analytical or numerical) to calculate the full frequency dependence of the self-energy for a single-impurity Anderson model defined by arbitrary input parameters (ε_f , U , T , and a manifestly energy-dependent hybridization function $\Delta(\omega)$). There are many methods besides the NRG available to calculate dynamic quantities for quantum impurity models and we shall not give an overview here (for reviews see, for example, Sec. VI in Georges *et al.* (1996), Sec. III in Maier *et al.* (2005), and Bulla (2006)), but rather concentrate on the application of the NRG method to the Hubbard model (see Sec. V.A), the periodic Anderson and Kondo lattice models (see Sec. V.B), and lattice models with coupling to phonons (see Sec. V.C) within the DMFT approach.

Before we discuss the results obtained for those models, let us comment on peculiarities of the NRG when applied to DMFT calculations. The DMFT self-consistency specifies at each iteration an input hybridization function $\Delta(\omega)$, the form of which depends on the model under investigation, its parameters and also on the history of the previous DMFT-iterations. The frequency dependence of $\Delta(\omega)$ has to be taken into account within the logarithmic discretization scheme, exactly as described in Sec. II and already employed in the NRG investigations of the soft-gap Anderson model, see Sec. IV.C.2.

Concerning the output, the quantity of interest is usually the self-energy Σ_{AM} of the effective single-impurity Anderson model, although in some cases, as for the Bethe lattice, the knowledge of the single-particle Green function is sufficient for the DMFT iteration (Georges *et al.*, 1996). It has proven advantageous to calculate, within DMFT, the self-energy Σ_{AM} via the ratio of a two-particle and a one-particle Green function, see Eq. (85).

As discussed in Bulla *et al.* (1998) (see also Sec. III.B.2) the calculation of the self-energy via Eq. (85) significantly improves the quality of the results. This approach has been used in most NRG calculations within DMFT.

A. Hubbard model

The simplest model for correlated fermions on a lattice is the single-band Hubbard model with the Hamiltonian

$$H = -t \sum_{\langle ij \rangle \sigma} (c_{i\sigma}^\dagger c_{j\sigma} + c_{j\sigma}^\dagger c_{i\sigma}) + U \sum_i c_{i\uparrow}^\dagger c_{i\uparrow} c_{i\downarrow}^\dagger c_{i\downarrow}. \quad (142)$$

Consequently the first applications of the NRG within DMFT focused on this model; in particular on the Mott-transition, which the Hubbard model displays in the half-filled paramagnetic case. These investigations and further generalizations are described in the following subsections.

1. Mott metal-insulator transition

Although the qualitative features of the Mott transition have been correctly described very early in the development of the DMFT (see the review by Georges *et al.* (1996)), the NRG helped to clarify a number of conflicting statements in the literature (see the discussion in Bulla (1999) and Bulla *et al.* (2001)). The NRG method appears to be ideally suited to investigate the Mott transition because (i) the transition occurs at interaction strengths of the order of the bandwidth which requires the use of a non-perturbative method, and (ii) at $T = 0$ the Mott transition is characterized by a vanishing energy scale, $T^* \rightarrow 0$, when approached from the metallic side. Thus, a method is needed that is able to resolve arbitrarily small energies close to the Fermi level.

The first investigation of the Mott transition with the NRG has been performed by Sakai and Kuramoto (1994) (see also Shimizu and Sakai (1995)). These calculations did not use an expression of the self-energy as in Eq. (85), but nevertheless a Mott transition and a hysteresis region have been observed, with critical values very close to the ones reported later in Bulla (1999).

A detailed discussion of the NRG calculations for the Hubbard model is given in Bulla (1999) for $T = 0$ and in Bulla *et al.* (2001) for finite temperatures. The main results are summarized in Fig. 24: Spectral functions calculated with NRG for the half-filled Hubbard model in the paramagnetic regime for different values of U and $T = 0$ are shown in Fig. 24a. Upon increasing U from the metallic side, the typical three-peak structure forms, with upper and lower Hubbard peaks at $\omega \approx \pm U/2$ and a central quasiparticle peak at $\omega = 0$. The width of this quasiparticle peak goes to zero when approaching the transition from below, $U \nearrow U_{c,2} \approx 1.47W$, with W the bandwidth of the noninteracting model. Right at the

transition, when the quasiparticle peak has disappeared, an insulating solution with a preformed gap is realized.

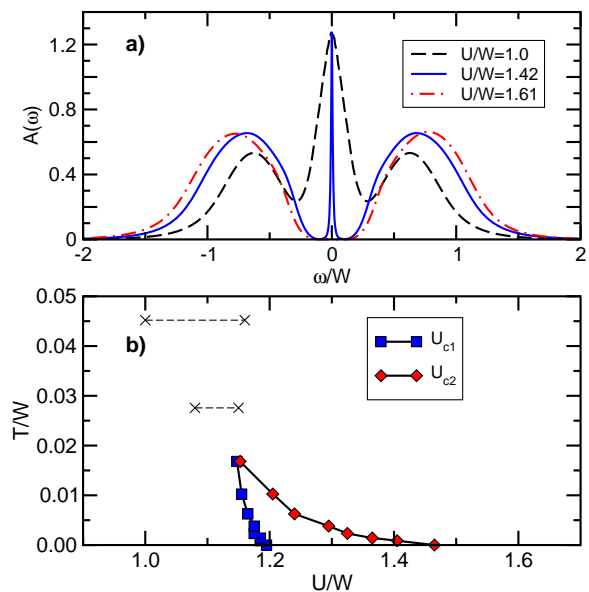


FIG. 24 (a) Spectral functions for the half-filled Hubbard model at $T = 0$ for various values of U (similar data as in Fig. 2 in Bulla (1999)); (b) phase diagram for the Mott transition. For a comparison with other methods see the corresponding Fig. 9 in Bulla *et al.* (2001).

We should remind the reader at that point that the NRG results for dynamic quantities have a certain fixed resolution on a *logarithmic* scale (c.f. the discussion in Sec. III.B). This means that structures close to $\omega = 0$ are much better resolved than structures at, for example, the band edges of the Hubbard bands. In contrast, the dynamical density-matrix renormalization group recently applied to the DMFT for the Hubbard model works with a fixed resolution on a *linear* scale, see for example Karski *et al.* (2005). The structures close to the inner band edges of the Hubbard bands seen in these calculations (see Fig. 2 in Karski *et al.* (2005)) cannot be resolved in present implementations of the NRG method.

Figure 24b shows the T - U phase diagram for the Mott transition, again only considering paramagnetic phases. As already observed earlier (Georges *et al.*, 1996), there are two transition lines, because the insulator-to-metal transition occurs at a lower critical value ($U_{c,1}(T)$) as the metal-to-insulator transition ($U_{c,2}(T)$). Within this hysteresis region, both metallic and insulating solutions can be stabilized within the DMFT self-consistency. With increasing temperature, the hysteresis region shrinks to zero at a critical T_c , above which there is only a crossover from metallic-like to insulating-like solutions; this crossover region is indicated by the dashed lines in Fig. 24b. The NRG values for $U_{c,1/2}(T)$ have later been verified by a number of other, non-perturbative techniques (see for example Tong *et al.* (2001) or Potthoff (2003)).

As discussed above, most of the NRG calculations

within DMFT have been performed using Eq. (85) for the calculation of the self-energy. This quantity itself shows interesting properties (see, for example, Fig. 3 in Bulla (1999) and Fig. 5 in Bulla *et al.* (2001)), and allows to calculate the U -dependence of the quasiparticle weight, see Fig. 1 in Bulla (1999).

The Mott transition can also be induced by moving away from half-filling, provided the value of U is larger than the U_c for the half-filled case. Unfortunately, no systematic NRG calculations have been published for this filling-induced Mott transition, despite the fact that the NRG can be easily extended to the Hubbard model away from particle-hole symmetry. Only a few results for the phase diagram (Ono *et al.*, 2001) and spectral functions (Freericks *et al.*, 2003; Krug von Nidda *et al.*, 2003) are available in the literature.

A nice feature of the DMFT is that it also allows for the calculation of physical quantities other than the single-particle Green function, in particular susceptibilities and also transport properties, both static and dynamic. This aspect of the DMFT has been intensively used already in the early applications (see for example the reviews by Pruschke *et al.* (1995) and Georges *et al.* (1996)), employing different methods to solve the effective quantum-impurity problem. However, apart from discussions of the A_{1g} Raman response (Freericks *et al.*, 2001, 2003) and calculations of the resistivity (Georges *et al.*, 2004; Limelette *et al.*, 2003) and the local dynamic susceptibility (Krug von Nidda *et al.*, 2003), no detailed studies of such quantities for the paramagnetic phase of the Hubbard model have been performed yet with the NRG.

2. Ordering phenomena

The Mott transition from a paramagnetic metal to a paramagnetic insulator is merely one of the many features in the rich phase diagram of the Hubbard model and its generalizations. In addition, various types of ordering phenomena occur, such as charge, orbital (in case of multi-orbital models), and magnetic ordering, and – possibly – superconductivity. The NRG has been used in particular to study magnetic ordering phenomena in a wide range of parameters.

For the investigation of symmetry broken phases within DMFT, the self-consistency equations have to be adapted appropriately (Georges *et al.*, 1996). The effective impurity models still have the structure of the single-impurity Anderson model so that the application of the NRG is straightforward, see the discussion in Zitzler *et al.* (2002). This work also contains a detailed study of the magnetic phases of the Hubbard model at $T = 0$ both at and away from half-filling. Right at half-filling and for a particle-hole symmetric band-structure, the groundstate is always antiferromagnetically ordered. Upon doping, the situation is more complicated as shown in Fig. 25: For small values of U , phase separation within the antiferromagnetic phase is observed, while for very

large U , ferromagnetic solutions can be stabilized. For intermediate U and finite doping, magnetic ordering ap-

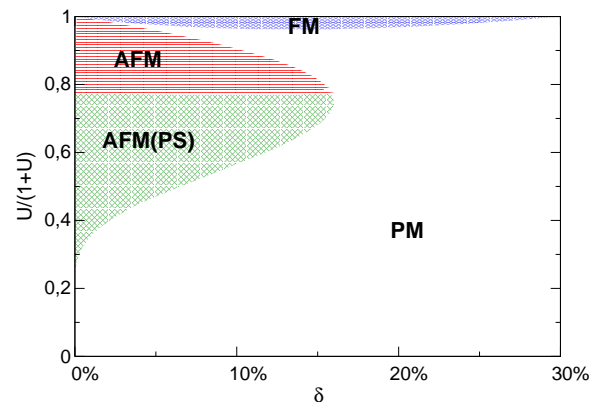


FIG. 25 Ground state magnetic phase diagram for the Hubbard model on a hypercubic lattice. The phases show antiferromagnetic (AFM) order, which for smaller U and doping $\delta > 0$ also shows phase separation (PS), and ferromagnetic order at large U . To display the whole interval $[0, \infty)$, the vertical axis was rescaled as $U/(1+U)$ (see also Fig. 10 in Zitzler *et al.* (2002)).

pears to exist but its type could not be determined yet.

In contrast to this work, the NRG calculations in Zitzler *et al.* (2004) concentrated on the antiferromagnetic phase at half-filling in a Hubbard model with frustration. As expected, the antiferromagnetic region in the T - U phase diagram is suppressed upon increasing frustration. However, the resulting phase diagram turns out to be significantly different from the one proposed for the frustrated Hubbard model in Georges *et al.* (1996), where it was claimed that the main effect of frustration is to suppress T_N such that the first-order Mott transition is visible above the antiferromagnetic region. This controversial issue certainly calls for more detailed calculations (with NRG and other methods); after all, the similarity of the phase diagram for the Hubbard model in DMFT and the experimental one for the transition metal oxide V_2O_3 has been claimed to be one of the early success of DMFT (Georges *et al.*, 1996).

The optical conductivity in the antiferromagnetic phase of the Hubbard model at half-filling and zero temperature has been studied in detail in Pruschke and Zitzler (2003). For small values of U , the antiferromagnetic phase shows signatures of a Slater insulator, while for large U a Mott-Heisenberg picture applies. There is a smooth crossover between these two limiting cases upon variation of U , in contrast to the Mott transition in the paramagnetic phase. The evidence from the optical data has been supported by a detailed discussion of the local dynamical magnetic susceptibility, giving additional insight into the subtle changes in the physics of charge- and spin-degrees of freedom across the Mott metal-insulator transition (Pruschke, 2005; Pruschke and Zitzler, 2003).

When the Hubbard model Eq. (142) is supplemented

by a nearest-neighbor Coulomb repulsion V , a transition to a charge ordered state is observed upon increasing V . This transition has been studied in Pietig *et al.* (1999) for the quarter-filled case. NRG calculations, together with results from non-crossing approximation and exact diagonalization show a phase diagram with a reentrant charge ordering transition, a feature which has also been observed in a variety of transition metal oxides. The NRG results in this work are restricted to $T = 0$, where the transition is of first order. It would be very interesting to extend the NRG calculations to a wider range of parameters, in particular to finite temperatures to study the change of the character of the transition which is continuous at higher T .

3. Multi-band Hubbard models

The application of the NRG to the investigation of multi-band Hubbard models within DMFT is still in a very early stage. This is because (i) the computational effort grows considerably with the number of orbitals and (ii) the DMFT requires a very high accuracy for the calculated dynamic properties. Furthermore, self-consistent solutions of the DMFT equations have to be obtained.

The first (and so far the only) DMFT results for a two-band Hubbard model using the NRG have been presented in Pruschke and Bulla (2005). In this work, two different strategies have been used to handle the complexity of the problem. The first one is to explicitly include the orbital quantum numbers in the iterative construction of the basis states. As for the impurity models discussed in Sec. IV.D, this additional quantum number significantly reduces the typical matrix size. However, this approach fails as soon as the Hamiltonian contains terms which break the orbital symmetry.

The second strategy is an asymmetric truncation scheme: Instead of adding both orbital degrees of freedom simultaneously, the Hilbert space is truncated after adding each orbital individually, which also leads to a significant reduction of the typical matrix size. This approach works quite well in a wide range of parameters, but it appears to violate the orbital symmetry, if present. However, in the presence of a crystal-field splitting of the orbitals, such a strategy might be usable.

The focus in Pruschke and Bulla (2005) was on the role of the Hund exchange coupling J on the Mott transition in the two-band Hubbard model. It was found that both the position in parameter space and the nature of the Mott transition depend on the value of J and the precise form of the coupling. For example, the replacement of a rotationally invariant Hund exchange by an Ising-like exchange leads to a significant change in the physics of the Mott transition. Note that such features can be partly understood already on the level of the corresponding effective impurity models, which underlines the importance to thoroughly investigate the properties of the impurity models appearing in the DMFT.

4. Other generalizations of the Hubbard model

Let us conclude this section with a brief overview of applications of the NRG to various other generalizations of the Hubbard model.

The influence of correlations in a conduction band (modeled by a Hubbard model within DMFT) on the physics of the single-impurity Anderson model has been investigated in Hofstetter *et al.* (2000). The DMFT approach allows to map this model on an effective impurity model with two coupled correlated sites, the first one corresponding to the original impurity and the second one coming from the DMFT treatment of the Hubbard model. This two-site cluster couples to a free effective conduction band. As discussed in Hofstetter *et al.* (2000), correlations in the conduction band have a significant influence on the low-energy scale and also lead to a suppression of the Kondo resonance.

Within the so-called Anderson-Hubbard model, disorder effects can be incorporated via a random distribution of the local energies ε_i . This model has been studied in Byczuk *et al.* (2004) within DMFT for binary alloy disorder. The application of the NRG here is standard – two independent single-impurity Anderson models have to be considered at each iteration step. Nevertheless, the physics of this model is already quite interesting, in particular the occurrence of a Mott transition at *non-integer* filling. The DMFT treatment in Byczuk *et al.* (2004) does not allow for true Anderson localization (as far as disorder is concerned, the DMFT is equivalent to the coherent potential approximation and the main effect of the binary disorder is to split the bands). This deficiency has been cured in Byczuk *et al.* (2005) where a generalization of the DMFT approach has been used, based on the geometrically averaged (typical) local density of states. This allows to study both Mott insulating and Anderson insulating phases, see Fig. 1 in this paper. The calculation has been performed using a continuous probability distribution, approximated by up to 30 different values of ε_i , so that in each DMFT step a corresponding number of independent single-impurity Anderson models have to be considered. All the NRG calculations for the Anderson-Hubbard model have been so far restricted to $T = 0$ and to phases without long-range order.

Recently, the NRG has been used within an extension of the standard DMFT. The ‘DMFT+ Σ_k ’ approach as introduced in Sadovskii *et al.* (2005) and Kuchinskii *et al.* (2005) adds to the local self-energy a k -dependent part Σ_k . Applied to the one-band Hubbard model, the effective single-impurity Anderson model is still of the same type as the one appearing in standard DMFT, the only difference is in the structure of the self-consistency equations.

For details of the NRG calculations and the discussion of the physics of the Falikov-Kimball model (Anders and Czycholl, 2005) and the ionic Hubbard model (Jabben *et al.*, 2005) we refer the reader to the respective references. Both papers show the usefulness of

the NRG approach to a wide range of correlated lattice models within DMFT, in particular for the calculation of dynamic quantities at low temperatures.

B. Periodic Anderson and Kondo lattice models

A variety of Lanthanide- and Actinide-based compounds can be characterized as heavy fermion systems with a strongly enhanced effective mass of the quasiparticles. These compounds contain well localized $4f$ or $5f$ orbitals coupling via a hybridization to a conduction band consisting of s , p or d orbitals. The appropriate microscopic model for these materials is the periodic Anderson model (PAM)

$$H = \varepsilon_f \sum_{i\sigma} f_{i\sigma}^\dagger f_{i\sigma} + U \sum_i f_{i\uparrow}^\dagger f_{i\uparrow} f_{i\downarrow}^\dagger f_{i\downarrow} + \sum_{k\sigma} \varepsilon_k c_{k\sigma}^\dagger c_{k\sigma} + \sum_{ij\sigma} V_{ij} (f_{i\sigma}^\dagger c_{j\sigma} + c_{j\sigma}^\dagger f_{i\sigma}) . \quad (143)$$

When charge fluctuations of the f orbitals are negligible, the low energy physics of the PAM can equally be described by the Kondo lattice model

$$H = J \sum_i \vec{S}_i \cdot \vec{s}_i + \sum_{k\sigma} \varepsilon_k c_{k\sigma}^\dagger c_{k\sigma} . \quad (144)$$

The large effective mass in these models arises from a strongly reduced lattice coherence scale T_0 ; this is one of the reasons why the NRG is very well suited for the investigation of heavy fermion behavior when the PAM or the Kondo lattice model are treated within DMFT. The main difference for the NRG treatment (as compared to the Hubbard model) lies in the DMFT self-consistency. This means that the structure of the effective impurity model is changed only via the effective hybridization $\Delta(\omega)$ (which may lead to complications as discussed later).

The PAM with on-site hybridization $V_{ij} = V\delta_{ij}$ and particle-hole symmetry on a hypercubic lattice has been discussed in Shimizu and Sakai (1995), Pruschke *et al.* (2000), and Shimizu *et al.* (2000). In this case, a hybridization gap at the Fermi level appears in the spectral functions for both conduction and f electrons. This effect for the f spectral function is shown in Fig. 26 by the full lines in the main panel and left inset. Apparently, the Kondo resonance of the corresponding single-impurity Anderson model (dashed curves in the main panel and left inset in Fig. 26), for which the hybridization function is given by the bare density of states of the lattice, is split in the periodic model. The energy scale of the gap in the PAM (proportional to the lattice coherence scale T_0) depends exponentially on the model parameters, similar as for the width of the Kondo resonance in the impurity model (proportional to the Kondo temperature T_K). Further analysis shows that the lattice coherence scale T_0 is enhanced over the impurity scale T_K (for details see Pruschke *et al.* (2000)).

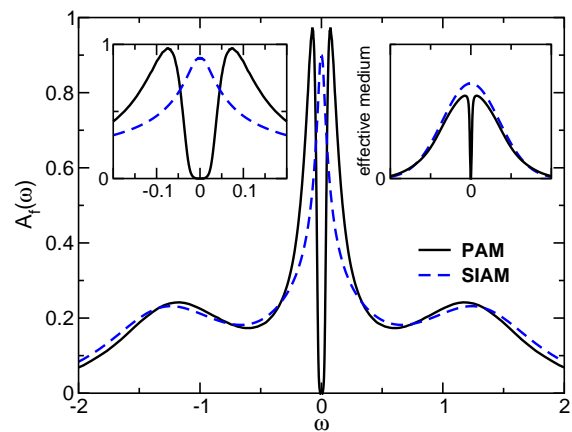


FIG. 26 Comparison of dynamic properties for the particle-hole symmetric periodic Anderson model (solid lines) and the corresponding single-impurity Anderson model (dashed lines). Main panel: f electron spectral function; left inset: enlarged view of the region around the Fermi energy; right inset: (effective) hybridization function. (Figure adapted from Pruschke *et al.* (2000)).

The right inset to Fig. 26 shows the hybridization function of the effective impurity model after self-consistency has been reached (full line) in comparison to the same quantity entering the isolated impurity (dashed line). At first sight, the only difference seems to be the gap at the Fermi level. However, for the particle-hole symmetric case, one can show that $\Delta(\omega)$ has a pole at the Fermi level. At first sight, this pole appears to be a problem for the NRG as the logarithmic discretization explicitly excludes the point $\omega = 0$, i.e. such a pole cannot be incorporated in the mapping to the semi-infinite chain. The way out is to take the pole into account via an extra site which couples directly to the impurity, thus removing the pole from the hybridization function.

Due to the appearance of the hybridization gap, the particle-hole symmetric PAM seems rather suitable to describe so-called Kondo insulators, but not the metallic heavy fermion behavior. There are various ways to drive the PAM into the metallic regime, two of which we will discuss in the following. One possibility is to use asymmetric parameters for the f electrons ($\varepsilon_f \neq -U/2$) and to keep the conduction band symmetric so that $n_c \approx 1$. More interesting (and also physically more relevant) is the opposite case, namely keeping $\varepsilon_f = -U/2$ and shifting the conduction band center-of-mass away from the Fermi level, so that n_c is reduced from 1. This situation has been discussed in the context of Nozières exhaustion principle (Nozières, 1998) which states that, upon decreasing n_c , there will not be enough conduction electrons available to screen the impurity spins. Collective screening then becomes effective only at a strongly reduced lattice coherence scale. We do not want to go into the details here and refer the reader to the discussion in Sec. 5.4 of Vidhyadhiraja and Logan (2004), which is based on results for the PAM obtained with the local-

moment approach.

There is one particular feature found in the DMFT calculations which at first sight seems to support Nozières idea, namely that, as shown in Fig. 6b in Pruschke *et al.* (2000), the effective hybridization function is strongly reduced in a region close to the Fermi level. Since this quantity can be interpreted as being proportional to the conduction band density of states effectively seen by the f -states, it seems that indeed there are less conduction electrons available to screen the moments of the f electrons. Figure 6a in Pruschke *et al.* (2000) shows the corresponding f -spectral function, which consequently now displays metallic (heavy fermion) behavior. The corresponding lattice coherence scale is now reduced as compared to T_K , see Fig. 8 in Pruschke *et al.* (2000) where the dependence of both T_0 and T_K on n_c is plotted. However, in contrast to Nozières original claim, i.e. $T_0 \propto (T_K)^2$, a behavior $T_0 \propto T_K$ is found, with a prefactor decreasing exponentially with decreasing n_c . Again, the ability of the NRG to accurately identify exponentially small energy scales proves to be of great value here.

Another route to metallic behavior in the PAM is to incorporate a dispersion of the f electrons of the form

$$t_f \sum_{\langle ij \rangle, \sigma} \left(f_{i\sigma}^\dagger f_{j\sigma} + f_{j\sigma}^\dagger f_{i\sigma} \right). \quad (145)$$

The effect of such a dispersion term – in particular the closing of the gap upon increasing t_f – has been studied in detail in Shimizu *et al.* (2000) for both the particle-hole symmetric and asymmetric cases. The authors of this work also study the relation between charge and spin gaps in the dynamical susceptibilities and the hybridization gap in the spectral function.

A metallic ground state of the particle-hole symmetric PAM can also be realized when the hybridization between f electrons and c electrons is only between nearest neighbors:

$$V_{ij} = \begin{cases} V & : i, j \text{ nearest neighbors} \\ 0 & : \text{otherwise} \end{cases}. \quad (146)$$

For $T = 0$, the PAM with nearest-neighbor hybridization shows a notable difference to the models discussed above: the low-energy scale T_0 does no longer depend exponentially on U but vanishes at a *finite* critical U_c (Held and Bulla, 2000). This behavior is reminiscent of the physics of the Mott-transition in the Hubbard model. The difference, however, is that in the PAM defined by (143) and (146) the Mott-transition occurs only in the subsystem of the f electrons – a gap opens in the f electron spectral function while the c electron part still has finite spectral weight at the Fermi level (see Fig. 3 in Held and Bulla (2000)) so that the overall system remains metallic.

The calculations described so far have all been restricted to $T = 0$. Finite temperature calculations for single-particle and magnetic excitation spectra have been presented in Costi and Manini (2002) for the Kondo lattice model. As in Pruschke *et al.* (2000), one focus

of these studies has been the variation of the spectra with conduction band filling n_c . For this case it was found that the spectra exhibit *two* energy scales, one being the Kondo temperature T_K of the corresponding single-impurity Kondo model, the other one being the Fermi liquid coherence scale T_0 which, for low carrier densities, $n_c \ll 1$, is strongly reduced as compared to T_K , similar to the observations made in Pruschke *et al.* (2000) for the PAM. A comparison of the temperature dependence of the photoemission spectra with experimental data on YbInCu₄ showed good agreement. A ferromagnetic version of the Kondo lattice model with Coulomb interactions in the conduction band was studied by Liebsch and Costi (2006) in the context of the orbitally selective Mott phase of the two-band Hubbard model with inequivalent bands. The physics of this model is quite different to the usual Kondo lattice model. In particular, one finds, as in Biermann *et al.* (2005), non-Fermi liquid or bad metallic behavior, depending on whether the ferromagnetic exchange is isotropic or anisotropic, respectively.

All these results have been obtained for the paramagnetic phases of the PAM or Kondo lattice model. Of course, the presence of localized moments implies the possibility for magnetic ordering, which is frequently observed in heavy fermion compounds, partly in close vicinity to superconducting phases. These issues have not been addressed yet with the NRG, but, as has been demonstrated for the Hubbard model, are of course accessible with this method and are surely a promising project for future NRG calculations for the PAM or Kondo lattice model within the DMFT.

Magnetic quantum phase transitions in the Kondo lattice model have been the focus of calculations within the extended DMFT (Si *et al.*, 2001), for which the effective impurity model includes a coupling to both fermionic and bosonic baths. The NRG has been generalized to such types of impurity models, see Sec. IV.E, and recent applications of the NRG within the extended DMFT are discussed in Glossop and Ingersent (2006b); Zhu *et al.* (2006).

C. Lattice models with phonons

Let us consider the Hubbard model Eq. (142) and supplement it by a local coupling of the electron density to the displacement of Einstein phonons with frequency ω_0 . This results in the Hubbard-Holstein model with the Hamiltonian

$$H = \varepsilon \sum_{i\sigma} c_{i\sigma}^\dagger c_{i\sigma} - t \sum_{\langle ij \rangle \sigma} c_{i\sigma}^\dagger c_{j\sigma} + U \sum_i c_{i\uparrow}^\dagger c_{i\uparrow} c_{i\downarrow}^\dagger c_{i\downarrow} + g \sum_{i\sigma} \left(b_i^\dagger + b_i \right) c_{i\sigma}^\dagger c_{i\sigma} + \omega_0 \sum_i b_i^\dagger b_i. \quad (147)$$

The limit $U \rightarrow 0$ of this Hamiltonian gives the Holstein model, still a highly non-trivial model as discussed in the following.

Within DMFT, the model Eq. (147) maps onto the Anderson-Holstein (impurity) model, to which the NRG method has been first applied by Hewson and Meyer (2002), see Sec. IV.E. The self-consistency equations are the same for both Hubbard-Holstein and the pure Hubbard model, the only difference lies in the calculation of the self-energy for the effective impurity model which now contains an additional contribution from the coupling to the phonons. This contribution can also be calculated as a ratio of two correlation functions.

From a technical point of view, there is no difference in the NRG-treatment of the Hubbard-Holstein model with either finite or zero value of U . Historically, the first applications of the NRG have been for the $U = 0$ -case (the Holstein model, see Meyer *et al.* (2002) and Meyer and Hewson (2003)) and have already revealed a number of interesting results. As compared to other methods applied to the Holstein-model, the advantage of the NRG combined with the DMFT is that it is non-perturbative in both g and U and that it allows to study the case of a *macroscopic* electron density (in contrast to the few electron case).

For the half-filled case, the investigations of Meyer *et al.* (2002) showed some unexpected properties for the transition from a metal to a bipolaronic insulator at a critical coupling g_c . In contrast to the Mott transition in the Hubbard model, no hysteresis and no preformed gap is observed here (at least for small values of ω_0) which indicates that the physics of the transition to the bipolaronic insulator might be completely different (whether it is connected to locally critical behavior is an interesting subject for future research).

For large values of ω_0 , the physics of the transition is getting closer to that of the Hubbard model (Meyer and Hewson, 2003). This is because in the $\omega_0 \rightarrow \infty$ -limit the Holstein model can be mapped onto the attractive Hubbard model which has the same behavior as the repulsive Hubbard model when charge and spin degrees of freedom are interchanged.

The phase diagram of the Hubbard-Holstein model at half-filling, $T = 0$, and neglecting any long-range ordered phases has been discussed in detail in Koller *et al.* (2004b), Jeon *et al.* (2004), and Koller *et al.* (2004a). The main features are summarized in Fig. 27 which shows the position of the phase boundaries between metallic, Mott-insulating, and bipolaronic insulating phases. The nature of these various transitions, together with the behavior of dynamic quantities has been discussed in detail in Koller *et al.* (2004a). Let us point out here the behavior of the phonon spectral function which shows a considerable phonon softening upon approaching the transition to the bipolaronic insulator. Such a softening is absent in the approach to the Mott insulator, for the simple reason that close to the Mott transition, where charge fluctuations are strongly suppressed, the phonons are effectively decoupled from the electrons. One of the interesting topics for future research are models which do show such a phonon softening even close to the Mott transition; this

can possibly be accomplished by considering additional orbital degrees of freedom.

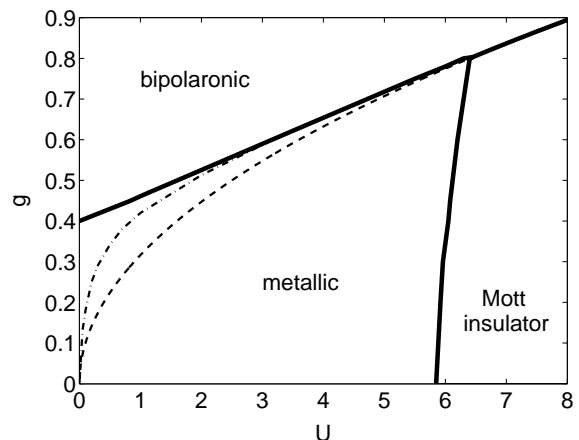


FIG. 27 Phase diagram of the half-filled Hubbard-Holstein model for $T = 0$ (figure adapted from Koller *et al.* (2004a)). The thick solid lines denote the phase boundaries while the dashed line corresponds to $U_{\text{eff}} = U - 2g^2/\omega_0 = 0$. The dashed and dot-dashed lines are polaronic lines, see Koller *et al.* (2004a).

Recently, the Hubbard-Holstein model has been studied for the quarter-filled case and large values of U (Koller *et al.*, 2005a). In this situation, a strongly renormalized band of polaronic quasiparticle excitations occurs within the lower Hubbard band of the electronic spectral function.

All the investigations of lattice models with electron-phonon coupling described in this section have been restricted to $T = 0$ and to phases without long-range order. Generalizations to finite temperatures and ordered phases (such as superconducting and charge ordered phases) appear to be possible within the DMFT/NRG approach and will certainly give interesting results and new insights. Other possible generalizations are different types of lattice models, such as the periodic Anderson model and multi-orbital models, and models with a different type of coupling between electrons and phonons.

VI. SUMMARY

Let us first summarize here the main purpose of this review:

- (i) To give a general introduction to the basic concepts of the numerical renormalization group approach (Sec. II) and to the general strategy for the calculation of physical quantities within this method (Sec. III).
- (ii) To cover the whole range of applications over the last 25 years, following the seminal work of Wilson (1975a) on the Kondo problem and the work of Krishna-murthy *et al.* (1980a) on the Anderson impurity model (Secs. IV and V).

Apparently, the range of applicability of the NRG widened considerably, in particular over the last ten years. This can be easily seen in the list of references in which more than 50% of the entries are from the years starting with 2000. In physical terms, the NRG is now being used to study very different phenomena of condensed matter physics: Typical correlation phenomena such as the Mott transition and heavy-fermion behavior, the physics of a two-state system in a dissipative environment, Kondo correlations in artificial atoms such as quantum dots, to name but a few. Of course, we expect that there are still very many problems to which the NRG will be applied in the future, and we hope that this review will be helpful as a starting point for such investigations.

Some of the concepts discussed in Secs. II and III are fairly recent developments: For example the generalization of the NRG to quantum impurities coupled to a bosonic environment (see also Sec. IV.E) and the calculation of time-dependent quantities (transient dynamics, see Sec. III.B.3). As only a few applications of these new concepts have been considered so far, one line of future research of the NRG is their generalization to a broader class of impurity models.

We already discussed some open issues and ideas for further investigations in the various subsections of Secs. IV and V. Let us mention here a few suggestions for further generalizations and applications of the NRG:

- Application of the bosonic NRG to generalizations of the spin-boson models such as coupled spins in a dissipative environment.
- Magnetic, orbital and charge ordering in lattice models within DMFT.
- Application of multiple-shell techniques (Sec. III.B) to further improvement of the dynamics, particularly at the lowest temperatures.

What are the main open issues of the NRG approach? As discussed in Sec. IV.D, multi-site and multi-orbital models pose severe technical problems for the NRG, because the Hilbert space increases dramatically with the number of orbitals. This limits, in particular, the accuracy in the calculation of dynamical quantities which in turn restricts the applicability of the NRG to multi-band models within DMFT (see Sec. V.A) or its extensions. Concerning dynamical quantities, another shortcoming of the present implementations of the NRG is the rather poor resolution at high frequencies, for example features such as the band edges of upper and lower Hubbard bands in the Hubbard model or the sharply peaked and highly asymmetrical spin-resolved Kondo resonance at high magnetic fields, as shown in Fig. 7.

A gradual improvement of the accuracy can, of course, be achieved by simply increasing the computational effort, but for a real breakthrough (concerning multi-band models and the high-energy resolution) we probably need completely new ideas and concepts.

From a conceptual point of view it will be very interesting to view the NRG in a broader context. One step in this direction has been made in Verstraete *et al.* (2005). The authors of this work interpret the NRG iteration in terms of matrix product states, and establish a connection to the widely used density matrix renormalization group method.

Concerning the future prospects of the numerical renormalization group, let us conclude with a remark from Wilson's original paper (Wilson (1975a), page 777), about the prospects of the renormalization group in general:

... However, most of the unsolved problems in physics and theoretical chemistry are of the kind the renormalization group is intended to solve (other kinds of problems do not remain unsolved for long). It is likely that there will be a vast extension of the renormalization group over the next decade as the methods become more clever and powerful; there are very few areas in either elementary particle physics, solid state physics, or theoretical chemistry that are permanently immune to this infection.

Acknowledgments

It is a pleasure to acknowledge many useful discussions on the topic of this review with present and former colleagues, including F.B. Anders, J. Bonča, L. Borda, S. Florens, J. Freericks, A.C. Hewson, W. Hofstetter, K. Ingersent, S. Kehrein, J. Kroha, D. Logan, N. Manini, A. Rosch, C. Varma, M. Vojta, D. Vollhardt, J. von Delft, P. Wölfle, G. Zaránd, A. Zawadowski, and V. Zlatić. This work was supported in part by the DFG through the collaborative research centers SFB 484 and SFB 602. We acknowledge supercomputer support by the Leibniz Computer Center, the Max-Planck Computer Center Garching under grant h0301, the *Gesellschaft für wissenschaftliche Datenverarbeitung Göttingen* (GWDG), the *Norddeutscher Verbund für Hoch- und Höchstleistungsrechnen* (HLRN) under project nip00015 and the John von Neumann Institute for Computing (Jülich).

References

- Affleck, I., and A. W. W. Ludwig, 1992, Phys. Rev. Lett. **68**, 1046.
- Affleck, I., A. W. W. Ludwig, and B. A. Jones, 1995, Phys. Rev. B **52**, 9528.
- Affleck, I., A. W. W. Ludwig, H.-B. Pang, and D. L. Cox, 1992, Phys. Rev. B **45**, 7918.
- Alascio, B., R. Allub, and C. A. Balseiro, 1986, Phys. Rev. B **34**, 4786.
- Allub, R., and A. A. Aligia, 1995, Phys. Rev. B **52**, 7987.

- Alzoubi, G. M., and N. O. Birge, 2006, Phys. Rev. Lett. **97**, 226803.
- Anders, F. B., 2005, Phys. Rev. B **71**, 121101.
- Anders, F. B., R. Bulla, and M. Vojta, 2006, cond-mat/0607443 .
- Anders, F. B., and G. Czycholl, 2005, Phys. Rev. B **71**, 125101.
- Anders, F. B., E. Lebanon, and A. Schiller, 2004, Phys. Rev. B **70**, 201306.
- Anders, F. B., E. Lebanon, and A. Schiller, 2005, Physica B **359-361**, 1381.
- Anders, F. B., and T. Pruschke, 2006, Phys. Rev. Lett. **96**, 086404.
- Anders, F. B., and A. Schiller, 2005, Phys. Rev. Lett. **95**, 196801.
- Anders, F. B., and A. Schiller, 2006, cond-mat/0604517 .
- Anderson, P. W., 1961, Phys. Rev. **124**, 41.
- Anderson, P. W., 1967, Phys. Rev. Lett. **18**, 1049.
- Bäuerle, C., F. Mallet, F. Schopfer, D. Mailly, G. Eska, and L. Saminadayar, 2005, Phys. Rev. Lett. **95**, 266805.
- Biermann, S., L. de'Medici, and A. Georges, 2005, Phys. Rev. Lett. **95**, 206401.
- Boese, D., W. Hofstetter, and H. Schoeller, 2002, Phys. Rev. B **66**, 125315.
- Borda, L., 2006, cond-mat/0611208 .
- Borda, L., G. Zaránd, W. Hofstetter, B. I. Halperin, and J. von Delft, 2003, Phys. Rev. Lett. **90**, 026602.
- Borda, L., G. Zaránd, and P. Simon, 2005, Phys. Rev. B **72**, 155311.
- Bradley, S. C., R. Bulla, A. C. Hewson, and G.-M. Zhang, 1999, Eur. Phys. J. B **11**, 535.
- Bray, J. W., and S. T. Chui, 1979, Phys. Rev. B **19**, 4876.
- Brito, J. J. S., and H. O. Frola, 1990, Phys. Rev. B **42**, 6378.
- Bulla, R., 1999, Phys. Rev. Lett. **83**, 136.
- Bulla, R., 2006, Phil. Mag. **86**, 1877.
- Bulla, R., T. A. Costi, and D. Vollhardt, 2001, Phys. Rev. B **64**, 045103.
- Bulla, R., M. T. Glossop, D. E. Logan, and T. Pruschke, 2000, J. Phys.: Condens. Matter **12**, 4899.
- Bulla, R., and A. C. Hewson, 1997, Z. Phys. B **104**, 333.
- Bulla, R., A. C. Hewson, and T. Pruschke, 1998, J. Phys.: Condens. Matter **10**, 8365.
- Bulla, R., A. C. Hewson, and G.-M. Zhang, 1997a, Phys. Rev. B **56**, 11721.
- Bulla, R., H.-J. Lee, N.-H. Tong, and M. Vojta, 2005, Phys. Rev. B **71**, 045122.
- Bulla, R., T. Pruschke, and A. C. Hewson, 1997b, J. Phys.: Condens. Matter **9**, 10463.
- Bulla, R., N.-H. Tong, and M. Vojta, 2003, Phys. Rev. Lett. **91**, 170601.
- Bulla, R., and M. Vojta, 2003, in *Concepts in Electron Correlations*, edited by A. C. Hewson and V. Zlatić (Kluwer Academic Publishers, Dordrecht), p. 209.
- Byczuk, K., W. Hofstetter, and D. Vollhardt, 2004, Phys. Rev. B **69**, 045112.
- Byczuk, K., W. Hofstetter, and D. Vollhardt, 2005, Phys. Rev. Lett. **94**, 056404.
- Campo, Jr., V. L., and L. N. Oliveira, 2003, Phys. Rev. B **68**, 035337.
- Campo, Jr., V. L., and L. N. Oliveira, 2004, Phys. Rev. B **70**, 153401.
- Campo, Jr., V. L., and L. N. Oliveira, 2005, Phys. Rev. B **72**, 104432.
- Castro Neto, A. H., E. Novais, L. Borda, G. Zaránd, and I. Affleck, 2003, Phys. Rev. Lett. **91**, 096401.
- Chen, K., and C. Jayaprakash, 1995a, J. Phys.: Condens. Matter **7**, L491.
- Chen, K., and C. Jayaprakash, 1995b, Phys. Rev. B **52**, 14436.
- Chen, K., and C. Jayaprakash, 1998, Phys. Rev. B **57**, 5225.
- Chen, K., C. Jayaprakash, and H. R. Krishnamurthy, 1987, Phys. Rev. Lett. **58**, 929.
- Chen, K., C. Jayaprakash, and H. R. Krishnamurthy, 1992, Phys. Rev. B **45**, 5368.
- Chen, K., C. Jayaprakash, and H. R. Krishnamurthy, 1995, Phys. Rev. Lett. **58**, 929.
- Choi, H.-Y., T.-H. Park, and G. S. Jeon, 2003a, Int. J. of Mod. Phys. B **17**, 3381.
- Choi, M.-S., N. Y. Hwang, and S.-R. E. Yang, 2003b, Phys. Rev. B **67**, 245323.
- Choi, M.-S., M. Lee, K. Kang, and W. Belzig, 2004a, Phys. Rev. B **70**, 020502.
- Choi, M.-S., D. Sánchez, and R. López, 2004b, Phys. Rev. Lett. **92**, 056601.
- Chui, S.-T., and J. W. Bray, 1978, Phys. Rev. B **18**, 2426.
- Coleman, P., 1984, Phys. Rev. B **29**, 3035.
- Coleman, P., L. B. Ioffe, and A. M. Tsvelik, 1995, Phys. Rev. B **52**, 6611.
- Coleman, P., and A. J. Schofield, 1995, Phys. Rev. Lett. **75**, 2184.
- Cornaglia, P. S., and C. A. Balseiro, 2003, Phys. Rev. B **67**, 205420.
- Cornaglia, P. S., and D. R. Grempel, 2005a, Phys. Rev. B **71**, 245326.
- Cornaglia, P. S., and D. R. Grempel, 2005b, Phys. Rev. B **71**, 075305.
- Cornaglia, P. S., D. R. Grempel, and H. Ness, 2005, Phys. Rev. B **71**, 075320.
- Cornaglia, P. S., H. Ness, and D. R. Grempel, 2004, Phys. Rev. Lett. **93**, 147201.
- Costa, S. C., C. A. Paula, V. L. Líbero, and L. N. Oliveira, 1997, Phys. Rev. B **55**, 30.
- Costi, T. A., 1997a, Phys. Rev. B **55**, 3003.
- Costi, T. A., 1997b, Phys. Rev. B **55**, 6670.
- Costi, T. A., 1998, Phys. Rev. Lett. **80**, 1038.
- Costi, T. A., 1999, in *Density-Matrix Renormalization - A New Numerical Method in Physics*, edited by I. Peschel, X. Wang, M. Kaulke, and K. Hallberg (Springer), p. 3.
- Costi, T. A., 2000, Phys. Rev. Lett. **85**, 1504.
- Costi, T. A., 2001, Phys. Rev. B **64**, 241310.
- Costi, T. A., 2003, in *Concepts in Electron Correlations*, edited by A. C. Hewson and V. Zlatić (Kluwer Academic Publishers, Dordrecht), p. 247.
- Costi, T. A., and A. C. Hewson, 1990, Physica B **163**, 179.
- Costi, T. A., and A. C. Hewson, 1991, Physica C **185-189**, 2649.
- Costi, T. A., and A. C. Hewson, 1992a, J. Magn. and Magn. Materials **108**, 129.
- Costi, T. A., and A. C. Hewson, 1992b, Phil. Mag. B **65**, 1165.
- Costi, T. A., and A. C. Hewson, 1993, J. Phys.: Condens. Matter **5**, L361.
- Costi, T. A., A. C. Hewson, and V. Zlatić, 1994a, J. Phys.: Condens. Matter **6**, 2519.
- Costi, T. A., and C. Kieffer, 1996, Phys. Rev. Lett. **76**, 1683.
- Costi, T. A., J. Kroha, and P. Wölffe, 1996, Phys. Rev. B **53**, 1850.
- Costi, T. A., and N. Manini, 2002, J. Low. Temp. Phys. **126**,

- 835.
- Costi, T. A., and R. H. McKenzie, 2003, Phys. Rev. A **68**, 034301.
- Costi, T. A., P. Schmitteckert, J. Kroha, and P. Wölfle, 1994b, Phys. Rev. Lett. **73**, 1275.
- Cox, D. L., H. O. Frota, L. N. Oliveira, and J. W. Wilkins, 1985, Phys. Rev. B **32**, 555.
- Cox, D. L., and A. Zawadowski, 1998, Adv. Phys. **47**, 599.
- Cragg, D. M., and P. Lloyd, 1979, J. Phys. C: Solid St. Phys. **12**, L215.
- Cragg, D. M., P. Lloyd, and P. Nozières, 1980, J. Phys. C: Solid St. Phys. **13**, 803.
- Cronenwett, S. M., T. H. Oosterkamp, and L. P. Kouwenhoven, 1998, Science **281**, 540.
- De Leo, L., and M. Fabrizio, 2004, Phys. Rev. B **69**, 245114.
- De Leo, L., and M. Fabrizio, 2005, Phys. Rev. Lett. **94**, 236401.
- Dias da Silva, L. G. G. V., N. P. Sandler, K. Ingersent, and S. E. Ulloa, 2006, Phys. Rev. Lett. **97**, 096603.
- Doniach, S., 1977, Physica B **91**, 231.
- Doniach, S., and M. Šunjić, 1970, J. Phys. C: Solid St. Phys. **3**, 285.
- Evangelou, S. N., and A. C. Hewson, 1982, J. Phys. C: Solid St. Phys. **15**, 7073.
- Fabrizio, M., A. F. Ho, L. De Leo, and G. E. Santoro, 2003, Phys. Rev. Lett. **91**, 246402.
- Ferreira, J. V. B., and V. L. Libero, 2000, Phys. Rev. B. **61**, 10615.
- Freericks, J. K., T. P. Devereaux, and R. Bulla, 2001, Phys. Rev. B **64**, 233114.
- Freericks, J. K., T. P. Devereaux, R. Bulla, and T. Pruschke, 2003, Phys. Rev. B **67**, 155102.
- Fritz, L., and M. Vojta, 2005, Phys. Rev. B **72**, 212510.
- Frota, H. O., 2004, cond-mat/0401005 .
- Frota, H. O., and K. Flensberg, 1992, Phys. Rev. B **46**, 15207.
- Frota, H. O., and L. N. Oliveira, 1986, Phys. Rev. B **33**, 7871.
- Galpin, M. R., D. E. Logan, and H. R. Krishnamurthy, 2006a, J. Phys.: Condens. Matter **18**, 6571.
- Galpin, M. R., D. E. Logan, and H. R. Krishnamurthy, 2006b, J. Phys.: Condens. Matter **18**, 6545.
- Gan, J., 1995, Phys. Rev. B **51**, 8287.
- Garst, M., S. Kehrein, T. Pruschke, A. Rosch, and M. Vojta, 2004, Phys. Rev. B **69**, 214413.
- Georges, A., S. Florens, and T. A. Costi, 2004, Journal de Physique IV **114**, 165.
- Georges, A., G. Kotliar, W. Krauth, and M. J. Rozenberg, 1996, Rev. Mod. Phys. **68**, 13.
- Gerland, U., J. von Delft, T. A. Costi, and Y. Oreg, 2000, Phys. Rev. Lett. **84**, 3710.
- Glazman, L. I., and M. E. Raikh, 1988, JETP Lett. **47**, 452.
- Glossop, M. T., and K. Ingersent, 2005, Phys. Rev. Lett. **95**, 067202.
- Glossop, M. T., and K. Ingersent, 2006a, cond-mat/0609589 .
- Glossop, M. T., and K. Ingersent, 2006b, cond-mat/0607566 .
- Goldenfeld, N., 1992, *Lectures on Phase Transitions and the Renormalization Group* (Perseus Books).
- Goldhaber-Gordon, D., J. Gores, M. A. Kastner, . H. Shtrikman, D. Mahalu, and U. Meirav, 1998, Phys. Rev. Lett. **81**, 5225.
- Gonzalez-Buxton, C., and K. Ingersent, 1998, Phys. Rev. B **57**, 14254.
- Goremychkin, E. A., R. Osborn, B. D. Rainford, . T. A. Costi, A. P. Murani, and C. A. Scott, 2002, Phys. Rev. Lett. **89**, 147201.
- Hallberg, K. A., 2006, Adv. Phys. **55**, 477.
- Hattori, K., 2005, J. Phys. Soc. Jpn. **74**, 3135.
- Hattori, K., and K. Miyake, 2005, J. Phys. Soc. Jpn. **74**, 2193.
- Hattori, K., S. Yotsuhashi, and K. Miyake, 2005, J. Phys. Soc. Jpn. **74**, 839.
- Held, K., and R. Bulla, 2000, Eur. Phys. J. B **17**, 7.
- Helmes, R. W., M. Sindel, L. Borda, and J. von Delft, 2005, Phys. Rev. B **72**, 125301.
- Hewson, A. C., 1993, *The Kondo Problem to Heavy Fermions* (Cambridge University Press, Cambridge).
- Hewson, A. C., 2005, J. Phys. Soc. Jpn. **74**, 8.
- Hewson, A. C., 2006, J. Phys.: Condens. Matter **18**, 1815.
- Hewson, A. C., J. Bauer, and A. Oguri, 2005, J. Phys.: Condens. Matter **17**, 5413.
- Hewson, A. C., and D. Meyer, 2002, J. Phys.: Condens. Matter **14**, 427.
- Hewson, A. C., A. Oguri, and D. Meyer, 2004, Eur. Phys. J. B **40**, 177.
- Hofstetter, W., 2000, Phys. Rev. Lett. **85**, 1508.
- Hofstetter, W., R. Bulla, and D. Vollhardt, 2000, Phys. Rev. Lett. **84**, 4417.
- Hofstetter, W., J. König, and H. Schoeller, 2001, Phys. Rev. Lett. **87**, 156803.
- Hofstetter, W., and H. Schoeller, 2002, Phys. Rev. Lett. **88**, 016803.
- Hofstetter, W., and G. Zaránd, 2004, Phys. Rev. B **69**, 235301.
- Hotta, T., 2006, Phys. Rev. Lett. **96**, 197201.
- Imada, M., A. Fujimori, and Y. Tokura, 1998, Rev. Mod. Phys. **70**, 1039.
- Ingersent, K., 1996, Phys. Rev. B **54**, 11936.
- Ingersent, K., B. A. Jones, and J. W. Wilkins, 1992, Phys. Rev. Lett. **69**, 2594.
- Ingersent, K., A. W. W. Ludwig, and I. Affleck, 2005, Phys. Rev. Lett. **95**, 257204.
- Ingersent, K., and Q. M. Si, 2002, Phys. Rev. Lett. **89**, 076403.
- Izumida, W., O. Sakai, and Y. Shimizu, 1997, J. Phys. Soc. Jpn. **66**, 717.
- Izumida, W., O. Sakai, and Y. Shimizu, 1998, J. Phys. Soc. Jpn. **67**, 2444.
- Izumida, W., O. Sakai, and S. Suzuki, 2001a, J. Phys. Soc. Jpn. **70**, 1045.
- Izumida, W., O. Sakai, and S. Tarucha, 2001b, Phys. Rev. Lett. **87**, 216803.
- Jabben, T., N. Grewe, and F. Anders, 2005, Eur. Phys. J. B **44**, 47.
- Jayaprakash, C., H. R. Krishna-murthy, and J. W. Wilkins, 1981, Phys. Rev. Lett. **47**, 737.
- Jeon, G. S., T.-H. Park, and H.-Y. Choi, 2003, Phys. Rev. B **68**, 045106.
- Jeon, G. S., T.-H. Park, J. H. Han, H. C. Lee, and H.-Y. Choi, 2004, Phys. Rev. B **70**, 125114.
- Jones, B., 1990, in *Field Theories in Condensed Matter Physics*, edited by Z. Tesanović (Adison-Wesley, Redwood City), p. 87.
- Jones, B. A., and C. M. Varma, 1987, Phys. Rev. Lett. **58**, 843.
- Jones, B. A., C. M. Varma, and J. W. Wilkins, 1988, Phys. Rev. Lett. **61**, 125.
- Kang, K., M.-S. Choi, and S. Lee, 2005, Phys. Rev. Lett. **71**, 045330.

- Karski, M., C. Raas, and G. S. Uhrig, 2005, Phys. Rev. B **72**, 113110.
- Killer, U., E.-W. Scheidt, G. Eickerling, H. Michor, J. Sereni, T. Pruschke, and S. Kehrein, 2004, Phys. Rev. Lett. **93**, 216404.
- Kim, T.-S., L. N. Oliveira, and D. L. Cox, 1997, Phys. Rev. B **55**, 12460.
- Koga, M., 2000, Phys. Rev. B **61**, 395.
- Koga, M., and D. L. Cox, 1999, Phys. Rev. Lett. **82**, 2575.
- Koga, M., and M. Matsumoto, 2002a, J. Phys. Soc. Jpn. **71**, 943.
- Koga, M., and M. Matsumoto, 2002b, Phys. Rev. B **65**, 094434.
- Koga, M., and H. Shiba, 1995, J. Phys. Soc. Jpn. **64**, 4345.
- Koga, M., and H. Shiba, 1996, J. Phys. Soc. Jpn. **65**, 3007.
- Kolesnychenko, O. Y., G. M. M. Heijnen, A. K. Zhuravlev, R. de Kort, M. I. Katsnelson, A. I. Lichtenstein, and H. van Kempen, 2005, Phys. Rev. B **72**, 085456.
- Kolf, C., and J. Kroha, 2006, cond-mat/0610631 .
- Koller, W., A. C. Hewson, and D. M. Edwards, 2005a, Phys. Rev. Lett. **95**, 256401.
- Koller, W., A. C. Hewson, and D. Meyer, 2005b, Phys. Rev. B **72**, 045117.
- Koller, W., D. Meyer, and A. C. Hewson, 2004a, Phys. Rev. B **70**, 155103.
- Koller, W., D. Meyer, Y. Ōno, and A. C. Hewson, 2004b, Europhys. Lett. **66**, 559.
- Krishna-murthy, H. R., J. W. Wilkins, and K. G. Wilson, 1980a, Phys. Rev. B **21**, 1003.
- Krishna-murthy, H. R., J. W. Wilkins, and K. G. Wilson, 1980b, Phys. Rev. B **21**, 1044.
- Krug von Nidda, H.-A., R. Bulla, N. Büttgen, M. Heinrich, and A. Loidl, 2003, Eur. Phys. J. B **34**, 399.
- Kuchinskii, E. Z., I. A. Nekrasov, and M. V. Sadovskii, 2005, JETP Letters **82**, 198.
- Kusunose, H., 2005, J. Phys. Soc. Jpn. **74**, 2157.
- Kusunose, H., and Y. Kuramoto, 1999, J. Phys. Soc. Jpn. **68**, 3960.
- Kusunose, H., K. Miyake, Y. Shimizu, and O. Sakai, 1996, Phys. Rev. Lett. **76**, 271.
- Lebanon, E., A. Schiller, and F. B. Anders, 2003a, Phys. Rev. B **68**, 041311.
- Lebanon, E., A. Schiller, and F. B. Anders, 2003b, Phys. Rev. B **68**, 155301.
- Lee, H.-J., R. Bulla, and M. Vojta, 2005, J. Phys.: Condens. Matter **17**, 6935.
- Lee, P. A., 1979, Phys. Rev. Lett. **42**, 1492.
- Leggett, A. J., S. Chakravarty, A. T. Dorsey, M. P. A. Fisher, A. Garg, and W. Zwerger, 1987, Rev. Mod. Phys. **59**, 1.
- Li, M.-R., K. Le Hur, and W. Hofstetter, 2005, Phys. Rev. Lett. **95**, 086406.
- Líbero, V. L., and L. N. Oliveira, 1990a, Phys. Rev. B **42**, 3167.
- Líbero, V. L., and L. N. Oliveira, 1990b, Phys. Rev. Lett. **65**, 2042.
- Liebsch, A., and T. A. Costi, 2006, Eur. Phys. J. B **51**, 523.
- Limelette, P., P. Wzietek, S. Florens, A. Georges, T. A. Costi, C. Pasquier, D. Jérôme, C. Mézière, and P. Batail, 2003, Phys. Rev. Lett. **91**, 016401.
- Logan, D. E., and M. T. Glossop, 2000, J. Phys.: Condens. Matter **12**, 985.
- Ma, S.-K., 1976, *Modern Theory of Critical Phenomena* (Addison-Wesley).
- Mahan, G. D., 1967, Phys. Rev. **163**, 612.
- Mahan, G. D., 1975, **29**, 75.
- Maier, T., M. Jarrell, T. Pruschke, and M. H. Hettler, 2005, Rev. Mod. Phys. **77**, 1027.
- Mallet, F., J. Ericsson, D. Maily, S. Ünlübayir, D. Reuter, A. Melnikov, A. D. Wieck, T. Micklitz, A. Rosch, T. A. Costi, L. Saminadayar, and C. Bäuerle, 2006, Phys. Rev. Lett. **97**, 226804.
- Martinek, J., M. Sindel, L. Borda, J. Barnaś, J. König, G. Schön, and J. von Delft, 2003, Phys. Rev. Lett. **91**, 247202.
- Matsumoto, M., and M. Koga, 2001, J. Phys. Soc. Jpn. **70**, 2860.
- Matsumoto, M., and M. Koga, 2002, Phys. Rev. B **65**, 024508.
- Mehta, P., N. Andrei, P. Coleman, L. Borda, and G. Zaránd, 2005, Phys. Rev. B **72**, 014430.
- Metzner, W., and D. Vollhardt, 1989, Phys. Rev. Lett. **62**, 324.
- Meyer, D., and A. C. Hewson, 2003, Acta. Phys. Pol. B **34**, 769.
- Meyer, D., A. C. Hewson, and R. Bulla, 2002, Phys. Rev. Lett. **89**, 196401.
- Micklitz, T., A. Altland, T. A. Costi, and A. Rosch, 2006a, Phys. Rev. Lett. **96**, 226601.
- Micklitz, T., T. A. Costi, and A. Rosch, 2006b, cond-mat/0610304 .
- Millis, A. J., B. G. Kotliar, and B. Jones, 1990, in *Field Theories in Condensed Matter Physics*, edited by Z. Tesaonović (Adison-Wesley, Redwood City), p. 159.
- Mohanty, P., E. M. Jariwala, and R. A. Webb, 1997, Phys. Rev. Lett. **78**, 3366.
- Müller-Hartmann, E., 1984, Z. Phys. B **57**, 281.
- Ng, T. K., and P. A. Lee, 1988, Phys. Rev. Lett. **61**, 1768.
- Noack, R. M., and S. R. Manmana, 2005, AIP Conf. Proc. **789**, 93.
- Novais, E., A. H. Castro Neto, L. Borda, I. Affleck, and G. Zaránd, 2005, Phys. Rev. B **72**, 014417.
- Nozières, P., 1974, J. of Low Temp. Phys. **17**, 31.
- Nozières, P., 1998, Eur. Phys. J. B **6**, 447.
- Nozières, P., and A. Blandin, 1980, J. Physique **41**, 193.
- Nozières, P., and C. T. De Dominicis, 1969, Phys. Rev. **179**, 1097.
- Oguri, A., Y. Tanaka, and A. C. Hewson, 2004, J. Phys. Soc. Jpn. **73**, 2494.
- Oliveira, L. N., and J. W. Wilkins, 1981, Phys. Rev. B **24**, 4863.
- Oliveira, L. N., and J. W. Wilkins, 1985, Phys. Rev. B **32**, 696.
- Oliveira, W. C., and L. N. Oliveira, 1994, Phys. Rev. B **49**, 11986.
- Ōno, Y., R. Bulla, A. C. Hewson, and M. Potthoff, 2001, Eur. Phys. J. B **22**, 283.
- Pang, H.-B., 1994, Phys. Rev. Lett. **73**, 2736.
- Pang, H.-B., and D. L. Cox, 1991, Phys. Rev. B **44**, 9454.
- Paula, C. A., M. F. Silva, and L. N. Oliveira, 1999, Phys. Rev. B **59**, 85.
- Perakis, I. E., and C. M. Varma, 1994, Phys. Rev. B **49**, 9041.
- Perakis, I. E., C. M. Varma, and A. E. Ruckenstein, 1993, Phys. Rev. Lett. **70**, 3467.
- Peters, R., and T. Pruschke, 2006, New J. Phys. **8**, 127.
- Peters, R., T. Pruschke, and F. B. Anders, 2006, Phys. Rev. B **74**, 245114.
- Pierre, F., A. B. Gougam, A. Anthore, H. Pothier, . D. Esteve, and N. O. Birge, 2003, Phys. Rev. B **68**, 085413.
- Pietig, R., R. Bulla, and S. Blawid, 1999, Phys. Rev. Lett.

- 82**, 4046.
- Pietri, R., K. Ingersent, and B. Andraka, 2001, Phys. Rev. Lett. **86**, 1090.
- Potthoff, M., 2003, Eur. Phys. J. B **36**, 335.
- Pruschke, T., 2005, Prog. Theor. Phys. Suppl. **160**, 274.
- Pruschke, T., and R. Bulla, 2005, Eur. Phys. J. B **44**, 217.
- Pruschke, T., R. Bulla, and M. Jarrell, 2000, Phys. Rev. B **61**, 12799.
- Pruschke, T., M. Jarrell, and J. K. Freericks, 1995, Adv. in Phys. **44**, 187.
- Pruschke, T., and R. Zitzler, 2003, J. Phys.: Condens. Matter **15**, 7867.
- Pustilnik, M., and L. I. Glazman, 2001, Phys. Rev. B **64**, 045328.
- Ramos, L. R., and V. L. Libero, 2006, Phys. Rev. B **73**, 073101.
- Ramos, L. R., W. C. Oliveira, and V. L. Libero, 2003, Phys. Rev. B **67**, 085104.
- Romeike, C., M. R. Wegewijs, W. Hofstetter, and H. Schoeller, 2006a, Phys. Rev. Lett. **96**, 206601.
- Romeike, C., M. R. Wegewijs, W. Hofstetter, and H. Schoeller, 2006b, Phys. Rev. Lett. **96**, 196601.
- Rosch, A., T. A. Costi, J. Paaske, and P. Wölfle, 2003, Phys. Rev. B **68**, 014430.
- Sadovskii, M. V., I. A. Nekrasov, E. Z. Kuchinskii, T. Pruschke, and V. I. Anisimov, 2005, Phys. Rev. B **72**, 155105.
- Sakai, O., and W. Izumida, 2003, Physica B-Condensed Matter **328**, 125.
- Sakai, O., and Y. Kuramoto, 1994, Solid State Commun. **89**, 307.
- Sakai, O., and Y. Shimizu, 1992a, J. Phys. Soc. Jpn **61**, 2333.
- Sakai, O., and Y. Shimizu, 1992b, J. Phys. Soc. Jpn **61**, 2348.
- Sakai, O., Y. Shimizu, and N. Kaneko, 1993a, Physica B **186-188**, 323.
- Sakai, O., Y. Shimizu, and T. Kasuya, 1989, J. Phys. Soc. Jpn. **58**, 3666.
- Sakai, O., Y. Shimizu, and T. Kasuya, 1990, Solid State Commun. **75**, 81.
- Sakai, O., Y. Shimizu, H. Shiba, and K. Satori, 1993b, J. Phys. Soc. Jpn. **62**, 3181.
- Sakai, O., S. Suzuki, and Y. Shimizu, 1997, Solid State Commun. **101**, 791.
- Sakai, O., S. Suzuki, Y. Shimizu, H. Kusunose, and K. Miyake, 1996, Solid State Commun. **99**, 461.
- Salmhofer, M., 1999, *Renormalization* (Springer Verlag Berlin-Heidelberg-New York).
- Sasaki, S., S. De Franceschi, J. M. Elzerman, W. G. van der Wiel, M. Eto, S. Tarucha, and L. P. Kouwenhoven, 2000, Nature **405**, 764.
- Satori, K., H. Shiba, O. Sakai, and Y. Shimizu, 1992, J. Phys. Soc. Jpn. **61**, 3239.
- Scheidt, E.-W., F. Mayr, U. Killer, W. Scherer, H. Michor, E. Bauer, S. Kehrein, T. Pruschke, and F. Anders, 2005, cond-mat/0506163 .
- Schoeller, H., and J. König, 2000, Phys. Rev. Lett. **84**, 3686.
- Schollwöck, U., 2005, Rev. Mod. Phys. **77**, 259.
- Schopfer, F., C. Bäuerle, W. Rabaud, and L. Saminadayar, 2003, Phys. Rev. Lett. **90**, 056801.
- Schrieffer, R., and P. A. Wolff, 1966, Phys. Rev. **149**, 491.
- Shimizu, Y., A. C. Hewson, and O. Sakai, 1999a, J. Phys. Soc. Jpn. **68**, 2994.
- Shimizu, Y., and O. Sakai, 1995, in *Computational Physics as a New Frontier in Condensed Matter Research* (The Physical Society of Japan), p. 42.
- Shimizu, Y., O. Sakai, and A. C. Hewson, 2000, J. Phys. Soc. Jpn. **69**, 1777.
- Shimizu, Y., O. Sakai, and T. Kasuya, 1990, Physica B **163**, 401.
- Shimizu, Y., O. Sakai, and S. Suzuki, 1998, J. Phys. Soc. Jpn. **67**, 2395.
- Shimizu, Y., O. Sakai, and S. Suzuki, 1999b, Physica B **261**, 366.
- Si, Q., S. Rabello, K. Ingersent, and J. L. Smith, 2001, Nature **413**, 804.
- Si, Q. M., J. L. Smith, and K. Ingersent, 1999, Int. Journ. Mod. Phys. B **13**, 2331.
- Silva, J. B., W. L. C. Lima, W. C. Oliveira, J. L. N. Mello, L. N. Oliveira, and J. W. Wilkins, 1996, Phys. Rev. Lett. **76**, 275.
- Simon, P., P. S. Cornaglia, D. Feinberg, and C. A. Balseiro, 2006, cond-mat/0607794 .
- Sindel, M., W. Hofstetter, J. von Delft, and M. Kindermann, 2005, Phys. Rev. Lett. **94**, 196602.
- Suzuki, S., O. Sakai, and Y. Shimizu, 1996, J. Phys. Soc. Jpn. **65**, 4034.
- Takayama, R., and O. Sakai, 1993, Physica B **188**, 915.
- Takayama, R., and O. Sakai, 1997, J. Phys. Soc. Jpn. **66**, 1512.
- Takegahara, K., Y. Shimizu, N. Goto, and O. Sakai, 1993, Physica B **186-188**, 381.
- Takegahara, K., Y. Shimizu, and O. Sakai, 1992, J. Phys. Soc. Jpn. **61**, 3443.
- Tong, N.-H., S.-Q. Shen, and F.-C. Pu, 2001, Phys. Rev. B **64**, 235109.
- Tong, N.-H., and M. Vojta, 2006, Phys. Rev. Lett. **97**, 016802.
- Tornow, S., N.-H. Tong, and R. Bulla, 2006a, J. Phys.: Condens. Matter **18**, 5985.
- Tornow, S., N.-H. Tong, and R. Bulla, 2006b, Europhys. Lett. **73**, 913.
- v. Löhneysen, H., A. Rosch, and P. W. M. Vojta, 2006, cond-mat/0606317 .
- Vavilov, M. G., and L. I. Glazman, 2003, Phys. Rev. B **67**, 115310.
- Verstraete, F., A. Weichselbaum, U. Schollwöck, J. I. Cirac, and J. von Delft, 2005, cond-mat/0504305 .
- Vidhyadhiraja, N. S., and D. E. Logan, 2004, Eur. Phys. J. B **39**, 313.
- Vojta, M., 2006, Phil. Mag. **86**, 1807.
- Vojta, M., and R. Bulla, 2002a, Eur. Phys. J. B **28**, 283.
- Vojta, M., and R. Bulla, 2002b, Phys. Rev. B **65**, 014511.
- Vojta, M., R. Bulla, and W. Hofstetter, 2002a, Phys. Rev. B **65**, 140405.
- Vojta, M., N.-H. Tong, and R. Bulla, 2005, Phys. Rev. Lett. **94**, 070604.
- Vojta, M., R. Zitzler, R. Bulla, and T. Pruschke, 2002b, Phys. Rev. B **66**, 134527.
- Weichselbaum, A., and J. von Delft, 2006, cond-mat/0607497 .
- White, S. R., and R. M. Noack, 1992, Phys. Rev. Lett. **68**, 3487.
- van der Wiel, W. G., S. De Franceschi, J. M. Elzerman, S. Tarucha, and L. P. Kouwenhoven, 2002, Phys. Rev. Lett. **88**, 126803.
- van der Wiel, W. G., S. De Franceschi, T. Fujisawa, J. M. Elzerman, S. Tarucha, and L. P. Kouwenhoven, 2000, Science **289**, 2105.
- Wilson, K. G., 1975a, Rev. Mod. Phys. **47**, 773.
- Wilson, K. G., 1975b, Adv. in Math. **16**, 170.

- Wilson, K. G., and J. Kogut, 1974, Phys. Rep. **12**, 75.
- Withoff, D., and E. Fradkin, 1990, Phys. Rev. Lett. **64**, 1835.
- Yanson, I. K., V. V. Fisun, R. Hesper, A. V. K. =, J. M. Krans, J. A. Mydosh, and J. M. van Ruitenbeek, 1995, Phys. Rev. Lett. **74**, 302.
- Yoshida, M., M. A. Whitaker, and L. N. Oliveira, 1990, Phys. Rev. B **41**, 9403.
- Yoshioka, T., and Y. Ohashi, 1998, J. Phys. Soc. Jpn. **67**, 1332.
- Yoshioka, T., and Y. Ohashi, 2000, J. Phys. Soc. Jpn. **69**, 1812.
- Yotsuhashi, S., and H. Maebashi, 2002, J. Phys. Soc. Jpn. **71**, 1705.
- Zaránd, G., L. Borda, J. von Delft, and N. Andrei, 2004, Phys. Rev. Lett. **93**, 107204.
- Zaránd, G., C.-H. Chung, P. Simon, and M. Vojta, 2006, Phys.Rev.Lett. **97**, 166802.
- Zhu, J.-X., S. Kirchner, R. Bulla, and Q. Si, 2006, cond-mat/0607567 .
- Zhu, L., and C. M. Varma, 2006, cond-mat/0607426 .
- Zhuravlev, A. K., V. Y. Irkhin, and M. I. Katsnelson, 2005, cond-mat/0512512 .
- Zhuravlev, A. K., V. Y. Irkhin, M. I. Katsnelson, and A. I. Lichtenstein, 2004, Phys. Rev. Lett. **93**, 236403.
- Žitko, R., and J. Bonča, 2006a, cond-mat/0604287 .
- Žitko, R., and J. Bonča, 2006b, Phys. Rev. B **74**, 045312.
- Zitzler, R., T. Pruschke, and R. Bulla, 2002, Eur. Phys. J. B **27**, 473.
- Zitzler, R., N.-H. Tong, T. Pruschke, and R. Bulla, 2004, Phys. Rev. Lett. **93**, 016406.
- Zlatić, V., T. A. Costi, A. C. Hewson, and B. R. Coles, 1993, Phys. Rev. B **48**, 16152.